Noble gases in mantle sources from accretion to the present-day

Rita Parai[1,2]

[1]Dept. of Earth and Planetary Sciences
Washington University in St. Louis
1 Brookings Drive, Saint Louis, MO 63130

[2]McDonnell Center for the Space Sciences
Washington University in St. Louis
1 Brookings Drive, Saint Louis, MO 63130

parai@wustl.edu

Author's archival copy
R. Parai (2025). Noble gases in mantle sources from accretion to the present-day. In: Weis, D and Anbar, A. (eds.) ***Treatise on Geochemistry***, 3e. vol. 1, pp. 513-564. UK: Elsevier. https://dx.doi.org/10.1016/B978-0-323-99762-1.00111-X

Abstract (82 words)
Noble gas isotopes offer a uniquely comprehensive, multi-faceted story of Earth's interior, from accretion to the present-day. Signatures of volatile delivery, extensive gas loss during accretion, early-formed heterogeneity, and differential mantle processing on billion-year timescales are all superimposed in the noble gas record. The large array of noble gas isotopes available for study enables systematic investigation of each of these signatures. A story of early separation of terrestrial reservoirs and divergent paths of mantle outgassing and atmospheric influx emerges from these investigations.

Keywords
accretion
argon
degassing
helium
influx
krypton
neon
noble gas
outgassing
regassing
volatiles
xenon

Key points / objectives

- Terminology, concepts, samples and methods are reviewed for audiences new to noble gas geochemistry.
- Many potential sources of volatiles may have delivered noble gases to the Earth during accretion, but mantle noble gases are most consistent with a mixture of solar nebula and gases trapped in carbonaceous solids.
- There are at least two broad distinct mantle reservoirs, sampled at mid-ocean ridges and by plumes, respectively. These reservoirs carry heterogeneities from accretion that have survived ~4.5 Gyr of convective mixing.
- MORB and plume mantle sources have experienced different histories of long-term outgassing.
- Influx of atmospheric gases affects mantle source Ne, Ar, Kr and Xe compositions of MORB and plume sources. This influx was likely inefficient early in Earth history, and became more efficient as the Earth cooled.
- There might not be any single reservoir that hosts a given specific noble gas signature (*e.g.*, high $^{3}He/^{4}He$) in Earth's interior. Noble gases record a different set of processes than refractory lithophile elements and should be viewed as providing distinct layers of information to characterize mantle sources.
- Noble gases in mantle sources can be explained as signatures intrinsic to highly processed mantle reservoirs that have experienced extensive outgassing and incorporation of subducted slabs bearing atmospheric gas. No primordial mantle or contributions from other hidden reservoirs (such as the core) are required to explain mantle compositions.

1. INTRODUCTION

The study of noble gases in Earth's interior provides key insights into Earth's accretion, early differentiation, and long-term evolution. These rare, inert, volatile elements have quietly witnessed and recorded critical events and planetary processes, including transport processes that played key roles in the establishment and sustenance of clement, habitable conditions on Earth's surface. The set of events and processes tracked by the noble gases is unique among geochemical tracers – much of the information encoded in noble gas elemental and isotopic compositions is not recorded in the compositions of other elements. Accordingly, these valuable tools deserve emphasis in our study of the geochemistry of Earth's interior.

Mantle noble gas geochemists work to address a difficult set of challenges to make precise and accurate determinations of mantle noble gas compositions, including low initial gas concentrations, loss of sample gas from sample materials, and pervasive contamination with atmospheric gases during and after sample formation. Great progress in analytical techniques has enabled major advances in understanding in the past decade, and the field is currently poised for another big step forward. This contribution reviews the current data, interpretations and outstanding discussions in the field. Brief reviews of prior thinking are given where they are useful to understanding how the current discussion developed. This work builds on chapters from prior editions of the Treatise on Geochemistry and many other review papers (Farley and Neroda, 1998; Graham, 2002; Hilton and Porcelli, 2014a, b; Moreira, 2013; Moreira and Kurz, 2013; Mukhopadhyay and Parai, 2019; Parai et al., 2019; Porcelli and Pepin, 2014; Zhang, 2014).

There are five noble gas elements discussed in this chapter: helium (He), neon (Ne), argon (Ar), krypton (Kr) and xenon (Xe). Radon (Rn) is not discussed as it is not typically applied to the study of the mantle (see Section 2.1). Table 1 lists the isotopes of each noble gas element and

categorizes them based on whether they are produced in appreciable quantities over time by nuclear reactions in the mantle or not. For each noble gas element listed, at least one isotope is produced by nuclear reactions, and at least one is not. For an account of the important role that noble gases played in the discovery of isotopes and early geochemistry, the reader is referred to Hilton and Porcelli (2014a), Burnard et al. (2013) and Moreira (2013). Below is a guide to terminology frequently used in mantle noble gas geochemistry, including distinctions from and connections to the broader mantle geochemistry terminology, and background information about samples used to characterize mantle source noble gas signatures. In the sections that follow, we develop the stories of volatile delivery and retention during accretion, early outgassing, and long-term volatile exchange between the mantle and surface reservoirs that are recorded by the noble gases.

2. TERMINOLOGY AND BACKGROUND INFORMATION

2.1 Isotopes and radioactive decay

The nucleus of any given isotope of an element has some intrinsic stability that reflects its makeup (protons, neutrons) and the nuclear orbitals these particles occupy. The less stable a nucleus, the greater the probability that it will undergo spontaneous decay at any given moment. The stability of a nucleus is described by its decay constant, λ, which is larger for less-stable nuclei. The *half-life* of a given isotope is a metric that translates the decay constant into an easier thing to think about: the amount of time it would take for a collection of atoms of that isotope to be halved in number by spontaneous decay (Figure 1).

Isotopes are classified as *stable* or *radioactive* based on their half-lives, but in a manner that is strongly context-dependent – a mantle geochemist would consider ^{147}Sm to be a very

important radioactive isotope that generates variations in $^{143}Nd/^{144}Nd$ among mantle rocks, but its half-life is ~103 billion years, longer than the age of the universe. Scientists who study the very recent past, or fleeting radioactive isotopes that decay away in seconds in the laboratory, might consider many of the mantle geochemist's *long-lived* radioactive isotopes to be effectively stable for their purposes, but as long as they produce measurable quantities of their daughter products on relevant (>Myr) timescales, these are useful radioactive decay systems. In the context of mantle geochemistry, radioactive isotopes are typically categorized as *short-lived* if their half-lives are ~100 million years or less. The short-lived radioactive isotopes became *extinct* (*i.e.*, ceased to generate appreciable amounts of their decay products) early in the history of the Earth, and the stable products of their decay record processes that occurred in the Hadean and early Archean eons.

<Figure 1 near here>

Radioactive *parent isotopes* decay to produce *radiogenic daughter isotopes*, which themselves could be either stable or radioactive. Most radiogenic isotopes discussed in mantle geochemistry are stable (that is, they do not decay appreciably on age-of-the-Earth timescales), with exceptions such as isotopes produced as intermediaries in the $^{235,238}U$ and ^{232}Th α-decay series. Radiogenic is only one of the terms applied to noble gas isotopes that are produced over time. The four heaviest isotopes of Xe are produced by spontaneous fission (of radioactive ^{244}Pu and ^{238}U) and are called *fissiogenic*. The isotope ^{21}Ne is produced in the mantle by nuclear reactions in association with alpha decay and fission, and is referred to as *nucleogenic* (Section 4). Other noble gas isotopes are produced by nuclear reactions in small amounts in specific geologic contexts (*e.g.*, there is significant nucleogenic ^{22}Ne production in continental crust due to its higher concentration of the reactant, ^{19}F, compared to that in the mantle) or in very ancient samples (e.g.,

Moreira, 2007). Note that interactions with cosmic rays produce some isotopes of noble gases (called *cosmogenic*); these signatures can be seen in some mantle-derived samples that have long histories of exposure at Earth's surface, but are negligible when discussing mantle source compositions. The term *produced* is used here to described radiogenic, fissiogenic and nucleogenic isotopes, collectively.

In mantle noble gas geochemistry, the term *primordial* is used to describe non-radiogenic stable isotopes, as the budgets of these isotopes were largely established during Earth's accretion. The phrase *primordial isotope* is not used in this way outside of the noble gas field, but the concept is universal, and the terminology could be extended to other elements. To draw an analogy, the U-Th-Pb decay system involves three radioactive isotopes (^{238}U, ^{235}U, ^{232}Th), three radiogenic isotopes of lead (^{206,207,208}Pb) and one primordial isotope of lead (^{204}Pb). The primordial Pb isotope is used as the denominator of Pb isotope ratios so that ingrowth of the radiogenic isotopes is distinguishable in a sensible way (e.g., high U/Pb ratios lead to high ratios of ^{206}Pb/^{204}Pb). Each noble gas element has at least one primordial isotope (Table 1), except for radon – the longest-lived isotope of radon has a half-life of 3.8 days, which is why radon is not used in mantle geochemistry (Bellotti et al., 2015). Primordial noble gas isotopes (*e.g.*, ^{3}He, ^{22}Ne, ^{36}Ar, ^{130}Xe) are typically used as the denominator of noble gas isotope ratios, with either a radiogenic isotope or another primordial isotope in the numerator depending on the application. However, literature convention is to use the inverse for helium isotopes: these are frequently reported as ^{3}He/^{4}He ratios with the much more abundant radiogenic isotope in the denominator – this is similar to the convention for light stable isotope ratios, such as ^{18}O/^{16}O or ^{13}C/^{12}C. Some laboratories report ^{4}He/^{3}He ratios in alignment with the broader convention in radiogenic isotope geochemistry (e.g., Allègre et al., 1983; Moreira et al., 1998; Parai and Mukhopadhyay, 2021). The practice of

reporting $^{3}He/^{4}He$ ratios is nonetheless ingrained in much of the literature, and so both ratios are given in this chapter.

The phrase *time-integrated ratio* is widely used to describe certain ratios that have long-term consequences for radiogenic isotope systems. A common example is that a high (or low) parent-daughter ratio translates over time to a high (or low) radiogenic-primordial ratio. It is thus said that a high $^{4}He/^{3}He$ ratio reflects high time-integrated $(U+Th)/^{3}He$. One should not take the phrase literally and attempt to actually integrate the $(U+Th)/^{3}He$ ratio with respect to time; the result would not be meaningful. Similarly, a high time-integrated $^{3}He/^{22}He$ ratio denotes that a mantle reservoir evolved over long (Gyr) timescales with a relatively high ratio of primordial ^{3}He compared to primordial ^{22}Ne, and may therefore have relatively unradiogenic He isotopes paired with nucleogenic Ne isotopes (Graham, 2002).

It is important to note that the word *primordial* is used throughout mantle geochemistry literature to describe anything that persists from accretion (e.g., Gülcher et al., 2020; Hallis et al., 2015), including primordial mantle, a hypothetical mantle composition representing the bulk silicate Earth prior to silicate differentiation. It is particularly important to note that the existence of primordial noble gas isotopes (*e.g.,* ^{3}He, ^{130}Xe) in the mantle only means that some gas from accretion has been retained, and does not signify that a truly primordial mantle reservoir (meaning a portion of the mantle unchanged since accretion) exists or has been sampled.

Another potential source of confusion is that the phrase “primordial volatiles” is used when discussing the inventories of noble gases that were delivered to Earth during accretion and retained at the end of accretion. This can be confusing when discussing isotopes, as some amount of every noble gas isotope budget originates from accretion, including the radiogenic isotopes, prior to any production by radioactive decay on Earth. To avoid confusing constructions (like “the primordial

budget of ^{40}Ar"), these are referred to here as *initial* budgets: *e.g.*, the initial budget of ^{40}Ar, or the initial mantle ^{132}Xe concentration.

2.2 Noble gas isotopes

Each of the five noble gas elements discussed in this chapter has multiple isotopes. A list of isotopes, production mechanisms (if any) and other pertinent details are given in Table 1. There are two isotopes of helium: ^{3}He, which is primordial, and ^{4}He, which is produced by alpha decay (mainly of long-lived ^{238}U, ^{235}U and ^{232}Th in the mantle). There are three isotopes of neon: ^{20}Ne and ^{22}Ne are considered primordial in the mantle, while ^{21}Ne is nucleogenic. Two nuclear reactions produce ^{21}Ne in association with decay of U and Th in the mantle: ^{18}O(α,n)^{21}Ne and ^{24}Mg(n, α)^{21}Ne (Wetherill, 1954). Note that in the continental crust, higher fluorine concentrations lead to significant nucleogenic ^{22}Ne production by the ^{19}F(α,n)^{22}Ne reaction. There are three isotopes of argon: ^{36}Ar and ^{38}Ar are primordial, while ^{40}Ar is produced as long-lived ^{40}K decays by electron capture. There are six isotopes of krypton, and the heaviest three are fissiogenic while the rest are primordial. There are nine isotopes of xenon: ^{124,126,128,130}Xe are primordial, ^{129}Xe was produced for the first ~100 Myr of Earth history by decay of the now-extinct short-lived radioactive isotope ^{129}I, and ^{131,132,134,136}Xe are produced in distinct, characteristic proportions by spontaneous fission of extinct, short-lived ^{244}Pu and extant, long-lived ^{238}U.

<Table 1 near here>

2.3 Mantle processing: outgassing, ingassing, degassing, regassing, and influx

Noble gases are volatile and atmophile, and accordingly they trace a distinctive set of planetary processes, beginning from Earth's accretion through to the present day. Common

terminology describing these processes is given here. The dissolution of gases into an early terrestrial magma ocean is referred to as *ingassing*. Transfer of gas out of the silicate mantle is called *outgassing* or *degassing* (generally used interchangeably). This could reflect exsolution from a magma ocean early in Earth history, or loss from the solid mantle by partitioning of incompatible gases into melt, which then erupts and degasses at the surface. *Regassing* has been used to describe the transport of gas from the surface (atmosphere, oceans, crust) into the mantle, typically in association with subducting tectonic plates. However, it is important to note that *regassing* gives the erroneous impression that these atmospheric gases were all initially derived from the mantle, outgassed into the atmosphere, and subsequently returned to the mantle. Some portion of atmospheric gases are indeed derived from outgassing of the interior, but that portion varies among individual isotopes of different elements and in many cases must be small (e.g., ^{36}Ar and Xe isotopes; Marty, 1989; Marty et al., 2017; Zhang et al., 2023). For example, the vast majority of ^{40}Ar in the atmosphere is likely from volcanic outgassing, but most ^{36}Ar was delivered directly to the atmosphere during accretion (Zhang et al., 2023). *Influx* would be a more accurate term for the injection of atmospheric volatiles into the deep interior, and that is adopted here.

There is clear evidence for at least two distinct broad noble gas isotopic signatures in the mantle: one signature generally found in mid-ocean ridge basalts (MORBs), and another in samples from localities influenced by mantle plumes (Morgan, 1971). The compositions of samples carrying magmatic gas are often altered from the original mantle composition, which is called the *mantle source* composition, by contamination and fractionation (see Section 2.6). The mantle that melts to produce MORBs is called the *MORB source*; it is also sampled by some CO_2 well gases (Section 2.4). Ocean island basalts (OIBs) and volcanic gases from hotspots seem to sample a distinct reservoir with a signature that is referred to here as the *plume source*.

There is an offset in the terminology used for noble gases compared to other radiogenic isotope systems, because these systems trace different geochemical aspects of the same geodynamical processes. Most mantle geochemistry terminology originates from studies of relatively refractory, lithophile radiogenic isotope systems (*e.g.*, Rb-Sr, Sm-Nd, U-Th-Pb) in MORBs and OIBs. Systematic variations among these radiogenic isotope signatures (among others) have defined distinct geochemical components in the mantle (FOZO, C, DMM, HIMU, EM-I, EM-II, etc; Chauvel et al., 1992; Hanan and Graham, 1996; Hart et al., 1992; Weis et al., 2023; White, 1985; Zindler and Hart, 1986; Zindler et al., 1982), whose signatures are thought to be generated by partial melting and silicate differentiation, subduction of surface materials, and mixing, all in association with mantle processing through plate tectonics and convection (e.g., Chauvel et al., 1992; Donnelly et al., 2004; Hofmann and White, 1982).

Noble gas signatures don't easily fit into the framework of depleted and enriched components. Part of this is because data coverage for the full suite of noble gases (particularly Ar, Kr and Xe) is much more sparse than for the other systems, and some simplification of the discussion of "plumes" will persist until more data are obtained from EM-I EM-II, and HIMU endmember samples. However, part of it is a conceptual mismatch, as these terms describe systematics of refractory lithophiles, not volatile atmophiles. Enriched recycled oceanic crust and depleted lithospheric mantle are both gas-poor slab components that would carry low concentrations of very radiogenic gas and potentially an influx of atmospheric noble gases upon subduction into the mantle. Furthermore, mixing between materials with dramatic differences in gas concentration can lead to a misleading lack of correlation ("decoupling") between noble gases and other isotopic signatures. For example, addition of a small material amount of a gas-rich component can dominate noble gas signatures without strongly affecting lithophile elements; *e.g.*,

low $^{4}He/^{3}He$ (high $^{3}He/^{4}He$) ratios are found among ocean island basalts with distinct Sr, Nd and Pb isotopic signatures (Jackson et al., 2007). Instead of attempting to identify a single host of a specific noble gas signature (like high $^{3}He/^{4}He$), the noble gases can instead be viewed as having recorded distinct layers of information about the components observed in mantle sources.

2.4 Types of samples carrying mantle noble gases

Noble gases behave incompatibly during partial melting and are concentrated in melts (Graham et al., 2016). The melts are buoyant and rise, degassing as they ascend, and ultimately either stall and solidify or erupt at the surface. Samples of the mantle (typically found as xenoliths in lavas), of the erupted lavas, of phenocryst separates, and of degassed volatiles all have been analyzed to shed light on mantle source noble gas compositions (Figure 2). Mantle gases have been measured in diamonds (Honda et al., 1987; Ozima, 1989) and in ultramafic nodules and xenoliths (e.g., Gautheron et al., 2005; Buikin et al., 2005; Kaneoka and Takaoka, 1980; Kaneoka et al., 1983; Poreda and Farley, 1992). Gases concentrated (due to their incompatibility) in melts have been measured in fluid or melt inclusions hosted within phenocrysts carried in the lavas (Hanyu and Kaneoka, 1997; Hilton et al., 2000; Horton et al., 2019), and in glass from the rims of pillow basalts erupted in submarine or subglacial environments (e.g., Condomines et al., 1983; Craig and Lupton, 1976; Kaneoka et al., 1978). Rapid quenching seems to be favorable for the trapping of magmatic vesicles in glassy pillow basalt rims. The slower-cooled fine-grained basalt in pillow interiors does not seem to effectively preserve magmatic gases (Roubinet and Moreira, 2018), even when the pillow interior is vesicular. However, coarse-grained crystalline intrusive rocks may contain magmatic gas trapped in inclusions within crystals (Jeffery, 1971).

Volatiles exsolved and degassed from magmas percolate through the surrounding crust (or lithosphere) and can be sampled within hydrothermal vent fluids (Hilton et al., 1998; Kennedy, 1988), fumarolic gases, fluids from hot springs and other volcanic gas emissions (Sano and Fischer, 2013). Continental well gases, collected from wells developed for industrial production of natural CO_2, are in some cases dominated by magmatic CO_2 and bear mantle noble gases (Ballentine et al., 2005; Butler et al., 1963; Caffee et al., 1999; Holland and Ballentine, 2006; Phinney et al., 1978; Zartman et al., 1961). Compared to the solid samples discussed above, gas samples have the advantage of providing a much larger quantity of gas for analysis, which enables excellent precision (Seltzer and Bekaert, 2022). However, interpretation of the data can be more complicated than for solid samples: (1) gases are contaminated by both atmospheric gas and non-magmatic crustal gas (see Section 2.6), and (2) very high-precision measurements indicate that isotopic compositions are mass-fractionated during circulation of the gas in the subsurface environment (Bekaert et al., 2023).

<Figure 2 near here>

2.5 Gas processing and mass spectrometry

Sample preparation depends on the type of sample and degree of alteration of solid samples. Highly altered samples (for example, olivine phenocrysts from old, altered ocean island basalts) are sometimes leached in dilute acid and cleaned ultrasonically (Parai et al., 2009) or, in rare cases, abraded by hand under a microscope (Zhang et al., 2024) to avoid gas loss during ultrasonic cleaning. Altered basalt glass chips may be crushed to pick out clean glass pieces, but it may be better to remove surface alteration and keep large glass chips intact to increase the chances of preserving gas trapped in large vesicles within the sample (Kurz et al., 1982; Parai, 2023; Sarda et al., 1985).

Gases are typically extracted from solid samples in multiple steps by crushing, laser ablation or heating by laser or furnace. Step-release of gas enables sub-sampling of gases held in different sites in the sample. Ideally, random mixtures of magmatic gas and contaminants enable elucidation of the uncontaminated magmatic composition (see Section 2.6). Samples can be crushed by using an electromagnet to drive a slug of metal within the crushing chamber up and down in strokes (Kurz et al., 1987; Moreira et al., 1998; Sarda et al., 1988), or by means of a pestle or ram situated within a compressible bellows (Burnard et al., 2003; Mukhopadhyay, 2012; Parai, 2023; Parai et al., 2009). Laser ablation has been used to release gas from diamonds (Johnson et al., 2000) or to analyze single vesicles in basalt glass (Burnard et al., 1997; Colin et al., 2015; Péron et al., 2016; Raquin et al., 2008). Step-release by heating in a furnace or by means of a laser is also used for a variety of samples (Kaneoka et al., 1983; Marty, 1989; Poreda and Farley, 1992; Sarda et al., 1985).

Gas extracted from solids is typically purified by exposure to reactive alloys called getter pumps; the reactive gases are adsorbed or chemisorbed, while the inert gases are theoretically unaffected and remain free in the processing volume (Burnard et al., 2013). For volcanic gas samples, gas aliquots are taken and purified prior to analysis (Bekaert et al., 2023; Broadley et al., 2020; Seltzer and Bekaert, 2022). The purified noble gases may be separated using a cryogenic trap, leveraging the sorption characteristics and release temperatures for the different noble gases on sorbents like activated charcoal or stainless steel (Lott III, 2001; Péron et al., 2020; Reynolds et al., 1978). Elemental separation allows for better sample-standard bracketing: if elemental abundance patterns differ significantly between sample and standard gases (*e.g.*, much lower Ar/Ne in sample gas compared to atmospheric gas standards), then the calibration provided by analysis of standard gas may not accurately capture conditions in the mass spectrometer during

sample gas analysis. Analysis of purified, separated noble gas elements avoids this potential complication during analysis.

Noble gas isotopes are typically measured in a gas source magnetic sector mass spectrometer, using sample-standard bracketing to calibrate instrument sensitivity and mass discrimination (Burnard et al., 2013; Zeitler and Tremblay, 2020). For solid samples with very small quantities of gas, measurements are made by static mass spectrometry: the mass spectrometer is isolated from the ion pump that usually maintains ultra-high vacuum, sample gas is expanded from the processing line into the mass spectrometer, the inlet valve is closed, and the gas is consumed by measurement. Dynamic mass spectrometry involves continuous gas flow (alternating between sample and standard gases) into a mass spectrometer that is being actively pumped, and requires orders of magnitude more sample gas than static mass spectrometry (Seltzer and Bekaert, 2022). The newest instruments have sufficient mass resolving power to resolve ^{3}He from HD^{+}, $^{20}Ne^{+}$ from $^{40}Ar^{++}$, and various hydrocarbons from Kr and Xe isotopes, but corrections generally must be made for CO_2^{++} interference on ^{22}Ne, and HCl^{+} on ^{36}Ar and ^{38}Ar. The exact corrections are specific to each instrument and must be calibrated periodically (Mukhopadhyay et al., 2012; Parai, 2023; Parai et al., 2009).

2.6 Hard luck and trouble: from measured compositions to the mantle source

Noble gas geochemistry differs from other mantle isotope geochemistry fields in that the set of processes that affect measured compositions and obscure the mantle source composition is distinct from the set of common processes affecting non-volatile elements. There are two major categories of headache faced specifically by noble gas geochemists trying to backtrack from measured compositions to source compositions: contamination and degassing.

Most samples are affected to some degree by shallow atmospheric contamination. The only noble gas that is largely unaffected by atmospheric contamination in mantle samples is He, as it is light enough to escape from the atmosphere and is present at a very low concentrations in atmospheric gas. Magmatic He concentrations are orders of magnitude higher than those of the heavier gases, so atmospheric contamination can strongly affect Ne, Ar, Kr and Xe isotopes without detectably affecting He isotopes. Samples may be contaminated through assimilation of altered oceanic crust during magma transit towards the surface (Fisher, 1997; Fisher and Perfit, 1990; Marty and Zimmermann, 1999; Stroncik and Niedermann, 2016), through interaction with seawater (Patterson et al., 1990), during eruption, or during storage and handling in the laboratory, either by surface adsorption (Stroncik and Niedermann, 2016) or if microfractures from rapid sample decompression (*e.g.,* upon dredging of submarine basalt glass that erupted under kilometers of water) allowed infiltration of atmospheric gas into vesicles and then subsequently healed (Ballentine and Barfod, 2000; Mungall et al., 1996; Roubinet and Moreira, 2018). In some samples, the first few gas release steps show the greatest degree of atmospheric contamination (Ballentine and Barfod, 2000; Moreira et al., 1998), but that is not uniformly true for all samples and may depend on the method of gas release (Burnard et al., 2003; Parai and Mukhopadhyay, 2021; Parai et al., 2012).

Samples that erupted or circulated through crust may be additionally affected by crustal contamination. If melts assimilate altered oceanic crust, the contamination should be more or less atmospheric in composition. However, if the melts erupt or circulate through old continental crust with high concentrations of radioactive U, Th and K, they would be affected by a crustal contaminant rich in isotopes produced by nuclear reactions (^{4}He, ^{21}Ne, ^{22}Ne, ^{40}Ar and fissiogenic Xe). For example, crustal signatures are evident in compositions measured in continental well

gases from New Mexico (Ballentine et al., 2005) and volcanic gases from Yellowstone (Broadley et al., 2020). Circulation in hydrothermal systems has also been shown to generate mass-dependent isotopic fractionation in hydrothermal gases (Bekaert et al., 2023).

The critical question when examining measured data: can a correction for contamination (or contamination and fractionation; Bekaert et al., 2023) be made? On some level, the ability to determine magmatic gas compositions prior to contamination is a matter of luck: one analyzes samples with unrelenting optimism, and seeks samples that have sufficient gas for multiple precise analyses, preferably showing variable contamination. If mixing systematics are evident, corrections can be made to estimate the magmatic gas composition without contamination. If not, hard luck – one tries again with another sample.

Corrections for solid samples are made by assuming some model uncontaminated mantle primordial isotope ratio (such as $^{20}Ne/^{22}Ne$) and using either linear or hyperbolic fitting to estimate the uncontaminated magmatic endmember with some uncertainty. A detailed description of this correction is given by Parai et al. (2019), and the method is summarized for determinations of mantle source $^{21}Ne/^{22}Ne$, $^{40}Ar/^{36}Ar$ and Xe isotopes in Section 4. For isotopic ratios, the corrected composition is the mantle source isotopic composition. For elemental ratios, the corrected composition may or may not reflect the mantle source composition due to the other category of noble gas trouble: magma degassing.

Equilibrium or kinetic effects can alter noble gas elemental ratios[1] during magma degassing. The noble gases have different solubilities in magma at near-surface pressures, with He

[1]Diffusive fractionation of helium isotopes during magma degassing has been suggested (Burnard, P., 2004. Diffusive fractionation of noble gases and helium isotopes during mantle melting. Earth and Planetary Science Letters 220, 287-295.), but isotopic fractionation of the heavier elements (with smaller proportional mass

being the most soluble and Xe being the least soluble (Broadhurst et al., 1992; Carroll and Stolper, 1993; Carroll and Webster, 1994; Jambon et al., 1986; Lux, 1987; Shibata et al., 1998). As the pressure decreases during magma ascent, dissolved CO_2 exsolves at a relatively early stage and forms vesicles (Bottinga and Javoy, 1989). The noble gases exsolve but are not abundant enough to form their own vesicles. Accordingly, exsolved noble gases are only degassed from the magma if they diffuse into CO_2-rich bubbles that carry them out. The diffusivities of noble gases differ based on mass: the lightest atoms diffuse the fastest in silicate melts (Behrens, 2010). If there is sufficient time for all noble gases to come to equilibrium between the vesicles and the magma, then the elemental ratios in the degassed fluid and residual magma will be related to the mantle source composition based on solubilities. If there is insufficient time (*e.g.,* if bubbles ascend rapidly through the melt and only helium diffuses fast enough to equilibrate with the vesicles), then kinetic effects are at play and elemental ratios in the resulting degassed fluid and residual magma will have a more complicated relationship with the mantle source (Gonnermann and Mukhopadhyay, 2007; Tucker et al., 2018; Weston et al., 2015).

The effects of degassing on elemental ratios can be assessed by computing sample radiogenic isotope ratios, such as $^{4}He^{*}/^{40}Ar^{*}$ (where the star denotes the portion of each isotope derived from radioactive decay; see Graham, 2002), and comparing these to production ratios expected in the mantle. If the computed sample ratio is similar to the expected production ratio, then elemental ratios have not been significantly affected by degassing. If the computed sample ratio differs from the expected production ratio, either the assumed mantle composition was

differences) during magmatic degassing has not been demonstrated and may be too small to detect with present methods.

incorrect (e.g., K/U in the mantle source differed from bulk silicate Earth; Hanyu et al., 2011; Zhang et al., 2024); or noble gas elemental abundances were altered from the source composition. By leveraging coupled production ratios for three or more noble gas elements, the nature of that alteration may be investigated (Graham, 2002; Tucker et al., 2018). Multi-element coupled production ratios suggest that non-equilibrium degassing is prevalent in oceanic basalts: He and Ne achieve near-equilibrium partitioning between melt and vesicles, but kinetic effects prevent the slow-diffusing heavier noble gases from equilibrating and these are overabundant in the residual melts (Tucker et al., 2018). In some solid samples, additional loss of He beyond modeled loss by degassing is sometimes observed, and potentially occurs due to diffusive loss from the samples.

In light of these difficulties, the best estimates of mantle source noble gas elemental ratios come from samples with radiogenic isotope ratios that are similar to mantle production ratios, and we largely focus on these in the discussion of mantle source noble gases that follows. We discuss mantle source isotopic compositions from samples where corrections for contamination were possible, or where relevant systematics are apparent in the step release data.

3. SETTING THE SCENE: NOBLE GASES FROM ACCRETION

Noble gases delivered to Earth during accretion are still retained within the interior of the planet today. Helium isotopes provided the first indication that this rather astonishing assertion – the Earth is very old and geologically active – was true. Based on the good agreement between the observed heat flux through the ocean floor and calculated heat production in the solid Earth, Suess and Wänke (1965) suggested that He produced within the solid Earth by U and Th decay should also diffuse out through the crust, and observed an excess in helium concentration in deep Pacific ocean water. To distinguish between helium from the crust (expected to be mostly ^{4}He) and excess

atmospheric gas entrained and trapped in ocean water, Clarke et al. (1969) measured helium isotopes in deep ocean waters from the South Pacific. Rather than atmospheric or ^{4}He-rich compositions, they instead found a surprising excess in ^{3}He compared to atmospheric helium, and concluded that ^{3}He from accretion was still present in Earth's interior and was leaking out even today. Clarke et al. (1969) used their observations to calculate a lower limit initial ^{3}He concentration in the solid Earth, and noted that a significant proportion of accreted gases might remain in the interior. This early example highlights the potency of noble gas isotopes as tools to investigate terrestrial volatile origins.

3.1 Formation of the Earth

The formation of the Solar System began with the collapse of a local region of the interstellar molecular cloud under its own gravity. The molecular cloud is thought to have been made of ~99% gas and ~1% dust (Bohlin et al., 1978), with hydrogen and helium making up most of the gas and the other elements of the periodic table appearing either as gaseous atoms or in dust grains less than a micrometer across (Weingartner and Draine, 2001). Most of the mass of the collapsing cloud fell into the central object, which became our Sun once temperatures were high enough to ignite hydrogen fusion. About 1% of the nebular mass remained in a rotating disk structure orbiting around the central star, called the protoplanetary disk or nebular disk.

Much of the dust from the molecular cloud was vaporized in the high temperature environment of the early disk. Early evidence for the survival of some solid dust grains from the molecular cloud (summarized in Zinner, 2014) included mysterious Xe (Reynolds and Turner, 1964) and Ne (Black and Pepin, 1969; Black, 1972b) isotopic signatures measured in chondritic meteorites. Efforts to isolate the host phases of these exotic noble gas isotopic compositions

culminated in the discovery of diamond (Lewis et al., 1987), silicon carbide (Zinner et al., 1987) and graphite (Amari et al., 1990) grains that had survived the collapse of the molecular cloud in the solid state. The survival of presolar grains (including silicates; Hoppe et al., 2022) and their heterogeneous distribution among meteorites raised the interesting prospect that these carriers of distinct isotopic compositions might not be homogeneously distributed throughout the protoplanetary disk.

Early studies assumed that the nebular disk was well-mixed and had a single, uniform composition (see discussion in Podosek, 1978), and that as the hot nebular gas cooled, new solids condensed in a sequence reflecting the temperatures and pressures at a given distance from the Sun (Lodders, 2003; Petaev and Wood, 1998). Temperatures were higher closer to the Sun compared to the outer Solar System at any given time, but at all distances the disk was cooling and condensing solids. The first Solar System solids are believed to be refractory calcium-aluminum inclusions found in undifferentiated meteorites (Gray et al., 1973). Dust grains that condensed within the proto-planetary disk accreted together to formed larger and larger solids, though the mechanism of building planetary bodies is debated (Burkhardt et al., 2021; Morbidelli et al., 2012; Raymond and Morbidelli, 2022).

Isotopic evidence that the proto-planetary disk was not well-mixed is now abundant. Different classes of undifferentiated meteorites sample distinct cosmochemical reservoirs, with a primary distinction made between carbonaceous chondrites and non-carbonaceous (ordinary and enstatite) chondrites in multiple non-radiogenic isotope systems (*e.g.*, Bermingham et al., 2020; Kleine et al., 2020; Kruijer et al., 2020; Trinquier et al., 2009; Warren, 2011). One possible interpretation is that non-carbonaceous solids formed from a reservoir in the inner Solar System, while volatile-rich carbonaceous solids formed from a distinct reservoir in the outer Solar System,

with incomplete mixing of material between these domains. The rapid formation of Jupiter may have inhibited mixing of material from inside and outside the gas giant's orbit for the first few Myr of Solar System history; subsequent growth and migration of Jupiter and Saturn (the Grand Tack scenario; Walsh et al., 2011) may have driven radial mixing that brought carbonaceous outer Solar System materials into the inner Solar System (see reviews by Broadley et al., 2022; Kruijer et al., 2020). While an outer Solar System origin for carbonaceous materials is widely discussed, the formation of carbonaceous materials within the inner Solar System is a distinct possibility (*e.g.*, Alexander et al., 2017; Marrochi et al., 2018), and our understanding of mixing in the proto-planetary disk is still developing. Observations of circumstellar disks around other stars indicate that rings and gaps are common (Huang et al., 2018), and pressure variations within the disk have been suggested to play an important role in planetary formation (Izidoro et al., 2022; Morbidelli, 2020). Pressure bumps and the position of the snow line (the radial distance from the Sun beyond which H_2O condenses as ice) during accretion may have also played a role in generating distinct isotopic reservoirs in the proto-planetary disk (Charnoz et al., 2021; Lichtenberg et al., 2021).

During the later stages of planet growth, giant impacts between planetary embryos (referring to planetary bodies roughly the size of Mars) had important consequences for planetary volatiles. Earth is thought to have experienced at least one giant impact: this is the leading hypothesis for the origin of our Moon (Cameron and Ward, 1976; Lock et al., 2020; Lock et al., 2018). However, Earth could potentially have experienced multiple giant impacts (Tucker and Mukhopadhyay, 2014), culminating in the Moon-forming giant impact. In the aftermath of any giant impact, the growing Earth likely experienced a magma ocean stage. It is important to note that the nebular gas was present in the Solar System only for the first several million years of accretion, before it was dispersed by intense radiation from the young Sun (e.g., Hillenbrand,

2008). A magma ocean stage that occurred prior to gas dispersal would have presented an opportunity for ingassing of nebular gases into the molten silicate of the proto-planet. Magma oceans that formed after gas dispersal likely drove strong outgassing of the silicate Earth, though strictly speaking, these may have driven different gases into or out of the magma, depending upon their respective partial pressures in whatever atmosphere was present on the proto-Earth at the time. Overall, giant impacts represent opportunities to fundamentally shape or reset the volatile inventory of the growing Earth.

A fraction of a percent of Earth's mass was accreted after the last giant impact. This late accreted material is called the *late veneer* and is inferred to account for the observation that highly-siderophile elements, which should partition into the core during metal-silicate equilibration, are present in Earth's mantle in chondritic proportions at higher concentrations than expected (Chou, 1978). The composition of the late veneer is debated (Dauphas et al., 2024; Fischer-Gödde et al., 2020; Hopp et al., 2022), and a better understanding is critical to our knowledge of volatile contributions from late-accreted material to the Earth's mantle and atmosphere.

3.2 Potential sources of volatiles during accretion

3.2.1 Solar nebular gas

The early stages of planetary accretion occurred in the presence of solar nebular gas, before the cooling nebular gas was dispersed by intense radiation from the young Sun. Some nebular gas was incorporated into proto-Earth bodies. The composition of solar nebular gas is expected to have been the same as the composition of the Sun, since ~99% of the mass of the collapsing nebula formed the Sun. However, the composition of the Sun has been altered by hydrogen fusion for the past ~4.5 billion years, which has affected He abundances and isotopic compositions. For an

estimate of the nebular He isotope ratio, we instead look to the atmosphere of Jupiter, since this gas giant planet rapidly grew massive enough to gravitationally bind hydrogen and helium, effectively trapping a solar nebular gas atmosphere, prior to the dispersal of the gas from the protoplanetary disk. Jovian helium isotopes were measured by a mass spectrometer on the NASA Galileo probe (Table 3; Mahaffy et al., 1998), and these are used as an estimate of the nebular He composition.

Estimates of the abundance pattern and isotopic composition of heavy noble gases in the solar nebula are derived from measurements of solar wind, as this is the most accessible sample of the Sun that can be measured with high precision in terrestrial laboratories. NASA's Genesis mission (Burnett and Team, 2011), spent 27 months collecting solar wind implanted on a variety of ultrapure foils and plates, and returned these samples to Earth, where they were analyzed for elemental abundance patterns and isotopic compositions (Crowther and Gilmour, 2013; Grimberg et al., 2006; Grimberg et al., 2008; Grimberg et al., 2007; Heber et al., 2012; Heber et al., 2009; Meshik et al., 2014; Meshik et al., 2020; Pepin et al., 2012; Vogel et al., 2011; Vogel et al., 2019). There is some mass-dependent isotopic fractionation that occurs during the formation and acceleration of solar wind (as well as during implantation into solid materials; see next section). A correction for this isotopic fractionation must be made to estimate the composition of the solar outer convective zone, which is believed to represent the bulk solar composition (though gravitational settling could also generate some isotopic fractionation within the Sun). Isotopic fractionation is expected to be more pronounced for the light noble gases due to their large relative mass differences; accordingly, mass-fractionation corrections are made for Ne and Ar, while measured solar wind compositions for Kr and Xe are typically used as estimates of the solar nebular composition (Heber et al., 2012; Wieler, 2002).

3.2.2 Solar noble gases implanted in dust

Dust irradiated by solar wind in the protoplanetary disk may also have contributed solar noble gases to the growing Earth (e.g., Ballentine et al., 2005; Moreira and Charnoz, 2016; Péron et al., 2018; Trieloff et al., 2000). To follow the current thinking on this topic, it is necessary to briefly review the development of earlier concepts regarding noble gases in meteorites. It was observed that the elemental abundance patterns of gas-rich meteorites typically fell into one of two patterns: a solar-like pattern enriched in He and Ne, or a "planetary" pattern depleted in light gases but with high abundances of Ar, Kr and Xe (Signer and Suess, 1963).

Noble gas measurements in solar-pattern meteorites thought to be formed from dust compacted on asteroid surfaces (Eberhardt et al., 1965a; Suess et al., 1964; Wänke, 1965) showed high concentrations of gas near the surfaces of individual grains, consistent with long-term irradiation of dust exposed to solar wind on bodies with weak magnetic fields and very thin (if any) atmospheres. Similar signatures were evident in lunar soils (Pepin et al., 1970; Reynolds et al., 1970). $^{20}Ne/^{22}Ne$ in the outermost portions of these grains was found to be high, around ~13.8, and agreed well with the solar wind $^{20}Ne/^{22}Ne$ of 13.7 ± 0.3 determined from the Apollo Solar Wind Composition experiments, which collected solar wind implanted onto foil collectors placed on the lunar surface during extra-vehicular activities on five Apollo missions (Geiss et al., 2004 and references therein). The solar wind $^{20}Ne/^{22}Ne$ was later confirmed by both the SOHO spacecraft (13.8 ± 0.7; Kallenbach et al., 1997) and the Genesis mission (13.78 ± 0.01; Heber et al., 2012).

A second solar component implanted more deeply within the grains was suggested to exist based on clustering of $^{20}Ne/^{22}Ne$ measurements around ~11.2 (Black and Pepin, 1969), initially

proposed to be solar flare particles (Black, 1972a), but later discussed as particles with greater fluxes and lower energies than expected for solar flares (Wieler et al., 1986). This second solar component was given the name "solar energetic particles" (SEP), but was later shown by studies of the Genesis samples to be an artifact of mass-dependent fractionation with depth as solar wind was implanted into grains (Grimberg et al., 2006; Grimberg et al., 2008; Grimberg et al., 2007; see Wieler, 2023 for a nice review of this story).

Early studies of neon isotopes in carbonaceous chondrites and other gas-rich "planetary" pattern meteorites indicated the existence of two distinct components trapped within these rocks: one with $^{20}Ne/^{22}Ne$ of ~8 labeled Ne-A (discussed below), and the other with $^{20}Ne/^{22}Ne$ of ~12.5 labeled Ne-B (Black and Pepin, 1969; Black, 1972b; Mazor et al., 1970; Pepin, 1967). Cosmogenic Ne (with very low $^{20}Ne/^{22}Ne < 1$; Mazor et al., 1970), produced within the meteorites over time while they were exposed to cosmic rays, is also present in variable amounts. The composition of Ne-B is moderately depleted in light isotopes compared to solar wind. Earlier studies interpreted the Ne-B composition as either mass-fractionated implanted solar wind (Podosek, 1978) or mixing between implanted solar wind and solar energetic particles (Black, 1972a). However, in light of the Genesis mission results, the SEP component is obsolete (Grimberg et al., 2006; Grimberg et al., 2008; Grimberg et al., 2007). Recent models for the origin of Ne-B favor solar wind implantation into dust grains, with the heaviest isotopes implanted more deeply, followed by sputtering to erode and remove the light isotope-enriched outer layers of the grains (Moreira and Charnoz, 2016; Moreira and Raquin, 2007; Raquin and Moreira, 2009). These models predict a steady-state $^{20}Ne/^{22}Ne$ of ~12.7, if erosion and implantation rates are equal. However, a more sophisticated treatment considering dust grain size and dust particle motion within a turbulent proto-planetary disk can yield values of ~12.9 (Moreira and Charnoz, 2016). If solar-wind

irradiated dust was prevalent during planet formation, this material could potentially have contributed noble gases to the Earth during accretion.

3.2.3 Noble gases in rocky solids

Noble gases trapped in solid materials early in Solar System history (or trapped even earlier in presolar grains) have compositions distinct from solar nebula and solar wind. Meteorites provide our best record of the gas compositions trapped in rocky solids[2] during planet formation, as these are leftovers from planet-building in a nearby region of the Solar System. A fundamental feature of rocky solids is that they are depleted in all noble gases compared to the Sun (in terms of atoms of element per atom of silicon; Dauphas and Morbidelli, 2014; Lodders, 2021), and are particularly depleted in He and Ne (Figure 3; widely discussed in the literature as the "planetary" pattern)[3]. This pattern reflects poor retention of noble gases overall, but preferential retention of Ar, Kr and Xe compared to He and Ne in some carrier phases within the rocky solids. The pronounced contrast in elemental abundance patterns for solar and rocky noble gases has important ramifications for the origins of terrestrial noble gases.

<Figure 3 near here>

There is detailed literature regarding the specific carriers of trapped noble gases in rocky solids and their compositions and origins (see Ott, 2014 and references therein). To understand

[2] Note that the phrase "rocky solids" is used here to describe a mixture of rock and metal (*i.e.*, undifferentiated meteorites are considered rocky solids) to differentiate from icy solids from further out in the Solar System

[3] Compare Figure 3 to Brown (1949) for a historical perspective; that study captured the essential points by showing that the Earth was overall depleted in noble gas atoms normalized to Si compared to cosmic abundances, and was particularly depleted in the light noble gases. That fundamental picture has not changed much in 75 years.

what noble gases could have been brought by rocky solids to the growing Earth, a bird's-eye view is merited: what is the bulk gas composition expected to be carried in rocky solids that accreted during planet formation in the inner Solar System? In this view, it is important to note extreme variations in noble gas concentrations among meteorite classes. Chondritic (undifferentiated) meteorites have orders of magnitude higher concentrations of noble gases than typical differentiated meteorites (Busemann and Eugster, 2002; Busemann et al., 2006; Krietsch et al., 2021; Patzer et al., 2003). Even if most of material that contributed to the growing Earth were differentiated and gas-poor, a few percent by mass of undifferentiated materials would contribute enough gas to dominate the final terrestrial noble gas budget. Likewise, among chondrites, carbonaceous chondrites have orders of magnitude higher gas concentrations than the non-carbonaceous (ordinary and enstatite) chondrites (Crabb and Anders, 1981; Krietsch et al., 2021; Okazaki et al., 2010; Patzer and Schultz, 2002; Schultz et al., 1990, 1991). If the Earth accreted entirely from material similar to enstatite chondrites, their noble gas compositions could be important to our understanding of the initial composition of terrestrial noble gases. However, if even a fraction of a percent of Earth's mass came from undifferentiated carbonaceous solids, gas carried by these materials could swamp out the weaker contributions from relatively gas-poor solids, whether these were differentiated or non-carbonaceous undifferentiated materials (Parai, 2022).

The isotopic compositions of noble gases in carbonaceous chondrites are reviewed here. Ar, Kr and Xe in carbonaceous chondrites are dominated by the Q phase ("quintessence"), which is enriched in heavy isotopes compared to solar wind (Busemann et al., 2000; Ott, 2014) and seems to be closely associated with refractory organic compounds (Marrocchi et al., 2005; Ott et al., 1981). The average carbonaceous chondrite (AVCC) Xe composition (Pepin, 2000; Pepin and

Porcelli, 2002) is consistent with a mixture between Q phase Xe and Xe hosted by presolar diamonds (Ott, 2014). While the Q phase dominates trapped Xe in chondrites, it contributes only a small fraction of trapped Ne (Nakamura et al., 1999). Rather, trapped Ne in carbonaceous chondrites has the Ne-A isotopic composition, with $^{20}Ne/^{22}Ne$ of ~8 (Krietsch et al., 2021; Marty, 2022; Mazor et al., 1970). The Ne-A composition is thought to reflect a mixture of presolar diamonds and phases hosting pure ^{22}Ne from decay of ^{22}Na (Ott, 2014). Carbonaceous chondrite Ne isotopes also evidence an implanted solar component (Ne-B or solar wind; Krietsch et al., 2021; Marty, 2022), but this solar component may have been implanted during secondary processing of the meteorite materials (see Marty, 2022 for a detailed discussion; Nakamura et al., 1999) and it is unknown whether the solar signature was acquired prior to planet formation.

If undifferentiated materials similar to enstatite chondrites contributed significantly to the terrestrial noble gas budget, the isotopes and elemental abundance ratios in the delivered gas could be distinct from gas delivered by carbonaceous materials. Neon isotopes in some enstatite chondrites are similar to Ne-B (Marty, 2022). Some enstatite chondrites carry a distinctive heavy noble gas component with very high Ar/Ne, Ar/Xe and Kr/Xe ratios, dubbed the "subsolar" component as it is less fractionated compared to solar wind than other trapped components (Crabb and Anders, 1981; Okazaki et al., 2001; Ott, 2014). The subsolar component may be hosted within the mineral enstatite (Crabb and Anders, 1981; Okazaki et al., 2010). Potential mechanisms to generate the subsolar signature are discussed by Marty (2022). The subsolar Ne isotopic composition is intermediate (~11.65; Busemann et al., 2001) among accreted components. Kr and Xe isotopic compositions are similar but not identical to solar wind (Crabb and Anders, 1981). Given the lower typical heavy noble gas concentrations in enstatite chondrites compared to carbonaceous chondrites (e.g., Okazaki et al., 2010; Patzer and Schultz, 2002; Krietsch et al.,

2021), a high proportion of planetary mass from enstatite chondrite-like material would be required for these isotopic compositions to manifest in the final accreted noble gas budgets of a planet.

3.2.4 Noble gases in icy solids (comets)

Comets are thought to have contributed a limited portion of Earth's atmospheric noble gas inventory (~20% of Xe; Marty et al., 2017). It is possible that icy solids also contributed some noble gases to the accreting solid Earth. Estimates of the elemental and isotopic compositions of noble gases trapped in icy solids are based on experiments (Bar-Nun et al., 2007; Notesco et al., 2003; Owen and Bar-Nun, 2000) and measurements made at the comet 67P/Churyumov-Gerasimenko by the Rosetta Orbiter Spectrometer for Ion and Neutral Analysis (Marty et al., 2017; Rubin et al., 2018).

3.3 Noble gases from accretion in mantle reservoirs

Earth's mantle noble gases are consistent with mixing between two main accretionary sources: solar nebular gas and material similar to carbonaceous chondrites. Mantle light noble gas (He and Ne) isotopes require a solar contribution and are consistent with ingassing of solar nebula during a terrestrial magma ocean stage (Section 3.3.2). Heavy noble gases (Ar, Kr, Xe) from accretion are consistent with delivery by rocky solids similar to carbonaceous chondrites (Section 3.3.4). The apparent dual sourcing is explained well by two-component mixing when the extreme contrast in elemental abundance patterns is taken into account: solar gases are very rich in He and Ne, and rather poor in Ar, Kr and Xe. Conversely, carbonaceous material is strongly depleted in He and Ne, but has Ar/Ne, Kr/Ne and Xe/Ne ratios that are orders of magnitude greater than solar. Accordingly, a simple mixture of solar gas and gas from carbonaceous solids can explain the

observed duality in noble gas isotopic signatures (Marty and Zimmermann, 1999; Parai, 2022; Trieloff et al., 2002; Williams and Mukhopadhyay, 2019).

Further detail on this scenario and alternate scenarios for the origins of accreted noble gases are discussed below. The budget of primordial helium and ratios of primordial isotopes of all noble gases (*e.g.*, ^{3}He, ^{20,22}Ne, ^{36}Ar, ^{82}Kr, ^{130}Xe; see Table 1 for full list) are used to better understand sources of noble gases from accretion. Ratios of primordial isotopes differ among various potential accreted sources of noble gases, and these may be used as fingerprints of volatile origins. Various processes can fractionate elemental or isotopic ratios based on their mass or solubility, but these processes should produce systematic, internally-consistent variations that can be assessed while evaluating potential volatile sources during accretion.

3.3.1 Solar-derived helium

Helium isotopes in samples of the mantle have much lower ^{4}He/^{3}He ratios than expected for in-situ production in the mantle (^{4}He/^{3}He > 10^{7}; (Graham, 2002), evidence of the retention of helium from accretion[4] in the modern mantle (Clarke et al., 1969). The lowest ^{4}He/^{3}He (highest ^{3}He/^{4}He) ratios observed to date were measured in 62 Myr old samples from Baffin Island (Horton et al., 2023), with multiple measurements of ^{4}He/^{3}He = 10,700 ± 300 in a single sample (^{3}He/^{4}He of 67.2 ± 1.8 Ra, where Ra is the atmospheric ratio of 1.39 × 10^{-6}) and a lowest individual measurement of ^{4}He/^{3}He = 7,930 ± 340 (the highest individual measurement of ^{3}He/^{4}He = 90.7 ±

[4]Subduction of ^{3}He-rich interplanetary dust particles (IDPs) and micrometeorites into a strongly outgassed mantle over time was suggested as a possible alternative explanation for the observed low mantle ^{4}He/^{3}He, rather than retention of gases from accretion (Anderson, 1993). However, Allègre et al. (1993) showed that subduction of cosmic dust was not sufficient to sustain the flux of magmatic ^{3}He emitted from the mantle, and this possibility has not gained traction.

3.9 Ra) in another sample. For comparison, the $^{4}He/^{3}He$ ratio measured in Jupiter's atmosphere, which provides our best estimate of nebular He isotopes, is 6,020 ± 180 (~120 Ra; Mahaffy et al., 1998). If He were delivered exclusively by rocky solids to Earth's mantle during accretion, this gas would have been subject to degassing and loss during energetic impacts, which are thought to have driven >97% loss during accretion (Porcelli et al., 2001). Harper and Jacobsen (1996) suggested that in light of inefficient volatile retention during accretion, rocky solids would not have high enough trapped ^{3}He concentrations to have delivered enough He to keep $^{4}He/^{3}He$ in the modern mantle this low after ~4.5 Gyr of Earth history given estimates of terrestrial U and Th concentrations. Instead, dissolution of solar nebular gas into a terrestrial magma ocean formed by a giant impact could have provided sufficient solar-like helium (Harper and Jacobsen, 1996; Mizuno et al., 1980; Olson and Sharp, 2018). However, rocky material bearing solar wind irradiated material with high concentrations of He could also have delivered sufficient solar-like helium to the mantle during accretion (Péron et al., 2018; Trieloff et al., 2000). To distinguish between a solar nebular origin (which requires a giant impact and magma ocean stage before dissipation of the nebular gas) and delivery of gases via solar wind irradiated material, primordial neon isotopes provide a powerful tool.

3.3.2 Primordial neon isotopes

The ratio of the two primordial Ne isotopes, $^{20}Ne/^{22}Ne$, is high in the mantle compared to Earth's atmosphere (Hiyagon et al., 1992; Honda et al., 1991; Honda et al., 1987; Marty, 1989; Sarda et al., 1988) (Figure 4) and can be used to assess the origins of Ne in terrestrial reservoirs. The highest measured mantle-derived $^{20}Ne/^{22}Ne$ values are from plume-influenced locations, including in a dunite from the Kola Peninsula in Russia (13.0 ± 0.2; Yokochi and Marty, 2004), a

subglacial basalt glass from Iceland (12.88 ± 0.06; Mukhopadhyay, 2012), and a submarine basalt glass from the Discovery plume-influenced section of the southern Mid-Atlantic Ridge (13.03 ± 0.02; Williams and Mukhopadhyay, 2019). All of these measurements are likely affected by some degree of contamination with atmospheric $^{20}Ne/^{22}Ne$ of 9.8 (Eberhardt et al., 1965b; Györe et al., 2024), and so the mantle source $^{20}Ne/^{22}Ne$ could be even higher. The Ne-A composition that dominates the trapped composition of rocky solids (Section 3.2.3) has $^{20}Ne/^{22}Ne$ that is a bit low compared to atmosphere (Figure 4); the atmospheric $^{20}Ne/^{22}Ne$ signature likely reflects direct delivery by impact degassing of late-accreting materials bearing Ne-A (Marty, 1989) mixed with a limited amount of Ne from mantle outgassing (Marty, 2012; Marty, 2022; Zhang et al., 2023). In contrast, Ne-A is clearly not the main source of neon accreted to the mantle. The highest ratios measured in plume-influenced samples are significantly higher than the Ne-B composition prevalent in meteorites, higher than the steady-state models of dust irradiated and eroded by solar wind ($^{20}Ne/^{22}Ne$ of ~12.7; Raquin and Moreira, 2009), and higher than $^{20}Ne/^{22}Ne$ ratios generated by models of irradiation of dust in a turbulent disk (up to ~12.9; Moreira and Charnoz, 2016), suggesting their derivation from dissolution of solar nebular gas ($^{20}Ne/^{22}Ne$ of 13.36 ± 0.09; Heber et al., 2012) into a terrestrial magma ocean.

The highest precise measurements of $^{20}Ne/^{22}Ne$ in mid-ocean ridge basalts have a maximum around ~12.6 (Parai and Mukhopadhyay, 2021). This could indicate that MORBs experience greater degrees of atmospheric contamination, and even the least-contaminated measurement in MORBs has a greater degree of shallow atmospheric contamination than is seen in plume samples. However, measurements of Ne isotopes in continental well gases, thought to be sourced from the upper mantle, pointed towards an uncontaminated mantle source $^{20}Ne/^{22}Ne$ of ~12.5 (Ballentine et al., 2005; Holland and Ballentine, 2006). Low $^{20}Ne/^{22}Ne$ compared to plume

sources may therefore be a signature that is characteristic of the MORB source mantle. Pető et al. (2013) suggested that mantle sources that incorporate a mix of plume and MORB mantle have intermediate mantle source $^{20}Ne/^{22}Ne$. Williams and Mukhopadhyay (2019) showed that compiled mantle Ne data support this interpretation. If low $^{20}Ne/^{22}Ne$ (<12.6) is a MORB source signature, then there are three potential explanations: (1) Ne in the MORB source mantle has an entirely different origin from the mantle source of plumes, and was delivered by solar wind irradiated material (Ne-B; Ballentine et al., 2005); (2) solar nebular Ne was ingassed to the whole mantle, and the MORB source mantle additionally received Ne trapped in rocky solids (Ne-A) that lowered the accreted $^{20}Ne/^{22}Ne$; or (3) solar nebular Ne was ingassed to the whole mantle, and the MORB source mantle $^{20}Ne/^{22}Ne$ has been lowered by an influx of atmospheric Ne through subduction over Earth history (Figure 4). Primordial isotope and elemental ratios show that (1) is not supported: solar wind irradiated material would not provide sufficient solar Ar or Xe to the mantle (Section 3.3.5; (Marty, 2012; Marty, 2022; Williams and Mukhopadhyay, 2019). Parai (2022) showed that a combination of (2,3) is required to explain He, Ne and Xe isotopes simultaneously (see Section 3.3.5).

<Figure 4 near here>

3.3.3 Primordial argon is of indeterminate origin

The primordial Ar isotope ratio, $^{38}Ar/^{36}Ar$, has received less attention than $^{20}Ne/^{22}Ne$. Earth's atmospheric $^{38}Ar/^{36}Ar$ (0.1880; Porcelli et al., 2002) is higher than solar (Pepin and Becker, 1990; Wiens et al., 2004) and is also distinct from the ratios associated with the solar wind irradiated component (Ne-B) or the trapped component (Ne-A) in chondrites (Black, 1972b). Studies that reported MORB and OIB $^{38}Ar/^{36}Ar$ distinct from the atmospheric composition

(Niedermann et al., 1997; Valbracht et al., 1997) were interpreted as signatures of solar $^{38}Ar/^{36}Ar$ (Pepin, 1998), but this was later challenged (see Moreira, 2013). Instead, it seems that $^{38}Ar/^{36}Ar$ is indistinguishable from the atmospheric composition in mantle samples (Kunz, 1999; Moreira and Raquin, 2007; Raquin and Moreira, 2009; Trieloff et al., 2002; Trieloff et al., 2000), potentially due to the influx of atmospheric Ar into the mantle over time associated with subduction (Section 5.1.3; see discussion in Moreira and Raquin, 2007; Raquin and Moreira, 2009). However, since it is unclear whether the mantle $^{38}Ar/^{36}Ar$ signature is a source composition or contamination, this ratio cannot be used to shed light on the origins of primordial argon.

3.3.4 Mantle primordial Kr and Xe isotopes are chondritic

All six isotopes of Kr are effectively primordial in the mantle. The heavier isotopes can be produced by spontaneous fission, but the relevant branch ratios and fission yields are small, and the expected concentration of fissiogenic Kr would be very small compared to Kr concentrations in the mantle (Péron et al., 2021). However, a small correction for fissiogenic Kr must be made for gas samples affected by crustal contamination due to the high concentration of U in continental crust (Holland et al., 2009). Kr isotopes in continental CO_2 well gas from New Mexico (Holland et al., 2009), volcanic gas from Yellowstone (Broadley et al., 2020), and basalts from Iceland and Galápagos (Péron et al., 2021) indicate that accreted mantle Kr is chondritic in origin, and not solar or subsolar. In particular, the Galápagos and Yellowstone Kr data indicate a primordial Kr composition that is similar to that in average bulk carbonaceous chondrites, rather than to Kr in

pure Phase Q (Figure 5)[5]. Notably, Péron et al. (2021) pointed out that the mantle data exhibit a deficit in ^{86}Kr compared to AVCC, which they suggest is nucleosynthetic in origin. This ^{86}Kr deficit is consistent with deficits in neutron-rich isotopes of non-volatile elements in Earth's mantle compared to chondrites (e.g., Akram et al., 2015; Fischer-Gödde et al., 2020; Render et al., 2017), and suggests that there were nucleosynthetic heterogeneities among carbonaceous materials in the proto-planetary disk.

<Figure 5 near here>

The four primordial isotopes of Xe (^{124,126,128,130}Xe) are also the rarest isotopes of Xe, and their low abundances make precise measurement difficult in most samples. For both Kr and Xe, influx of atmospheric gas over time has affected the composition of the mantle source (Holland and Ballentine, 2006; Mukhopadhyay, 2012; Parai and Mukhopadhyay, 2015; Péron et al., 2021), and shallow atmospheric contamination affects the measured compositions, reducing the magnitude of the primordial isotopic signal. Because of this difficulty, early studies could not distinguish mantle primordial Xe isotope ratios from the atmospheric composition, and assumed the primordial mantle Xe composition was the same as the atmospheric composition (Allègre et al., 1983)[6]. Later studies measured samples with sufficient precision to resolve primordial Xe

[5] This is the first of several isotope ratio diagrams in the chapter. Note that for any isotope ratio diagram, if the denominator isotopes are the same for the ratios shown on the x-axis and y-axis, then mixing between compositions on the diagram generates linear arrays. If the denominator isotopes differ, then mixing generates hyperbolic arrays, where the curvature of the hyperbola reflects the contrast in elemental ratios (see Parai et al., 2019).

[6] These early studies erroneously adopted a framework in which primordial mantle gas was residual to outgassing that formed the atmosphere, and therefore resembled the early atmosphere. Current understanding is that Earth's atmosphere was not outgassed from the mantle, and that the original atmospheric primordial Xe isotopic composition was similar to impact degassing of a mix of ~80% chondritic material and ~20% cometary material (Marty et al., 2017; other chapters in this work). After accretion, Earth's atmospheric Xe experienced protracted mass-dependent isotopic fractionation to reach the present day composition ~2.4 Ga (Pujol et al., 2009; Avice et al., 2018; Ardoin et al., 2022).

isotopic excesses from atmosphere. Measurements of continental well gas showed that the mantle preserved primordial Xe isotope ratios distinct from air (Caffee et al., 1999). Very precise measurements of primordial Xe in well gases, oceanic basalts and volcanic gases indicate that primordial Xe in the mantle is similar to AVCC or Q, and is not solar or cometary Xe (Figure 6; (Broadley et al., 2020; Caffee et al., 1999; Caracausi et al., 2016; Holland and Ballentine, 2006; Holland et al., 2009; Péron and Moreira, 2018). A small cometary contribution cannot be ruled out, but due to the exceedingly low solar $^{130}Xe/^{22}Ne$ ratio compared to the mantle $^{130}Xe/^{22}Ne$ (Section 3.3.5), the solar contribution to mantle Xe must be negligible (Parai, 2022). Accordingly, the Kr and Xe delivered to Earth during accretion was similar in composition to gases trapped in carbonaceous chondrites.

<Figure 6 near here>

3.3.5 The bigger picture: Elemental abundance patterns and primordial isotope ratios

The story of volatile origins recorded in Earth's mantle primordial noble gas isotopes has developed in recent years due to improved analytical precision and luck in finding samples that meet two criteria: (1) ratios of radiogenic isotopes (*e.g.*, $^{4}He/^{21}Ne^{*}$, $^{4}He/^{40}Ar^{*}$; (Graham, 2002) are similar to mantle production ratios, meaning that elemental ratios have not been significantly altered by degassing; and (2) corrections for atmospheric contamination can be made to determine mantle source compositions. This has enabled comparison of mantle source primordial isotope ratios (including elemental ratios, like $^{36}Ar/^{22}Ne$) with potential sources of accreted volatiles.

<Figures 7 and 8 near here>

Figure 7 shows $^{20}Ne/^{22}Ne$ plotted against $^{36}Ar/^{22}Ne$ (Marty, 2012; Marty, 2022; Mukhopadhyay, 2012; Williams and Mukhopadhyay, 2019). Mantle source compositions

estimated for samples with unfractionated elemental ratios are available from the N. Atlantic popping rock 2ΠD43 (Moreira et al., 1998; Parai and Mukhopadhyay, 2021; Péron and Moreira, 2018), Iceland (Mukhopadhyay, 2012), Rochambeau Rift (Pető et al., 2013) and Galápagos (Péron and Mukhopadhyay, 2022; Péron et al., 2021). Solar nebular gas, trapped gas in carbonaceous chondrites, compositions from enstatite chondrites, solar wind irradiated material, Earth's atmosphere, and atmosphere-derived compositions are shown for comparison. Several important points are illustrated in this diagram. First, the origin of the atmosphere cannot be from mantle outgassing followed by mass-fractionating loss to space to explain the low $^{20}Ne/^{22}Ne$ (e.g., Sasaki and Nakazawa, 1988), as the resulting $^{36}Ar/^{22}Ne$ would be too low compared to the atmosphere (Marty, 2012). Instead, the atmospheric composition is consistent with delivery by chondrites, potentially with a small amount of outgassed mantle Ne and Ar (Marty, 2022). The plume source mantle composition is explained well by mixing solar nebular gas with gas trapped within chondritic materials and/or influxed atmospheric gas with an elevated $^{36}Ar/^{22}Ne$ (Trieloff et al., 2002; Williams and Mukhopadhyay, 2019). Mukhopadhyay (2012) pointed out that the MORB source has a higher $^{36}Ar/^{22}Ne$ and lower $^{20}Ne/^{22}Ne$ than the plume source, and argued that these distinct primordial isotope ratios were signatures from accretion. While the $^{20}Ne/^{22}Ne$ ratio of MORB source mantle is similar to Ne-B, solar wind irradiated material has a much lower $^{36}Ar/^{22}Ne$ than that of the MORB source (Marty, 2022). If MORB source Ne originates from solar wind irradiated material, there are two potential ways to explain a high mantle $^{36}Ar/^{22}Ne$ ratio: (1) influx of Ne-free, Ar-rich atmospheric gas into the MORB mantle, or (2) incorporation of the "subsolar" composition carried by enstatite chondrites (Ott, 2014). The first option can be ruled out based on Ne-Xe arguments given below (Parai, 2022), while the second option calls for a very fortuitous mixture of Ne-B and subsolar gas from enstatite chondrites, which seems unlikely (Marty, 2022).

The simpler explanation is that the MORB source mantle composition is also explained by mixing solar nebular gas with gas trapped within carbonaceous materials and/or influxed atmospheric gas, with a greater contribution from the non-solar components than is found in the plume source mantle (Williams and Mukhopadhyay, 2019).

A similar picture emerges when $^{20}Ne/^{22}Ne$ is plotted against $^{130}Xe/^{22}Ne$ (Figure 8), only here we have additional isotopic constraints on origins of mantle primordial Xe isotopes (Section 3.3.4). The same samples and components from Figure 7 are shown, and similar systematics are evident. The plume mantle source has a lower $^{130}Xe/^{22}Ne$ than the MORB source (Mukhopadhyay, 2012), and is consistent with mixing of solar nebular gas with gas trapped within chondritic materials and/or influxed atmospheric gas with elevated $^{130}Xe/^{22}Ne$ (Williams and Mukhopadhyay, 2019). If $^{20}Ne/^{22}Ne$ of ~12.6 in the MORB source reflected a Ne-B origin, the high $^{130}Xe/^{22}Ne$ ratio in the MORB source would require either: (1) influx of Ne-free, Xe-rich atmospheric gas into the mantle, or (2) incorporation of the "subsolar" composition carried by enstatite chondrites, which has moderately elevated $^{130}Xe/^{22}Ne$ (Ott, 2014). Mass balance considerations and primordial Xe isotopic excesses compared to atmosphere (Section 3.3.4) rule out both of these options. Parai (2022) showed that if atmospheric influx compensated for the low $^{130}Xe/^{22}Ne$ of either solar nebular gas or solar wind irradiated material (Ne-B), then >99% of ^{130}Xe in the MORB source mantle would have to be influxed atmospheric Xe, and the mantle source primordial isotopic ratios ($^{124}Xe/^{130}Xe$, $^{126}Xe/^{130}Xe$, $^{128}Xe/^{130}Xe$) would all be indistinguishable from atmosphere, which is not the case (Figure 6; Peron and Moreira, 2018; Broadley et al., 2022; Caffee et al., 1999; Holland and Ballentine, 2006). Likewise, "subsolar" gases carried by enstatite chondrites cannot have provided the excess Xe to the mantle during accretion, because primordial Xe isotope ratios are not consistent with the "subsolar" Xe isotopic composition, nor with a mixture

between subsolar and atmospheric Xe isotopes (Figure 6). Instead, the MORB source primordial noble gas composition is well-explained as mixture of the same components as the plume source mantle: solar nebular gas mixing with gas trapped within carbonaceous chondritic material and influxed atmospheric gas, with a greater contribution from the non-solar components in the MORB source. Notably, linear decomposition of the MORB source primordial Ne and Xe isotopic signature requires a greater proportion of Ne from chondrites (as well a greater influx of atmospheric Ne into the MORB source mantle; Section 5.1.4) compared to the plume source mantle, signifying that a more carbonaceous material delivered noble gases to the MORB source than the plume source during accretion (Parai, 2022).

4. MANTLE SIGNATURES OF OUTGASSING

Transfer of noble gases from the mantle to the atmosphere and incorporation of subducted slabs is recorded by noble gas isotopes in mantle sources. Signatures of mantle outgassing from accretion through to the present-day are discussed below. There are two dominant signatures in mantle sources: one signature of a reservoir that has experienced less outgassing throughout Earth history, and another of a reservoir that has experienced more outgassing. Neither signature calls for primordial reservoir (meaning a reservoir that has largely been unchanged since accretion) in the mantle or in the core. Topics are ordered first by type of signature (primordial isotopes vs. radiogenic isotopes) and then by time in Earth history.

4.1 Primordial isotope ratio variations generated by outgassing

Mantle source $^{3}He/^{22}Ne$ ratios vary among oceanic basalts: low ratios are determined for plume-influenced locations, and higher ratios are computed for MORB sources. Mantle source

$^{3}He/^{22}Ne$ ratios are estimated by correcting for atmospheric contamination in samples with unfractionated elemental ratios (i.e., $^{4}He^{*}/^{21}Ne^{*}$ near the production ratio; Yatsevich and Honda, 1997), but can also be constrained by correcting for atmospheric contamination and making a correction for elemental fractionation due to magmatic degassing (Graham, 2002; Honda and McDougall, 1998; Tucker and Mukhopadhyay, 2014). Unlike the primordial isotope ratios discussed in Section 3.3, $^{3}He/^{22}Ne$ varies among mantle sources in a way that cannot be explained by two-component mixing between solar nebular gas and chondritic gases, and requires some other explanation. Generally, plume mantle sources are found to have lower $^{3}He/^{22}Ne$ ratios than MORB sources (Dygert et al., 2018; Graham, 2002; Honda and McDougall, 1998; Tucker and Mukhopadhyay, 2014). Horton et al. (2021; 2023) calculated a relatively high source $^{3}He/^{22}Ne$ ratio of ~7.5 to 10 for plume-related samples from Baffin Island with extremely low $^{4}He/^{3}He$ (high $^{3}He/^{4}He$). This result is anomalous in the context of He-Ne systematics among global oceanic basalts (Graham, 2002; Moreira, 2013; discussed in Section 4.2 and 4.3). Figure 9 shows $^{3}He/^{22}Ne$ data plotted against $^{20}Ne/^{22}Ne$ in samples with elemental ratios that are not strongly fractionated.

<Figure 9 near here>

Both plume and MORB $^{3}He/^{22}Ne$ ratios are higher than the solar nebular (1.4) and chondritic (0.89) ratios (Table 3), signifying that both mantle sources have seen some process that altered their $^{3}He/^{22}Ne$. Equilibration of gas between a magma ocean and the atmosphere above it fractionates noble gas elemental ratios in the magma based on solubility (Honda and McDougall, 1998; Jambon et al., 1986; Lux, 1987). Given the higher solubility of He in magma, it was suggested that nebular ingassing in a magma ocean explains the elevated $^{3}He/^{22}Ne$ in plumes compared to solar nebula (Honda and McDougall, 1998; Tucker and Mukhopadhyay, 2014), and that the MORB source $^{3}He/^{22}Ne$ originated from nebular ingassing followed by multiple magma

ocean events, where outgassing during each successive event raised $^{3}He/^{22}Ne$ in the residual magma ocean by a factor of ~2 based on the solubility contrast (Tucker and Mukhopadhyay, 2014). The elemental ratios of heavier noble gases (e.g., $^{36}Ar/^{22}Ne$, $^{130}Xe/^{22}Ne$) do not appear to have been significantly impacted by magma ocean outgassing. Parai (2022) argued that estimated ^{130}Xe concentrations in the mantle at the end of accretion were too high for the last magma ocean to have experienced equilibrium degassing given the low solubility of Xe compared to other volatiles like H_2O. One possibility is that the heavy noble gas ratios were less affected by magma ocean outgassing than $^{3}He/^{22}Ne$ because the heavier noble gases were not effectively degassed due to kinetic effects in the magma ocean.

An alternative explanation for mantle $^{3}He/^{22}Ne$ variations was suggested based on the difference in diffusivities for He and Ne (Dygert et al., 2018). In this scenario, He diffused preferentially out of channels of basaltic melt and into the surrounding mantle, generating slabs with high $^{3}He/^{22}Ne$. Incorporation of subducted slabs over time would thus generate the high $^{3}He/^{22}Ne$ in plume and MORB sources, and the higher $^{3}He/^{22}Ne$ in the MORB source mantle would reflect a greater contribution from subducted slabs (Dygert et al., 2018). In this case, mantle $^{3}He/^{22}Ne$ variations would not originate from early outgassing but rather from long-term mantle processing (Section 4.2.2).

4.2 Radiogenic isotope variations generated by outgassing

A standout feature of the noble gas family of elements is the variety of nuclear reactions that have produced specific noble gas isotopes in the mantle over time (Table 1). When a partial melt of the mantle is formed, all relevant radioactive parent isotopes (^{238}U, ^{235}U, ^{232}Th, ^{40}K, ^{244}Pu, and ^{129}I; Figure 1) are retained within the melt, while the noble gases are lost by outgassing to the

atmosphere or ocean. This loss of gas raises the parent-daughter ratio in the melt, and as long as the parent radioactive isotope is not yet extinct, the high parent-daughter ratio will translate over time into a high ratio of the radiogenic isotope compared to a primordial isotope of the same noble gas element. For example, outgassing generates a high (U+Th)/^{3}He ratio, which translates to a high ^{4}He/^{3}He ratio over time. Likewise, outgassing that occurs during the lifetime of the short-lived isotope ^{129}I generates a high ^{129}I/^{130}Xe ratio, which translates to a high ^{129}Xe/^{130}Xe ratio as the ^{129}I decays.

4.2.1 Early outgassing: I-Xe and Pu-Xe

4.2.1.1 I-Xe signatures

The short-lived ^{129}I-^{129}Xe system has recorded outgassing that occurred during accretion and the earliest part of Earth's history. Radiogenic ^{129}Xe was produced by β-decay of the now-extinct radioactive isotope ^{129}I ($t_{1/2}$ = 16.1 Myr; Table 1) in the first ~100 Myr of Earth history. The mantle exhibits high ^{129}Xe/^{130}Xe compared to the atmosphere (which has ^{129}Xe/^{130}Xe of 6.496; Porcelli et al., 2002) and potential sources of noble gases during accretion, indicating that Earth's interior had a comparatively high I/Xe ratio during the lifetime of ^{129}I. This high I/Xe ratio could reflect early outgassing (loss of Xe, potentially from outgassing of a magma ocean) and/or an enrichment in iodine in the mantle compared to the materials that delivered Xe to Earth's atmosphere.

Butler et al. (1963) measured Xe in CO_2 well gas and reported the first excess in ^{129}Xe compared to the atmospheric Xe composition. In light of evidence that the observed ^{129}Xe excess originated from decay of ^{129}I very early in Earth history, Butler et al. argued that the interior of the Earth was never completely outgassed or homogenized with the atmospheric Xe reservoir. Clarke

et al. (1969) reached the same conclusion about incomplete outgassing of the interior later in the same decade based on measurements of ^{3}He in seawater (Section 3). High $^{129}Xe/^{130}Xe$ ratios were subsequently measured in additional well gas samples (Boulos and Manuel, 1971; Phinney et al., 1978; Wasserburg and Mazor, 1965) and volcanic rock samples (Allègre et al., 1983; Hiyagon et al., 1992; Kaneoka and Takaoka, 1978, 1980; Marty, 1989; Poreda and Farley, 1992; Staudacher and Allegre, 1982; Trieloff et al., 2002; Trieloff et al., 2000). High precision Xe isotopic measurements showing mantle $^{129}Xe/^{130}Xe$ excesses are now available from basalts (Kunz et al., 1998; Moreira et al., 1998; Mukhopadhyay, 2012; Parai, 2023; Parai and Mukhopadhyay, 2015; Parai et al., 2012; Péron and Moreira, 2018; Péron et al., 2021; Pető et al., 2013; Tucker et al., 2012), spring and well gases (Bekaert et al., 2019; Caffee et al., 1999; Caracausi et al., 2016; Holland and Ballentine, 2006; Holland et al., 2009; Moreira et al., 2018), and volcanic hydrothermal gases (Bekaert et al., 2023; Broadley et al., 2020).

While mantle $^{129}Xe/^{130}Xe$ ratios are elevated compared to atmosphere for both plume and MORB sources, lower $^{129}Xe/^{130}Xe$ ratios have been shown to be characteristic of plume mantle sources compared to MORB mantle sources, and indicate that an early-formed radiogenic ^{129}Xe heterogeneity persists in the mantle today (Mukhopadhyay, 2012; Parai et al., 2012; Pető et al., 2013; Tucker et al., 2012). In early studies, based on the very small $^{129}Xe/^{130}Xe$ excesses measured in plume samples from Hawaii (Kaneoka and Takaoka, 1978, 1980; Staudacher and Allegre, 1982) compared to MORBs, Allègre et al. (1983) argued that the Hawaiian $^{129}Xe/^{130}Xe$ data represented sampling of an undegassed mantle reservoir. However, the conceptual framework underlying this interpretation was that the initial mantle Xe (and Ne and Ar) isotopic composition resembled the atmospheric composition, which has since been shown to be incorrect (Caffee et al., 1999; Holland and Ballentine, 2006; Péron and Moreira, 2018). Larger $^{129}Xe/^{130}Xe$ excesses were later measured

in Samoan xenoliths (Poreda and Farley, 1992), Loihi dunites (Trieloff et al., 2000), and Reunion xenoliths (Trieloff et al., 2002), but the highest of these was still lower than the maximum $^{129}Xe/^{130}Xe$ measured in MORBs. Three possible explanations were at hand: (1) plume samples were affected by a greater degree of syn- to post-eruptive atmospheric contamination (e.g., Ballentine and Barfod, 2000; Fisher, 1985; Patterson et al., 1990; Patterson et al., 1991); (2) plume source $^{129}Xe/^{130}Xe$ ratios were low due to preferential injection of atmospheric Xe into the plume mantle source (e.g., Holland and Ballentine, 2006; Sarda, 2004) (Section 5); or (3) the plume mantle had a lower I/Xe ratio than the MORB mantle during the lifetime of ^{129}I.

<Figure 10 near here>

High precision data generated by step crushing have enabled key advances in our understanding of mantle $^{129}Xe/^{130}Xe$ heterogeneity. Moreira et al. (1998) was the first study that was able to correct for syn- to post-eruptive atmospheric contamination[7] using Ne-Xe mixing systematics elucidated by step-crushing (Figure 10) of the very gas-rich North Atlantic MORB sample 2ΠD43 (a famous sample in mantle noble gas geochemistry, often called "the popping rock"). Mukhopadhyay (2012) measured noble gases in a subglacial basalt glass from Iceland and used Ne-Xe and Ar-Xe systematics to correct for syn- to post-eruptive atmospheric contamination, and showed that the Iceland mantle source had a low $^{129}Xe/^{130}Xe$ (~7) compared to the N. Atlantic MORB source (7.6; Moreira et al., 1998). By plotting step-released $^{129}Xe/^{130}Xe$ data against $^{3}He/^{130}Xe$ in two samples with unfractionated noble gas elemental ratios, Mukhopadhyay (2012) showed that these data formed distinct arrays radiating out from the atmospheric composition, and

[7] see Parai et al. (2019) for a detailed explanation of this correction for syn- to post-eruptive atmospheric contamination

that preferential incorporation of influxed atmospheric Xe (Holland and Ballentine, 2006) could not therefore account for the low mantle source $^{129}Xe/^{130}Xe$ at Iceland (Figure 11). Rather, the low $^{129}Xe/^{130}Xe$ in the Iceland mantle source indicated that early-formed $^{129}Xe/^{130}Xe$ heterogeneities in the mantle, which formed during the lifetime of ^{129}I, survived in the mantle today and had not been mixed away by ~4.45 Gyr of mantle convection (Mukhopadhyay, 2012). Additional high precision data generated by step-crushing of basalt from the Equatorial Atlantic (Tucker et al., 2012), Southwest Indian Ridge (Parai et al., 2012), N. Atlantic Ridge (Parai and Mukhopadhyay, 2021), and Rochambeau Rift (which samples the Samoan plume-influenced northern Lau Basin mantle; Pető et al., 2013) have yielded corrected mantle source $^{129}Xe/^{130}Xe$ estimates (Figure 11) that provide further support for early-formed mantle source $^{129}Xe/^{130}Xe$ heterogeneity.

<Figures 11 and 12 near here>

Analytical advances have enabled distinction of mantle primordial isotope ratios (e.g., $^{128}Xe/^{130}Xe$) from the atmospheric ratio in a wider array of samples in recent years. Plotting $^{129}Xe/^{130}Xe$ against $^{128}Xe/^{130}Xe$ provides additional support for ancient I/Xe heterogeneity as the origin of low $^{129}Xe/^{130}Xe$ in plume mantle sources compared to MORB mantle sources (Figure 12; Bekaert et al., 2023; Broadley et al., 2020; Caffee et al., 1999; Parai, 2023; Péron and Moreira, 2018; Péron et al., 2021). On this diagram, it is not necessary to have determined mantle source compositions corrected for syn- to post-eruptive atmospheric contamination: mixing is linear in this space, and the observation that plume data lie on a distinct slope compared to well gases and MORB is sufficient to show that early-formed $^{129}Xe/^{130}Xe$ heterogeneities persist.

Lower $^{129}Xe/^{130}Xe$ ratios indicate that plume mantle sources had low I/Xe during the lifetime of ^{129}I. This could either reflect less degassing of the plume mantle during the first 100 Myr, or indicate that the plume mantle acquired or retained less iodine than the MORB mantle

during accretion (discussed below in Section 4.2.1.3). Critically, the distinct slopes for MORB and plume data when $^{129}Xe/^{130}Xe$ is plotted against ratios of primordial isotopes ($^{3}He/^{130}Xe$, $^{128}Xe/^{130}Xe$) rule out models where the plume source supplies gas to the MORB source over time (Kellogg and Wasserburg, 1990; Porcelli and Wasserburg, 1995a; Porcelli and Wasserburg, 1995b) or a hidden reservoir such as the core supplies gas to both plume and MORB sources (e.g., Olson and Sharp, 2022).

4.2.1.2 Pu-Xe signatures

Spontaneous fission of ^{244}Pu (with a half-life of 80.0 Myr; Table 1) produced ^{131}Xe, ^{132}Xe, ^{134}Xe and ^{136}Xe during the first several hundred million years of Earth history. The same four isotopes of Xe are also produced by spontaneous fission of ^{238}U, but the fission yields differ, such that Pu-fission Xe has an isotopic composition that is distinct from U-fission Xe (Figure 13). Among early studies, Boulos and Manuel (1971) measured well gases from the Bueyeros field believed to carry mantle-derived gas and resolved fission Xe isotope excesses relative to air. The authors noted that their average compositions were consistent with a ~1:3 mixture of Pu-fission Xe and U-fission Xe, but could not rule out either a pure Pu-fission or pure U-fission origin due to the large uncertainties in the measurements. Distinguishing a signature of Pu-fission Xe in mantle Xe requires high precision measurements, and preferably an estimate of the mantle source composition corrected for syn- to post-eruptive atmospheric contamination. This section focuses on recent measurements made with sufficient precision to identify Pu-fission signatures.

<Figure 13 near here>

Kunz et al. (1998) reported precise Xe isotopic measurements of the N. Atlantic popping rock. The authors used a now-outdated “non-radiogenic air” composition for the initial mantle Xe

composition, and in comparing the data to mixing lines between their initial composition and Pu-fission or U-fission Xe in multiple Xe isotope ratio plots, estimated ~30% of the total fissiogenic ^{136}Xe was from Pu-fission (expressed as $^{136}Xe_{Pu}/^{136}Xe_{TF} = 0.3$, where $^{136}Xe_{TF} = ^{136}Xe_{Pu}+^{136}Xe_{U}$).

Caffee et al. (1999) reported high precision Xe isotopic data in well gases from continental CO_2 well gases from Colorado, New Mexico and South Australia, including precise primordial Xe isotope ratios that showed the initial mantle Xe composition was not the same as the atmosphere. This paper laid out a mathematical approach to determine the proportions of Xe from different sources with distinct isotopic compositions that mixed to generate the mantle Xe signature today. Variably described as a "decomposition" or "deconvolution," this linear least squares approach leverages the great number of Xe isotopes to shed light on many different aspects of the Xe isotope signature.

An explanation of the approach is given here. For studies with high precision Xe isotopic data, the mantle source (extrapolated) $^{129}Xe/^{132}Xe_E$ is determined using Ne-Xe or Ar-Xe mixing systematics, and linear correlations among Xe isotope ratios are used to compute the mantle source composition for other Xe isotope ratios (Mukhopadhyay and Parai, 2019; Parai and Mukhopadhyay, 2015; Parai et al., 2019). The $^{131,132,134,136}Xe$ budgets of mantle sources can be modeled as a mixture of four components: (1) initial Xe retained from accretion, likely chondritic in composition (Section 3.3); (2) atmospheric Xe influxed and incorporated into the mantle; (3) Pu-fission Xe produced within the first several hundred Myr of Earth history and retained in the mantle; and (4) U-fission Xe retained in the mantle. ^{244}Pu and ^{238}U each produce fissiogenic $^{131,132,134,136}Xe$ in characteristic proportions that are distinct from the $^{131,132,134,136}Xe$ composition of Earth's atmosphere, of primitive materials such as carbonaceous chondrites, and of each other. The mantle budget of any primordial Xe isotope (*e.g.*, ^{130}Xe) is a mixture of initial Xe and influxed

atmospheric Xe. Therefore, the Xe isotopic composition of the mantle source today may be described by a system of linear mixing equations of the form:

$$x_{init}\left(\frac{^{\zeta}Xe}{^{132}Xe}\right)_{init} + x_{atm}\left(\frac{^{\zeta}Xe}{^{132}Xe}\right)_{atm} + x_{Pu}\left(\frac{^{\zeta}Xe}{^{132}Xe}\right)_{Pu} + x_{U}\left(\frac{^{\zeta}Xe}{^{132}Xe}\right)_{U} = \left(\frac{^{\zeta}Xe}{^{132}Xe}\right)_{mantle} \quad \text{Eq. 1}$$

where $\zeta = {}^{130}$Xe, ^{131}Xe, ^{134}Xe and ^{136}Xe (the other primordial Xe isotopes are also included in some studies with high precision data); x is the molar mixing proportion of ^{132}Xe; *init* designates the initial mantle composition (assumed to be average carbonaceous chondrite; AVCC); *atm* designates influxed atmospheric Xe; *Pu* designates Pu-fission Xe; and *U* designates U-fission Xe. For primordial isotopes, the $^{\zeta}$Xe/^{132}Xe ratios of the Pu-fission and U-fission components are zero.

The least squares solution for A**x** = **b** (where A is a matrix of mixing endmember isotope ratios given in Table 4, **b** is a vector of mantle source isotope ratios, and **x** is a vector of ^{132}Xe mixing proportions) is determined, subject to the constraints that all values within the vector x are between 0 and 1 and the mixing proportions sum to 1:

$$x_{init} + x_{atm} + x_{Pu} + x_{U} = 1 \quad \text{Eq. 2}$$

The mathematical approach put forth by Caffee et al. (1999) enables determination of the fraction of a given Xe isotope (*e.g.*, ^{136}Xe) from Pu fission, U-fission, accretion ("initial"), or atmospheric influx. The Pu-derived $^{136}Xe_{Pu}$ is particularly powerful when interpreted in conjunction with other radiogenic isotope fractions: radiogenic ^{129}Xe* (below) and $^{136}Xe_{U}$ (Section 4.2.2).

4.2.1.3 I-Pu-Xe systematics

Wetherill (1975) formulated an expression for the I-Pu-Xe "closure age" of the Earth, which dates the end of accretion assuming quantitative, open system degassing of Xe from the

growing silicate Earth until accretion is complete, and closed system complete retention of Xe thereafter. ^{129}I decays away over the first ~100 Myr of Earth history, while ^{244}Pu continues to decay for several hundred million years (Figure 1). If the products of I- and Pu-decay are totally outgassed prior to closure, and completely retained after closure, then the ratio of radiogenic ^{129}Xe (^{129}Xe*) to Pu-fission ^{136}Xe is a function of the closure age and the I/Pu ratio.

Using the linear least squares approach outlined above to analyze mantle source compositions corrected for syn- to post-eruptive atmospheric contamination, ratios of ^{129}I-produced ^{129}Xe* to $^{136}Xe_{Pu}$ were determined for plume and MORB sources (Mukhopadhyay, 2012; Tucker et al., 2012; Pető et al., 2013; Parai and Mukhopadhyay, 2015; 2021). $^{129}Xe^*/^{136}Xe_{Pu}$ were found to be low in plume mantle sources compared to MORB source mantle sources (Figure 14). If I/Pu ratios were homogeneous throughout the mantle during accretion, then low $^{129}Xe^*/^{136}Xe_{Pu}$ ratios in the plume mantle would mean that open system outgassing of the MORB source mantle ceased, and then a significant time interval elapsed before the plume source closed to catastrophic volatile loss (Mukhopadhyay, 2012). If plumes sample a deep portion of the mantle, this is a physically puzzling result. Another potential explanation is that I/Pu ratios were distinct in the ancient plume and MORB sources, with low I/Pu in the ancient plume source mantle. Low I/Pu could either indicate that the plume source mantle accreted volatile-poor (Morbidelli et al., 2012; Parai, 2022; Schönbächler et al., 2010), or that iodine partitioned into the core at high pressures (Armytage et al., 2013; Jackson et al., 2018).

<Figure 14 near here>

4.2.2 Long-term outgassing (He, Ne, Ar and Xe isotopes)

Outgassing in association with mantle processing (partial melting of the mantle) has generated very large noble gas isotopic variations among mantle reservoirs. When trying to parse signatures of long-term outgassing in mantle sources, it is vital to understand that the outgassing of a specific melt at a volcanically active region is *not a process that directly imparts a signature upon the mantle reservoir from which the melt formed*. Cartoons depicting an outflux of mantle gas from the MORB source or plume source to the atmosphere are simplified depictions of net gas transport (Figure 15). When a melt is outgassed at the surface, the atmosphere receives the gas and the signature of outgassing is carried *within the melt* – it is not imparted to any deep mantle reservoir at all at the time of outgassing. It is imparted to a mantle reservoir when the lithosphere carrying the outgassed parcel (*e.g.*, an oceanic slab) is subducted and mixed into a mantle reservoir (Gonnermann and Mukhopadhyay, 2009). In this way, signatures of outgassing and atmospheric influx into the deep mantle (Section 5) are both mediated by incorporation of subducted slabs into the mantle.

It is helpful to conceptualize a simplified "box-model" to understand how mass transfer and gas transport are related at any given instant in time (Figure 15). When new partial melt is formed at a mid-ocean ridge, the mass of the melt and depleted lithospheric mantle is transferred from the MORB source reservoir to the lithosphere, and outgassing of the melt generates low gas concentrations and high parent-daughter ratios in the lithosphere. It can be assumed that the depleted residue of melting stays with the crust it generated and becomes lithospheric mantle as it cools. For the total mass of new lithosphere generated at ridges globally over a given period of time, an equal amount of mass is transferred from the lithosphere reservoir into the mantle at subduction zones globally. If that equal amount of subducted lithosphere mass is all mixed into

the MORB source mantle, then the size of the MORB source mantle reservoir does not change in this time period. In net, MORB source mantle material with some concentration of mantle noble gases is replaced with an equal amount of material that has been stripped of most of its mantle noble gases (and that potentially carries some atmospheric noble gases; Section 5). In this way, the concentration of mantle gas in mantle material is continuously diluted by incorporation of subducted slabs. We still broadly call this process outgassing, because in net, gas is transported from a mantle reservoir to the atmosphere, but technically a mantle reservoir that never gives rise to partial melts at all could attain an outgassed isotopic signature purely through incorporation of subducted slabs generated from melting of another reservoir. The term "processing" may be preferable and is used here — a less processed mantle has incorporated less material that was outgassed at the surface. This conceptual framework underpins a suite of recent numerical models of mantle noble gas isotopic evolution[8] (Gonnermann and Mukhopadhyay, 2009; Parai, 2022; Parai and Mukhopadhyay, 2018; Zhang et al., 2023).

<Figure 15 near here>

4.2.2.1 Radiogenic helium isotope signatures

Helium isotopic ratio variations among mantle samples have long been used to study mantle outgassing, and in particular, have been used to trace the influence of mantle plumes with distinctly low $^4He/^3He$ ratios (high $^3He/^4He$). The first studies reporting ^3He excesses in volcanic

[8] Note that neither the role of mantle metasomatism as a transport mechanism for noble gases and other fluid-mobile elements among deep Earth reservoirs (e.g., Vollmer, 1983), nor the role of the sub-continental lithospheric mantle as a deep Earth geochemical reservoir (Broadley et al., 2016; Dunai and Porcelli, 2002; Gautheron and Moreira, 2002), are captured in this simplified modeling framework. Future work should expand the framework to include these.

gases and rocks (Lupton and Craig, 1975; Tolstikhin et al., 1974 and references therein) argued that ^{3}He excesses indicated retention of gas from Earth's accretion. These were followed by numerous studies that confirmed high $^{3}He/^{4}He$ in the mantle compared to the atmosphere and characterized $^{3}He/^{4}He$ variations among different geographical locations (Condomines et al., 1983; Craig and Lupton, 1976; Graham et al., 1993; Graham et al., 1992a; Graham et al., 1992b; Kaneoka and Takaoka, 1978; Kaneoka et al., 1983; Kurz and Jenkins, 1981; Kurz et al., 1982a; Kurz et al., 1983; Kurz et al., 1982b; Kyser and Rison, 1982; Porcelli et al., 1986; Porcelli et al., 1987; Poreda et al., 1986; Rison and Craig, 1983).

Figure 16 shows the distribution of helium isotope ratios from MORBs and ocean island basalts compiled by Moreira (2013). OIBs exhibit a wider range of $^{4}He/^{3}He$ ratios than MORBs. The use of $^{4}He/^{3}He$ ratios has the advantage of consistency with other radiogenic isotope systems (including the other noble gases). Note that when $^{3}He/^{4}He$ ratios normalized to the atmospheric ratio (Ra) are considered, the mathematical transformation gives the erroneous impression that the majority of MORBs fall in a very narrow range (7-9 Ra) towards the more-outgassed end of the whole mantle spectrum (~4 to 63 Ra). Plotting the distribution of mantle $^{4}He/^{3}He$ ratios makes clear that the MORB $^{4}He/^{3}He$ ratios fall squarely in the middle of the whole mantle range: MORBs typically have $^{4}He/^{3}He$ between ~80,000 and 100,000, while the whole mantle varies from ~10,000 to 170,000 (Graham et al., 1992a; Horton et al., 2023). The peak for plume $^{4}He/^{3}He$ values falls to the low side of the MORB range. It is difficult to tell how much of the skew in the plume histogram stems from over-representation of samples from a handful of interesting plume locations that have been extensively studied (Iceland, Hawaii, Samoa, Galápagos, and continental hotspots like Yellowstone), which heavily populate the lower end of the plume mantle $^{4}He/^{3}He$ range, but it is

likely that the average plume source $^4He/^3He$ composition weighted by erupted volume is low compared to the MORBs.

<Figure 16 near here>

The origin of helium isotopic variations among mantle samples is generally attributed to differential outgassing of mantle sources. Both ^3He and ^4He are lost by outgassing, but only ^4He is generated in the mantle over time by decay of U and Th, such that outgassing generates high $^4He/^3He$ ratios in mantle reservoirs over time. A mantle reservoir that has preserved low $^4He/^3He$ (high $^3He/^4He$) has retained a greater proportion of its He from accretion, such that production of ^4He through radioactive decay has a smaller impact on the overall helium budget and therefore does not raise the $^4He/^3He$ as significantly as an outgassed reservoir.

While it is well-accepted that helium is incompatible during partial melting, conflicting experimental results were reported regarding whether helium is more incompatible than U and Th (Heber et al., 2007; Jackson et al., 2013a; Parman et al., 2005). It was suggested that if U and Th were more incompatible than He, then depleted residues of partial melting might be the carriers of low $^4He/^3He$ ratios (Parman et al., 2005), though these residues would have such low He concentrations that their He isotopic signatures would be easily swamped out (Porcelli and Elliott, 2008). This debate is reviewed by Hilton and Porcelli (2014) and discussed by Moreira (2013). A subsequent study of a global set of undegassed (CO_2 and H_2O undersaturated) MORBs demonstrated that helium is more incompatible than U and Th during melting that produces basalts in nature, indicating that depleted residues do not carry low $^4He/^3He$ ratios (Graham et al., 2016).

Regardless of how helium isotopic variations originate, the consistent observation is that the lowest $^4He/^3He$ ratios are found at ocean islands and other localities associated with mantle

plumes. Accordingly, low $^{4}He/^{3}He$ signatures are sought as a metric of plume influence where other metrics are ambiguous.

On the other end of the spectrum, the highest $^{4}He/^{3}He$ ratios are typically found at HIMU (high u, where u = $^{238}U/^{204}Pb$) localities with very radiogenic $^{206}Pb/^{204}Pb$ signatures[9]. The elevated $^{206}Pb/^{204}Pb$ ratios are generally attributed to the presence of recycled oceanic crust in the HIMU mantle source (Chauvel et al., 1992; Christensen and Hofmann, 1994). HIMU $^{4}He/^{3}He$ ratios range from ~100,000 to ~170,000 (e.g., Barfod et al., 1999; Class et al., 2005; Day, 2022; Day and Hilton, 2011; Graham et al., 1992a; Hanyu and Kaneoka, 1997; Hanyu et al., 1999; Hanyu et al., 2014; Hanyu et al., 2011; Hilton et al., 2000; Parai et al., 2009; Sandoval-Velasquez et al., 2023). Radiogenic helium isotopic signatures at HIMU localities are consistent with incorporation of ancient recycled slabs with high $(U+Th)/^{3}He$ into the mantle source, though the helium isotopes are less extreme than expected for pure ancient recycled crust. Completely-outgassed crust would develop a $^{4}He/^{3}He$ ratio > 10^{7} over Gyr timescales (Day and Hilton, 2011; Hanyu and Kaneoka, 1997; Parai et al., 2009). Possible explanations include diffusive exchange between the crust and ambient mantle (Hanyu and Kaneoka, 1998), closed system aging of trapped melts (Barfod et al., 1999) or the oceanic lithosphere (Moreira and Kurz, 2001), and mixing of ancient dehydrated recycled material with at least one other reservoir in the mantle with a lower $^{4}He/^{3}He$ than what is observed, which could be either the MORB source mantle or a less-degassed plume source (Hilton et al., 2000). Ne isotopes provide an additional dimension that points to mixing with a less-degassed plume source in the HIMU mantle source (Parai et al., 2009; Sandoval-Velasquez et al.,

[9] See Sturm et al. (1999) for discussion of the very highest mantle-derived $^{4}He/^{3}He$ (~200,000) in samples from the Chile Ridge that are not strictly associated with the HIMU mantle component found at ocean islands. The radiogenic He is associated with moderately radiogenic Pb, and is likely due to recycled material in the source.

2023; see below; Zhang et al., 2024), demonstrating that mantle helium isotopes provide only a partial picture of long-term volatile transport, and the full suite of noble gases should be leveraged when possible.

4.2.2.2 Nucleogenic neon isotope signatures

Outgassing generates high $^{21}Ne/^{22}Ne$ ratios ("nucleogenic Ne") in mantle reservoirs, as all isotopes of neon are lost but only ^{21}Ne is produced in significant quantities in the mantle[10] (Yatsevich and Honda, 1997). Neon isotopes in mantle samples can be strongly overprinted by atmospheric contamination during or after eruption (see Section 2.6 for discussion of atmospheric contamination and Section 3.3.2 for discussion of the origins of the distinct composition of Ne in the atmosphere). In order to interpret signatures of long-term outgassing in mantle sources, measured compositions must be corrected for syn- to post-eruptive atmospheric contamination to determine mantle source compositions (Figure 17). The corrections are typically made by determining a line of best fit for data in $^{20}Ne/^{22}Ne$ *vs.* $^{21}Ne/^{22}Ne$ space (Honda et al., 1993), preferably using multiple data points from the same sample generated by step release of gas and adopting an orthogonal least squares method accounting for correlated errors in these isotope ratios (York, 1969; York et al., 2004). The line of best fit is extrapolated to a model mantle source $^{20}Ne/^{22}Ne$ composition (Section 3.3.2), representing magmatic Ne free of syn- to post-eruptive atmospheric contamination, to determine the mantle source $^{21}Ne/^{22}Ne$ (Figure 17). These mantle source compositions are sometimes also referred to as "extrapolated" ratios ($^{21}Ne/^{22}Ne_E$).

[10] Note that in the continental crust, production of ^{22}Ne via nuclear reactions with fluorine is also significant (Yatsevich and Honda, 1997)

The modern understanding of mantle Ne isotope systematics emerged relatively recently. While Ne isotopic excesses compared to atmosphere were reported by some early studies, consensus was hampered by poor precision, atmospheric contamination and isobaric interferences within the mass spectrometer (e.g., Craig and Lupton, 1976; Ozima and Zashu, 1983; Poreda and Radicati di Brozolo, 1984). Improved analytical capabilities enabled resolution of mantle Ne from the atmospheric composition, in both MORB and plume-influenced samples (Farley and Poreda, 1993; Hiyagon et al., 1992; Honda et al., 1991; Marty, 1989; Sarda et al., 1988). Once non-atmospheric Ne signatures were resolved, correlated excesses in $^{20}Ne/^{22}Ne$ and $^{21}Ne/^{22}Ne$ emerged, and systematic variations in the slope of these correlations between MORBs and OIBs became apparent. In oceanic basalts, these correlated excesses generally reflect mixing between the mantle source Ne composition and atmospheric contamination (Figure 17).

<Figures 17 and 18 near here>

Figure 18 shows Ne isotopic systematics among a selection of plume and MORB studies. Plume source $^{21}Ne/^{22}Ne_E$ ratios vary across a wide range, but most plume $^{21}Ne/^{22}Ne_E$ ratios are lower than MORB mantle source $^{21}Ne/^{22}Ne_E$ ratios (Graham, 2002; Moreira, 2013). The steepest slopes radiating out from atmosphere are found in samples from Galápagos (Kurz et al., 2009; Péron et al., 2016; Péron et al., 2021; Raquin and Moreira, 2009); fitting a line to the data of Péron et al. (2021) and extrapolating to a solar nebular $^{20}Ne/^{22}Ne$ yields a $^{21}Ne/^{22}Ne_E$ of 0.0349 ± 0.0006, a modest excess compared to solar nebular $^{21}Ne/^{22}Ne$ (~0.0324; Williams and Mukhopadhyay, 2019). The $^{21}Ne/^{22}Ne_E$ determined for N. Atlantic MORB 2ΠD43 is 0.0590 ± 0.0002 at a $^{20}Ne/^{22}Ne$ at 12.6 (Parai and Mukhopadhyay, 2021; see Section 3.3 for explanation of distinct mantle source $^{20}Ne/^{22}Ne$ values). Low $^{21}Ne/^{22}Ne_E$ in plume mantle sources indicates a lower extent of mantle outgassing compared to MORB sources.

Global compilations of Ne isotopic data show continuous variation in slopes radiating out from atmosphere in the Ne three-isotope diagram (Graham, 2002; Moreira, 2013). Interestingly, this continuous spectrum of $^{21}Ne/^{22}Ne_E$ does not seem to reflect a continuum of different extents of mantle outgassing of an otherwise homogeneous reservoir. Instead, much of the variability seems to reflect two-component mixing between a less-outgassed mantle reservoir and the MORB source, with each having distinct long-term ("time-integrated") $^{3}He/^{22}Ne$ ratios. Figure 19 shows $^{21}Ne/^{22}Ne_E$ plotted against $^{4}He/^{3}He$ from Moreira (2013). The denominator isotopes are different for the two axes, so two-component mixing in this space is hyperbolic and depends on the contrast in $^{3}He/^{22}Ne$ between the mixing components. Mixing between two components that have identical $^{3}He/^{22}Ne$ would generate a special case of the hyperbola: a line. The larger the contrast in endmember $^{3}He/^{22}Ne$ ratios, the stronger the curvature of the mixing hyperbola. The curvature evident in this compilation indicates that the more-outgassed component with high $^{4}He/^{3}He$ and high $^{21}Ne/^{22}Ne_E$ (MORB source) has a high $^{3}He/^{22}Ne$ ratio compared to the less-outgassed component (plume source). This shows consistency with the high source $^{3}He/^{22}Ne$ ratios computed for MORB mantle sources compared to plumes (Section 4.1). These He-Ne systematics and implications for two distinct reservoirs in the mantle are discussed in detail by Moreira (2013). A few exceptions are noted: (a) samples from Loihi, Baffin Island and Rochambeau Rift seem to call for a weaker curvature (or even the opposite curvature), signifying a similar (or even a higher) $^{3}He/^{22}Ne$ in the plume mantle component compared to the MORB component (Fig. 19; Graham, 2002 and references therein; Horton et al., 2021); and (b) $^{21}Ne/^{22}Ne_E$ in HIMU OIBs may reflect mixing between the plume component and recycled material rather than the MORB mantle (see below). It is interesting that, due to the contrast in mantle source $^{3}He/^{22}Ne$ ratios, addition of a

small amount of plume mantle strongly affects Ne isotopes without significantly affecting He isotopes in a mixture.

<Figure 19 near here>

In that vein, measurements of Ne in HIMU samples with the highest $^{4}He/^{3}He$ (see above) provide valuable insight into the nature of the HIMU mantle source. While some HIMU Ne isotopic data are similar to the MORB range (Barfod et al., 1999) or fall towards the more nucleogenic side of the MORB range (Hanyu et al., 2011), multiple studies have now reported Ne isotopic compositions from HIMU samples with $^{21}Ne/^{22}Ne_E$ lower than the MORB range (Parai et al., 2009; Sandoval-Velasquez et al., 2023; Zhang et al., 2024). Parai et al. (2009) reported Ne data measured in olivines from the Cook-Austral Islands, and based on the observation that HIMU Ne isotopes were less nucleogenic than the MORB range, argued that a less-degassed mantle component contributed to the Cook-Austral HIMU mantle source. The samples with the largest isotopic excesses from atmosphere had relatively small deficits in $^{21}Ne/^{22}Ne_E$ compared to MORBs, and subsequent studies argued these data were similar to MORBs (Day, 2022; Hanyu et al., 2014; Hanyu et al., 2011). However, additional high precision Ne data from the Cook-Australs (Zhang et al., 2024) and La Palma (Sandoval-Velasquez et al., 2023) confirm that low $^{21}Ne/^{22}Ne_E$ are found in HIMU samples. Accordingly, HIMU Ne isotopes require that a less-degassed component contributes to these mantle sources, which was not evident from He isotopes.

4.2.2.3 Radiogenic argon isotope signatures

Radioactive ^{40}K decays with a half-life of 1.26 Gyr and ~10.6% of decay events produce ^{40}Ar by electron capture (Naumenko-Dèzes et al., 2018; Table 1). The atmosphere has a $^{40}Ar/^{36}Ar$ ratio of 298.6 (Lee et al., 2006), where most of the atmospheric ^{36}Ar budget originates from

delivery by impact degassing during accretion (potentially in part from degassing of the late veneer) and most of the ^{40}Ar comes from mantle outgassing over Earth history (Zhang et al., 2023). The ^{40}Ar/^{36}Ar ratios in gas sources during accretion are very low (<1; Ott, 2014; Wieler, 2002), so a less-outgassed mantle reservoir should have relatively low ^{40}Ar/^{36}Ar. Measurements of ^{40}Ar/^{36}Ar in mantle samples are affected by syn- to post-eruptive atmospheric contamination. In the prior section, it was discussed how linear correlations with ^{20}Ne/^{22}Ne could be used to correct ^{21}Ne/^{22}Ne for atmospheric contamination. The same approach can be extended to correlations between ^{40}Ar/^{36}Ar and ^{20}Ne/^{22}Ne, though in this case mixing is hyperbolic rather than linear (Farley and Poreda, 1993).

Even without correcting for atmospheric contamination, many early studies measured ^{40}Ar/^{36}Ar ratios orders of magnitude higher than the atmospheric ratio (Allègre et al., 1983; Fisher, 1975, 1983; Marty et al., 1983; Ozima and Zashu, 1983; Sarda et al., 1985; Sarda et al., 1988; Staudacher et al., 1989). Even though ^{40}K is present in the mantle at trace concentrations, it is still far more abundant than ^{36}Ar, and so the radiogenic isotope signatures are not subtle. It was noted that samples with the lowest ^{4}He/^{3}He ratios (highest ^{3}He/^{4}He) had lower maximum ^{40}Ar/^{36}Ar ratios compared to the maximum values measured in MORBs, and this was suggested to indicate a less-degassed plume mantle source (Allègre et al., 1983). However, the possibility of a less-degassed plume mantle source could not be distinguished from systematically greater atmospheric contamination in subaerially-erupted OIBs compared to MORBs (Ballentine and Barfod, 2000; Fisher, 1985; Patterson et al., 1990).

<Figures 20 and 21 near here>

Step-crushing data of oceanic basalts have enabled corrections for syn- to post-eruptive atmospheric contamination (Figure 20) to determine mantle source ^{40}Ar/^{36}Ar (Moreira et al., 1998;

Mukhopadhyay, 2012; Parai et al., 2012; Péron et al., 2016; Péron et al., 2019; Pető et al., 2013; Raquin and Moreira, 2009; Trieloff et al., 2002; Trieloff et al., 2000; Tucker et al., 2012). Measurements of well gases and laser analyses of single vesicles in MORBs have also yielded mantle source $^{40}Ar/^{36}Ar_E$ estimates (Bekaert et al., 2019; Holland and Ballentine, 2006; Péron et al., 2016; Raquin et al., 2008). The results demonstrate that $^{40}Ar/^{36}Ar_E$ in plume-influenced mantle sources are indeed low (<10,000) compared to $^{40}Ar/^{36}Ar_E$ in MORB mantle sources (~20,000 to 40,000; Figure 21). This is consistent with a greater extent of long-term outgassing of the MORB mantle source, recorded in He, Ne and Ar isotopes together. However, it has also been suggested that low $^{40}Ar/^{36}Ar$ ratios in plume sources reflect preferential incorporated of influxed atmospheric gases in plume mantle sources (Holland and Ballentine, 2006; Tucker et al., 2022). There are $^{40}Ar/^{36}Ar_E$ variations among MORB sources that are not associated with He or Ne isotopic variation at the Southwest Indian Ridge (Parai et al., 2012). This variability appears to be unrelated to outgassing, and may instead be due to incorporation of influxed atmospheric Ar in the Southwest Indian Ridge MORB mantle, potentially associated with subcontinental lithospheric mantle bearing atmospheric volatiles (Parai et al., 2012). Influx of atmospheric volatiles is discussed further in Section 5.

4.2.2.4 Pu-U-Xe signatures

An attractive metric with which to assess the extent of mantle outgassing is the fraction of Pu-fission Xe out of total fissiogenic Xe ($^{136}Xe_{Pu}/^{136}Xe_{TF}$). Spontaneous fission of the short-lived radioactive isotope ^{244}Pu produced fissiogenic Xe only for the first several hundred million years of Earth history. Spontaneous fission of the long-lived radioactive isotope ^{238}U has produced fissiogenic Xe throughout Earth history. In Section 4.2.1, the breakdown of a mantle source Xe

isotopic composition into component contributions was reviewed (Caffee et al., 1999; Mukhopadhyay and Parai, 2019; Parai and Mukhopadhyay, 2015; Parai et al., 2019). The fraction of ^{136}Xe from Pu-fission and fraction of ^{136}Xe from U-fission are used to compute $^{136}Xe_{Pu}/^{136}Xe_{TF}$. The $^{136}Xe_{Pu}/^{136}Xe_{TF}$ ratio sidesteps the uncertainty in interpretation discussed in the sections above, as it is affected only by outgassing – any influx of atmospheric Xe into the mantle source is explicitly separated ($^{136}Xe_{atm}$) when determining $^{136}Xe_{Pu}/^{136}Xe_{TF}$. A mantle reservoir that experienced no outgassing over Earth history would develop a $^{136}Xe_{Pu}/^{136}Xe_{TF}$ of ~0.97 (Tolstikhin et al., 2014). A mantle reservoir that experienced extensive outgassing would lose the Xe_{Pu} formed early in Earth history, and would only grow in $Xe_{\underline{U}}$ after ^{244}Pu went extinct, leading to low $^{136}Xe_{Pu}/^{136}Xe_{TF}$ in outgassed mantle reservoirs. Less-outgassed reservoirs preserve high $^{136}Xe_{Pu}/^{136}Xe_{TF}$ ratios.

Using AVCC as the initial mantle Xe composition (Broadley et al., 2020; Péron and Moreira, 2018), Parai et al. (2019) determined $^{136}Xe_{Pu}/^{136}Xe_{TF}$ ratios around ~0.3 for MORB and well gas mantle sources (Caffee et al., 1999; Holland and Ballentine, 2006; Parai and Mukhopadhyay, 2015; Tucker et al., 2012). Note that since well gases may have incorporated Xe_U-rich continental crustal contaminants, the $^{136}Xe_{Pu}/^{136}Xe_{TF}$ ratio for well gases is a lower limit. Well gas from Eifel agrees well with the MORB source mantle composition, with a $^{136}Xe_{Pu}/^{136}Xe_{TF}$ of ~0.2 (Bekaert et al., 2019). In contrast, (Péron and Moreira, 2018) presented high precision Xe measurements obtained from the N. Atlantic popping rock 2ΠD43 using a screened gas accumulation method that minimizes atmospheric contamination, and found a dominant Pu-fission signature. However, high precision data generated by step-crushing of 2ΠD43 (Parai and Mukhopadhyay, 2021) were not in agreement with the accumulated gas composition; the mantle source composition estimated from the step-crush data yielded a $^{136}Xe_{Pu}/^{136}Xe_{TF}$ of ~0.2, which is

consistent with other estimates from MORBs and well gases (Figure 14). High $^{136}Xe_{Pu}/^{136}Xe_{TF}$ ratios (>0.95) were determined for Iceland (Mukhopadhyay, 2012) and Rochambeau Rift (which samples the Samoan plume; Pető et al., 2013). The high $^{136}Xe_{Pu}/^{136}Xe_{TF}$ ratios found for plume mantle sources compared to MORB mantle indicate that the plume source has experienced less outgassing in association with mantle processing over Earth history, independent of the influx of atmospheric Xe into either mantle source.

4.3 Mantle outgassing: extent, rates, and hidden reservoirs

4.3.1 Initial gas concentrations and the extent of mantle outgassing

Box models of gas transport among terrestrial reservoirs and associated noble gas isotopic evolution provide important ways to test ideas about the origins of observed noble gas signatures, and to place constraints on important geophysical parameters like the extents and rates of mantle outgassing over time (Class and Goldstein, 2005; Coltice et al., 2009; Gonnermann and Mukhopadhyay, 2009; Kellogg and Wasserburg, 1990; Parai, 2022; Porcelli and Elliott, 2008; Porcelli and Wasserburg, 1995a; Porcelli and Wasserburg, 1995b) or the interplay between outgassing and atmospheric influx (Moreira and Raquin, 2007; Parai and Mukhopadhyay, 2018; Zhang et al., 2023).

In light of recent precise determinations of mantle source noble gas isotopic compositions and elemental ratios, Parai (2022) developed a box model of mantle evolution to identify model input parameters that could satisfy observed He, Ne and Xe isotope and elemental ratios simultaneously. Zhang et al. (2023) demonstrated that mantle Ar isotopic compositions could also be explained with the same model. Parai (2022) noted that the fissiogenic Xe isotopic composition of the Iceland mantle source (Mukhopadhyay, 2012) requires both a lower extent of outgassing

and a lower initial Xe concentration than that of the MORB mantle source. As discussed above, the $^{136}Xe_{Pu}/^{136}Xe_{TF}$ for the Iceland mantle source is high, and a Pu-fission signature manifests clearly in the mantle source composition when plotted in context with atmosphere, AVCC and fission components (Figure 22). A less-degassed mantle source would retain a greater proportion of its accreted initial Xe and Pu-fission Xe budgets, but the impact of fissiogenic Xe on the total mantle Xe budget depends on the initial Xe concentration, and will be muted for high Xe concentrations. Accordingly, an upper limit initial Xe concentration can be derived for the Iceland mantle source. Mantle He and Ne isotope ratios have long been used to calculate *lower* limit initial gas concentrations – for both of these gases, a lower limit concentration is calculated by assuming closed system isotopic evolution; a higher initial concentration can compensate for any outgassing (e.g., Harper and Jacobsen, 1996). Combined He-Ne-Xe systematics were used to determine the extent of outgassing of Iceland and N. Atlantic MORB mantle sources, and demonstrated that differential outgassing is necessary to explain mantle noble gas isotope systematics, but not sufficient – the initial concentration of Xe must also have been higher in the MORB source (Figure 23; Parai, 2022). However, initial ^{3}He concentrations were higher in the plume source due to a higher $^{3}He/^{130}Xe$ ratio in the plume mantle (closer to the solar ratio than MORB sources).

<Figures 22 and 23 near here>

The extent of outgassing over Earth history can be expressed in terms of the number of mantle reservoir masses processed by partial melting over Earth history (*e.g.*, Gonnermann and Mukhopadhyay, 2009); this is a bit easier to physically envision than alternative metrics. Parai (2022) estimated ~5 MORB source reservoir masses processed over Earth history, which translates to loss of ~99% of the initial accreted Xe. The estimated extent of outgassing of the Iceland plume

source over Earth history is ~2.8 reservoir masses, which translates to loss of ~94% of initial accreted Xe. The important thing to emphasize is that neither modeled mantle source is primitive, but both reservoirs still preserve a fraction of their initial noble gas budgets (^{3}He, ^{20}Ne, ^{22}Ne, ^{36}Ar, ^{130}Xe, *etc.*) in sufficient quantities to explain the observed mantle ^{4}He/^{3}He, ^{21}Ne/^{22}Ne, ^{40}Ar/^{36}Ar and Xe isotopic signatures (Parai, 2022; Zhang et al., 2023).

4.3.2 Mantle outgassing rates

Observational constraints on the magnitude of the flux of outgassed magmatic volatiles are important to our understanding of deep Earth volatile transport. The low concentration and distinct isotopic composition of helium in the atmosphere makes this element a valuable tracer of mantle outgassing. Estimates of the present-day outgassing rate of the MORB source mantle have been made based on helium isotope data from ocean waters and ocean general circulation models. These range from ~400 to 1000 moles ^{3}He/yr emitted from global ocean volcanism (Bianchi et al., 2010; Farley et al., 1995; Holzer et al., 2017; Schlitzer, 2016), though the more recent estimates seem to achieve some consensus around 550 ± 50 moles ^{3}He/yr (Jenkins, 2020). It is remarkable that Clarke et al. (1969) calculated a mantle outgassing flux by coupling their observed excess of ^{3}He in deep ocean water (compared to equilibrium concentrations) with a radiocarbon box model age of the deep ocean, and arrived at essentially the same figure – about 530 moles ^{3}He/yr – albeit with large uncertainties. Present-day outgassing rates for the other noble gases (or for other volatiles such as carbon dioxide, nitrogen and water) can be inferred using the ^{3}He flux and mantle source molar ratios (e.g., ^{36}Ar/^{3}He, CO_2/^{3}He).

Curiously, the oceanographic estimate of the mid-ocean ridge ^{4}He flux is significantly lower than expected based on the flux of radiogenic heat from the mantle; this problem is called

the “heat-helium paradox” (Ballentine et al., 2002; O’Nions and Oxburgh, 1983; van Keken et al., 2001). Outgassing rates can alternatively be computed by reconstructing noble gas concentrations in melts prior to magmatic degassing and combining these with estimates of the magmatic production rate. Tucker et al. (2018) determined a mid-ocean ridge ^{3}He flux of 800 ± 170 moles ^{3}He/yr. This higher value was determined independently of the oceanographic estimates, and may better represent the longer-term average MORB outgassing rate. However, it is still not high enough to match the expected He flux from heat flow arguments (Tucker et al., 2018).

It is worthwhile to note that outgassing flux from hotspot volcanism may be comparable to the mid-ocean ridge outgassing flux. While magmatic production rates are ~10 times lower at hotspots (Crisp, 1984), the plume mantle source may have higher ^{3}He concentrations (due to a lower extent of outgassing over Earth history; see Parai, 2022) which may compensate to yield comparable gas fluxes.

Given existing constraints on present-day fluxes, multiple lines of evidence indicate that the mantle outgassing rate must have been higher in the past. To explain the radiogenic noble gas isotope signatures that have traced mantle outgassing on different timescales (e.g., Pu-Xe, K-Ar, and U-Th-He; Sections 4.2.1-4.2.2), Yokochi and Marty (2005) argued for vigorous outgassing (at least an order of magnitude higher than present-day fluxes) in the first several hundred million years of Earth history. Using a box model of Xe isotopic evolution, Coltice et al. (2009) showed that it was necessary to process 4-9 times the mass of the mantle over Earth history to explain mantle Pu-U-Xe isotopes. Assuming the present day rate of mantle processing (producing 21 km^{3} of oceanic crust per year; Crisp, 1984) was sustained throughout Earth history, only ~0.7 times the mass of the mantle would have been processed over Earth history; present-day Xe isotopic observations necessitate a higher outgassing rate in the past. Parai and Mukhopadhyay (2018)

found a similar range for MORB Xe (5-9 mantle reservoir masses), and Parai (2022) provided narrower estimates of total processing (~3 reservoir masses for the plume mantle and ~5 reservoir masses for the MORB mantle). A distinct, complementary line of evidence comes from the paleo-atmospheric $^{40}Ar/^{36}Ar$ record: to account for a steep rise in atmospheric $^{40}Ar/^{36}Ar$ early in Earth history and slower subsequent evolution requires higher outgassing rates in the past (Tucker et al., 2022; Zhang et al., 2023).

4.3.3 No need for isolated reservoirs

Perhaps the most important result from recent box models of noble gas isotopic evolution is that observed noble gas isotopic compositions and elemental abundance patterns can be explained in full as characteristics of mantle reservoirs that have experienced extensive outgassing and incorporation of recycled materials bearing atmospheric volatiles. Gonnermann and Mukhopadhyay (2009) showed that high $^{3}He/^{4}He$ ratios could be preserved in mantle reservoirs that incorporated and mixed in recycled, depleted oceanic slabs over time, even if multiple reservoir masses were processed through partial melting and recycling over Earth history. As recycled slabs are mixed in, the concentration of primordial noble gases is diluted, but not driven to zero[11]. Sufficient ^{40}Ar could also be retained in a processed mantle to explain the bulk Earth ^{40}Ar budget (Gonnermann and Mukhopadhyay, 2009). The same modeling framework is able to reproduce $^{4}He/^{3}He$, $^{21}Ne/^{22}Ne$ and fissiogenic Xe isotopic compositions simultaneously for the Iceland plume and N. Atlantic MORB mantle source compositions (Parai, 2022). The radiogenic

[11] The only scenario where this would not hold true is if the characteristic slab mixing time is very slow; *i.e.*, slabs remain unmixed on billion year timescales within mantle reservoir that gives rise to melts, in which case the mantle reservoirs would simply shrink in size as they became displaced by pure "slab graveyards."

lithophile (Sr, Nd, Pb, Hf and others) isotopic compositions of the modeled mantle reservoirs would not resemble primordial bulk silicate Earth; an overall depleted radiogenic isotope character would be imparted by the long-term incorporation and mixing of slabs carrying the signature complementary to continental crust growth (Gonnermann and Mukhopadhyay, 2009). Enriched signatures (*e.g.*, sediments, altered oceanic crust) crop up where they have survived extensive mixing; it is possible that greater isotopic variability is observed in OIBs because they derived from a reservoir that mixes more sluggishly. The noble gas signatures of outgassing broadly observed in OIBs and MORBs thus do not require an isolated primordial mantle reservoir, nor do they require a flux of primordial gas from the core to the mantle.

The extremely high $^{3}He/^{4}He$ (low $^{4}He/^{3}He$) ratios measured in samples from Baffin Island (Horton et al., 2023; Horton et al., 2021; Rizo et al., 2016; Starkey et al., 2009; Stuart et al., 2003) stand out among OIBs and other plume-influenced samples. The highest measured values approach the solar nebular composition: Horton et al. (2023) reported a single measurement of $^{3}He/^{4}He$ = 90.7 ± 3.9 Ra ($^{4}He/^{3}He$ = 7,930 ± 340), whereas the solar nebular $^{3}He/^{4}He$ is ~120 Ra ($^{4}He/^{3}He$ of ~6,000; Mahaffy et al., 1998). The Baffin He isotope ratios are particularly puzzling in light of the Baffin Ne isotopic data that are indistinguishable from modern Iceland Ne (Horton et al., 2021; Mukhopadhyay, 2012; Parai, 2023), which requires substantial outgassing and ingrowth of nucleogenic ^{21}Ne compared to the solar composition (Parai, 2022). Something unusual had to happen in the Baffin Island source to impart near-solar He isotopes without changing $^{21}Ne/^{22}Ne_{E}$ from the composition of the broader proto-Iceland plume.

One possibility is that the solar He originates from the core (Bouhifd et al., 2020; Horton et al., 2023; Olson and Sharp, 2022; Porcelli and Halliday, 2001). In light of the high $^{3}He/^{22}Ne$ ratios required to explain Baffin He and Ne simultaneously, Horton et al. (2023) suggested that a

flux of solar-like He from the core raised $^{3}He/^{4}He$ and $^{3}He/^{22}Ne$ to ~7.5 to 10 in the portion of the proto-Iceland plume that was sampled at Baffin. It is important that only He be added for two reasons: (1) addition of bulk solar gas ($^{3}He/^{22}Ne$ of ~1.5; (Tucker and Mukhopadhyay, 2014) would lower the $^{3}He/^{22}Ne$ compared to the rest of the Iceland plume, not raise it; and (2) the requisite nucleogenic ^{21}Ne (needed to explain the high $^{21}Ne/^{22}Ne_E$ in Baffin and Iceland compared to solar) would not be generated in the core, as the $^{21}Ne^{*}/^{4}He$ production ratio would be much lower in the relatively oxygen-poor environment of the Earth's core (Fischer and McDonough chapter). The Baffin Ne isotopic composition must rather be native to the mantle. A flux of solar He from the core may explain the anomalous signature at Baffin Island (Horton et al., 2023) relative to other plume sources. However, no flux of solar He is required to explain the broader global plume dataset, and the full mantle noble gas (He, Ne, Ar, Kr and xe) compositional array is not well-explained by diffusive transport of gas out of the core.

Commented [RP1]: Unless fractionated by metal-silicate eq

5. SIGNATURES OF THE INFLUX OF ATMOSPHERIC GAS INTO MANTLE SOURCES

Atmospheric gases are transported into Earth's interior through subduction of tectonic plates. Noble gases are thought to be carried mostly in hydrous minerals in the subducting slab, making the influx of atmospheric noble gases a potential method to trace the influx of water from the surface into the interior over time. Signatures of the incorporation of atmospheric noble gases into the mantle are discussed below. Elemental abundances, isotopic evidence, fluxes and mass balance at subduction zones are covered. To avoid confusion when reading earlier literature, it is important to note that early studies discuss mantle heavy noble gas signatures based on the belief that primordial noble gases in the mantle resembled the atmosphere (*e.g.*, Allègre et al., 1983) –

this was born out of historical difficulty in measuring compositions resolved from the atmosphere, and the assumption that the atmosphere formed by outgassing of the mantle[12]. It is now understood that the accreted initial noble gases in the mantle are distinct from the atmospheric composition (Figures 4-8) and are consistent with a mixture of solar nebular and chondritic gases (Figures 7,8). Mantle reservoirs have retained a portion of their initial gas budgets (~1% to ~6% of the initial concentrations, Section 4.3). The present-day mantle source noble gas compositions reflect mixing between the retained initial gas, isotopes produced by nuclear reactions over Earth history, and any influx of atmospheric gas.

[12] Origins of the atmosphere are discussion in Chapters 2 and 168 of this edition of the Treatise on Geochemistry

5.1 Evidence for the influx of atmospheric noble gases into the mantle

The potential for "pollution" of the mantle by injection of atmospheric noble gases has long been discussed (e.g., Ozima et al., 1985; Porcelli and Wasserburg, 1995a; Porcelli and Wasserburg, 1995b; Staudacher and Allegre, 1982). However, it was unclear whether slabs would carry atmospheric noble gases beyond depths of magma generation, or release them during dehydration at subduction zones (e.g., Staudacher and Allègre, 1988). Distinguishing between an influx of atmospheric noble gases into mantle sources and shallow, syn- to post-eruptive atmospheric contamination was the main challenge in establishing whether atmospheric noble gases were injected into the mantle in significant quantities. The history of debate regarding the nature of $^{20}Ne/^{22}Ne$, $^{40}Ar/^{36}Ar$ and $^{129}Xe/^{130}Xe$ variations among mantle samples and terrestrial reservoirs was reviewed in Sections 3 and 4. The same determinations of mantle source compositions that enabled demonstration that, *e.g.*, plume mantle source $^{129}Xe/^{130}Xe$ ratios are low compared to MORB mantle source $^{129}Xe/^{130}Xe$ ratios (Figure 10; Mukhopadhyay, 2012; Mukhopadhyay and Parai, 2019), also enable us to identify and quantify the proportions of influxed atmospheric gas in mantle sources. This is easier to do when there are several isotopes of a given noble gas element to leverage in identifying atmospheric contributions to the mantle source (versus outgassing or a difference from accretion). The sections below discuss evidence for influxed atmospheric contributions to mantle source budgets of each of the noble gas elements, ordered from Xe to He.

5.1.1 There is a lot of influxed atmospheric Xe in the mantle

The nine isotopes of Xe provide powerful tools to examine mantle volatile origins. The diverse array of primordial and produced isotopes, and the fact that the composition of the

atmosphere is genetically distinct (Avice et al., 2018; Marty et al., 2017), all make it possible to fingerprint different Xe isotopic contributions to mantle sources. Holland and Ballentine (2006) presented measurements of heavy noble gases in CO_2 well gases from New Mexico and Colorado, and showed that these samples were affected by variable amounts of crustal and atmospheric contamination. By leveraging mixing systematics evident among the samples, the authors extrapolated away from the atmospheric and crustal contaminants, and towards the magmatic Xe isotopic composition. The intersection of their data array with the atmosphere-MORB mixing line from N. Atlantic popping rock Xe data (Kunz et al., 1998; Moreira et al., 1998) yielded a mantle source $^{129}Xe/^{130}Xe$ isotopic composition of ~7.9. Propagating this result to the primordial Xe isotope ratios gave a mantle source consistent with ~80% influxed atmospheric ^{130}Xe and 20% of accreted initial ^{130}Xe.

Holland and Ballentine (2006) further noted that the elemental abundance pattern of the well gases matched that of seawater, which has elemental ratios fractionated compared to air by the higher solubility of the heavier noble gases in water. Based on this similarity, the authors suggested that mantle budgets of the other heavy noble gases were likewise dominated by subducted seawater. They also argued that differential incorporation of atmospheric gas with low $^{129}Xe/^{130}Xe$ and $^{40}Ar/^{36}Ar$ is responsible for the difference between plume and MORB Xe and Ar. However, later studies showed that differential influx of atmospheric Xe could not explain plume and MORB isotopic variations (Figures 11, 12; Bekaert et al., 2023; Broadley et al., 2020; Mukhopadhyay, 2012; Parai, 2023; Parai and Mukhopadhyay, 2021; Parai et al., 2012; Péron et al., 2021; Pető et al., 2013; Tucker et al., 2012), though all of these studies required a large proportion of influxed atmospheric Xe to exist in mantle sources.

Studies of basalts analyzed by step-crushing and some well gases found mixing arrays that could, in favorable cases, be corrected for syn- to post-eruptive atmospheric contamination to determine mantle source Xe isotopic compositions (Bekaert et al., 2019; Moreira et al., 1998; Mukhopadhyay, 2012; Parai, 2023; Parai and Mukhopadhyay, 2021; Parai et al., 2012; Pető et al., 2013; Tucker et al., 2012). These studies leveraged Ne-Xe or Ar-Xe mixing systematics to determine mantle source Xe compositions that correspond to a model mantle $^{20}Ne/^{22}Ne$ free of atmospheric contamination (Figures 10, 17, 20; typical corrections use 12.5 for MORB mantle samples, 13.36 for plume samples, or intermediate values for mixed mantle sources; Pető et al., 2013; Williams and Mukhopadhyay, 2019). For some of the data, the range of measured compositions extended all the way to the corrected mantle source Xe isotope composition (Parai and Mukhopadhyay, 2021; Parai et al., 2012), so the measurements are not extremely far from the source compositions and the uncertainty derived from extrapolation remains small. Section 4.2.1 reviews the method to determine component contributions from initial accreted Xe, influxed atmospheric Xe, Pu-fission and U-fission to the corrected mantle source Xe composition (see Mukhopadhyay and Parai, 2019; Parai et al., 2019).

A striking outcome of the linear least squares analyses of mantle source Xe isotopic compositions is the dominance of the influxed atmospheric Xe component in both plume and MORB mantle sources (Bekaert et al., 2019; Mukhopadhyay, 2012; Parai and Mukhopadhyay, 2015; Parai et al., 2019; Pető et al., 2013; Tucker et al., 2012). For samples of the MORB mantle, ~80-90% of ^{132}Xe in the mantle source was found to be influxed atmospheric Xe (see Figure 24 for specific examples; Parai et al., 2019 for a compilation). Even in plume mantle sources with other noble gas isotopic signatures (*e.g.*, high $^{136}Xe_{Pu}/^{136}Xe_{TF}$) that signify very little outgassing by mantle processing and incorporation of slabs, the influxed atmospheric Xe signature is

dominant (Figure 24). To explain this latter observation, Parai (2022) suggested that a low initial concentration of Xe made a small amount of influxed atmospheric Xe stand out in the plume mantle source composition. However, it is also possible that, on average, slabs that mix into the plume mantle carry high concentrations of atmospheric Xe (Zhang et al., 2024). Notably, none of the studies called for complete overprinting of the mantle source with influxed atmospheric gas – all mantle sources still require retention of some small amount of initial accreted Xe.

<Figure 24 near here>

Another line of evidence for a high proportion of influxed atmospheric Xe is from primordial Xe isotope ratios in gases with minimal atmospheric contamination. Using a technique where measured $^{20}Ne/^{22}Ne$ ratios were used to screen gas released by step-crushing for atmospheric contamination, a pool of sample gas with minimal atmospheric contamination was accumulated and analyzed (Péron and Moreira, 2018; Péron et al., 2021). This technique yielded a very high Xe isotopic excess for the N. Atlantic popping rock sample 2ΠD43, with a measured $^{129}Xe/^{130}Xe$ of 7.41 ± 0.03, identical to the mantle source $^{129}Xe/^{130}Xe$ determined by hyperbolic fits to Ne-Xe and Ar-Xe mixing arrays for 2ΠD43 by Parai and Mukhopadhyay (2021). By accumulating a large quantity of mantle gas with their screening method, Péron and Moreira (2018) were able to measure mantle $^{124}Xe/^{130}Xe$, $^{126}Xe/^{130}Xe$, and $^{128}Xe/^{130}Xe$ ratios well in excess of the atmospheric composition, in good agreement with the variably-contaminated, high-precision well gas primordial Xe isotope data (Figure 6). Their result indicates a ~75:25 mix of influxed atmospheric Xe and initial accreted Xe in the N. Atlantic MORB mantle source, consistent with the estimates from Holland and Ballentine (2006) and the linear least squares analyses of the heavy Xe isotopes in other MORB mantle sources. The screened accumulated gas measurements from Iceland and Galápagos (Péron et al., 2021) do not show such high $^{129}Xe/^{130}Xe$, perhaps due to a

high $^{130}Xe/^{22}Ne$ ratio in the atmospheric contaminant compared to the magmatic gas, which would result in more atmospheric contamination of Xe isotopic compositions of these samples than manifests in the Ne isotopes (see Section 2.6 regarding hard luck). Nonetheless, three distinct approaches all produce similar results: there is a high proportion of influxed atmospheric Xe in mantle sources today.

5.1.2 There is most likely also influxed atmospheric Kr in the mantle

Studies of Kr in mantle-derived samples include well gases (Holland et al., 2009), volcanic gas from Yellowstone (Broadley et al., 2020), and screened accumulated gas from step-crushing of Iceland and Galápagos basalt samples (Péron et al., 2021). Broadley et al. (2020) examined the well gas and Yellowstone data in plots of primordial Xe isotope ratios against $^{86}Kr/^{84}Kr$, and showed hyperbolic mixing between atmosphere and AVCC components could explain the observed compositions. It is challenging to extract information about the amount of influxed atmosphere Kr in the mantle from such mixing hyperbolae: the observations could represent shallow atmospheric contamination of a mantle source free of influxed atmosphere, or the mantle source composition could be somewhere between atmosphere and AVCC. These particular systematics are further complicated by the potential for nucleosynthetic variations between Earth's mantle and chondrites: Péron et al. (2021) showed that the well gas, Yellowstone and Galápagos data all require a mantle source with a deficit in ^{86}Kr compared to AVCC (Figure 5).

Instead, the best evidence for an influx of atmospheric Kr into mantle sources comes from measurements of mantle gas where syn- to post-eruptive atmospheric contamination has been minimized. Péron et al. (2021) estimated ~40-70% of mantle Kr is influxed atmospheric for Iceland and Galápagos. Since the screened gas accumulation method reduces atmospheric contamination,

but does not eliminate it, these are maxima and the mantle source may have less influxed Kr than these estimates. Corrections for syn- to post-eruptive atmospheric contamination or other means of determining mantle source Kr isotopic compositions are needed to definitively demonstrate an influx of atmospheric Kr.

5.1.3 Influx of atmospheric Ar affects at least some parts of the mantle

The origins of $^{40}Ar/^{36}Ar$ variation (and lack of variation in $^{38}Ar/^{36}Ar$) in the global set of mantle samples are difficult to pin down. Substantial proportions of mantle ^{36}Ar have been suggested to originate from the influx of atmospheric Ar into the mantle (Sarda, 2004; Tucker et al., 2022; see discussions in Moreira and Raquin, 2007; Raquin and Moreira, 2009). Péron and Mukhopadhyay (2022) used estimates of the proportions of mantle source primordial noble gas isotopes from atmospheric influx to calculate mantle source elemental abundance patterns excluding the atmospheric-influx component. The authors argued that while some portion of the mantle ^{36}Ar budget could be atmospheric in origin, there was room for a large portion of mantle ^{36}Ar to be retained from accretion. Zhang et al. (2023) modeled He, Ne and Ar isotopic evolution in a model of mantle, continental crust and atmospheric evolution. Based on the ranges of model input parameters that could successfully replicate mantle and atmospheric observations, the authors found that mantle $^{40}Ar/^{36}Ar$ ratios could be explained with or without atmospheric Ar influx.

There is evidence that $^{40}Ar/^{36}Ar$ variations in specific regions of the mid-ocean ridge system reflect atmospheric Ar influx. Sarda et al. (2000) measured heavy noble gases in MORBs from the southernmost Mid-Atlantic Ridge (MAR). In samples exhibiting the Sr, Pb and Nd isotopic compositions consistent with the Dupal signature (Dupré and Allègre, 1983), Sarda et al.

(2000) found low estimated mantle $^{40}Ar/^{36}Ar$ (~15,000) compared to other MORBs. The authors suggested that these low ratios could be Dupal source signatures reflecting incorporation of delaminated subcontinental lithospheric mantle that had been metasomatized with atmospheric gases. Parai et al. (2012) presented data from basalts from the nearby Southwest Indian Ridge (SWIR), and showed that significant variation in mantle source $^{40}Ar/^{36}Ar_E$ (from ~20,000 to ~50,000) appeared in samples with very similar $^{4}He/^{3}He$ ratios (~100,000 to 110,000; Figure 25). Both the southernmost MAR and SWIR samples also exhibited low mantle source $^{129}Xe/^{130}Xe_E$. The occurrence of large variations in $^{40}Ar/^{36}Ar_E$ and $^{129}Xe/^{130}Xe_E$ without significant variation in $^{4}He/^{3}He$ or $^{21}Ne/^{22}Ne_E$ (which would be expected if outgassing generated the observed signatures) suggests that in this region of the MORB source mantle, atmospheric influx drives some portion of mantle source $^{40}Ar/^{36}Ar$ variability.

<Figure 25 near here>

5.1.4 The impact of atmospheric Ne influx has been muted because there is a lot of Ne in the mantle

The highest $^{20}Ne/^{22}Ne$ ratios measured in mantle samples approach the compositions of pure accreted components (Figure 4). This observation is the basis for using co-variations with $^{20}Ne/^{22}Ne$ to correct other isotopic ratios for atmospheric contamination: the mantle source composition is assumed to be close to that of accreted components, because such compositions have been measured at many settings (Figure 18). The high measured $^{20}Ne/^{22}Ne$ values limit the relative proportion of mantle Ne derived from the influx of atmospheric gas over time. However, that does not mean that there has been no influx of atmospheric Ne in an absolute sense.

Variations in $^{20}Ne/^{22}Ne$ among mantle sources were discussed in Section 3.3.2 as arising from mixing between solar nebular gas and chondritic gas during accretion, and the influx of atmospheric Ne into the mantle over time. Measurements of $^{20}Ne/^{22}Ne$ in MORB samples and CO_2 well gases indicate a lower source $^{20}Ne/^{22}Ne$ than that in plume sources (~12.6 vs. >13; Williams and Mukhopadhyay, 2019 and references therein; Figure 4). Recall that the MORB source mantle primordial noble gas isotopic composition is not reconcilable with solar wind irradiated material (Ne-B) as the source of mantle Ne, because of the orders-of-magnitude difference between mantle and solar Xe/Ne ratios and the ~25% of mantle ^{130}Xe from initial accreted sources (Section 3.3.5; Parai, 2022).

Williams and Mukhopadhyay (2019) suggested that the lower $^{20}Ne/^{22}Ne$ in the MORB source originated from a greater proportion of non-solar ^{22}Ne in the MORB mantle source. Parai (2022) used Ne-Xe isotope systematics to calculate that the MORB source had a greater proportion of ^{22}Ne from chondrites during accretion, but also had incorporated a greater proportion of ^{22}Ne from atmospheric influx (Figure 26). It makes physical sense that the plume mantle source, which has experienced less outgassing through mantle processing – that is, less incorporation of subducted slabs – would incorporate a smaller proportion of atmospheric Ne carried within those slabs. Parai (2022) suggested that the MORB mantle started off with a lower $^{20}Ne/^{22}Ne$ (~13) at the end of accretion, and that that ratio was lowered over time by atmospheric influx. Accordingly, a signature from long-term mantle processing is superimposed upon a difference from accretion in mantle Ne isotope signatures.

<Figure 26 near here>

Based on noble gas elemental abundance patterns measured in serpentinites and secondary peridotites, Kendrick et al. (2018) suggested that subduction of serpentinites should bring

significant quantities of atmospheric Ne into the mantle along with Xe, and could in part account for the lower $^{20}Ne/^{22}Ne$ in MORB sources compared to solar nebular gas. Parai (2022) used Ne and Xe primordial isotopes to calculate the weighted average $^{130}Xe/^{22}Ne$ ratio of atmospheric influx retained in mantle sources today, and found that this ratio (~0.04 to 0.06) was high compared to unfractionated atmosphere (~0.002), but similar to the ratios determined for serpentinites (Kendrick et al., 2013; Kendrick et al., 2018; Kendrick et al., 2011). This may indicate that noble gases are carried by serpentinites preserved within subducted slabs beyond depths of magma generation, or that Xe is preferentially retained in other hydrous phases and the subduction process raises Xe/Ne ratios relative to initial compositions.

Bekaert et al. (2021) compared estimates of the flux of Ne carried by slabs into subduction zones to the Ne flux from outgassing at arc volcanoes. Since the outgassing flux exceeded the estimated flux into the subduction zone, the authors argued for zero atmospheric Ne influx beyond depths of magma generation at subduction zones. A long-term zero Ne influx is not supported by the mantle noble gas data. The weighted average long-term $^{130}Xe/^{22}Ne$ ratio in subducted components that have carried atmospheric influx into mantle sources (~0.042 – 0.060; Parai, 2022; Figure 8) is elevated compared to unfractionated atmosphere (0.0021; Table 2), but these estimates are still significantly less than 1, which means that the absolute Ne influx in moles per year exceeds the Xe influx. While the mantle Xe isotopic composition sings prominently of influxed atmosphere, the impact of the influxed atmospheric Ne on the mantle Ne isotopic composition is muted by a low $^{130}Xe/^{22}Ne$ ratio in the mantle compared to the subducted components that bear influxed atmospheric gases into the deep mantle (Figure 8).

5.1.5 The atmospheric He influx is expected to be negligible

The concentration of He in atmospheric gas is very low due to continuous escape of He to space, whereas the concentration of He in the mantle is higher than for any other noble gas (Graham, 2002; Porcelli et al., 2002). Accordingly, it is unlikely that there is a detectable influx of atmospheric He to the mantle. Mantle $^{3}He/^{130}Xe$ ratios can be used to confirm this. Estimates of mantle $^{3}He/^{130}Xe$ range from ~600 to 1000 (Parai, 2022 and references therein). The atmospheric $^{3}He/^{130}Xe$ ratio is ~0.002 (Porcelli et al., 2002). We can imagine a mantle reservoir with 6000 parts ^{3}He to 10 parts ^{130}Xe. Of those 10 parts ^{130}Xe, about 8 are from atmospheric influx into the mantle (Péron and Moreira, 2018). Assuming the $^{3}He/^{130}Xe$ ratio of unfractionated atmosphere, that means 0.016 parts out of 6000 parts ^{3}He are from atmospheric influx. Using a fractionated atmospheric elemental ratio would give an even lower number, since seawater and mineral phases are enriched in Xe compared to He. Furthermore, it is possible that He is preferentially lost from slabs during subduction (Fukushima et al., 2024). The potential contribution of atmospheric influx He to mantle sources is therefore expected to be negligible.

5.2 Potential carriers of atmospheric noble gases into the mantle

Subducting slabs carry surface volatiles into the Earth's interior. Understanding the mass balance between volatiles that go into the subduction zone, what comes out via arc volcanism, and what is influxed into the mantle (e.g., Bekaert et al., 2021; Hilton et al., 2002; Marty and Tolstikhin, 1998; Parai and Mukhopadhyay, 2012; Plank and Manning, 2019) is of great importance to understanding how plate tectonics has affected the distributions of different volatiles between the deep Earth and surface reservoirs over time. Gases may be carried in pore fluids or within minerals in sediments, altered oceanic crust (AOC), or serpentinized lithospheric mantle

(Figure 15). As slabs reach higher pressures and temperatures in subduction zones, the breakdown of hydrous minerals in the subducting slab package results in a flux of slab volatiles to the overlying mantle wedge. The critical factor is the amount of any given volatile element that is retained within the subducting slab beyond depths of magma generation at a specific subduction zone. Even if the gas is carried in a phase that will become unstable at greater depths, upon breakdown that gas will be released into the mantle, and not returned to the surface through arc volcanism.

Based on the similarity between mantle noble gas elemental abundance patterns and seawater, air-saturated seawater carried in pore fluids was suggested as the vector carrying atmospheric noble gases into the mantle (Holland and Ballentine, 2006). However, pore fluids are thought to be largely expelled from slabs at shallow depths in the subduction zone (Connolly, 2010; Paulatto et al., 2017; Saffer and Tobin, 2011). Atmosphere-derived noble gases with elemental abundance patterns fractionated from air may instead be hosted within mineral phases in subducting slabs.

Studies of noble gas solubility in amphiboles, micas and serpentinites indicate that these phases may be important carriers of noble gases into the mantle (Baldwin and Das, 2015; Jackson et al., 2013b, 2015; Kendrick et al., 2013; Kendrick et al., 2018; Kendrick et al., 2011; Krantz et al., 2019; Smye et al., 2017). Altered oceanic crust hosts atmospheric noble gases with fractionated elemental abundance patterns (Chavrit et al., 2016; Kumagai et al., 2003; Staudacher and Allègre, 1988). Chavrit et al. (2016) measured noble gases and halogens in drill core samples of altered oceanic crust (AOC) of varying age and found elemental abundance patterns were strongly fractionated compared to seawater, with enrichment of heavier noble gases over light. Smye et al. (2017) argued that excessive elemental fractionation compared to seawater would not match the

seawater-like mantle elemental abundance pattern noted by Holland and Ballentine (2006), and showed that less fractionation occurs in cold subduction zones. The authors noted that it makes physical sense for slabs at cold subduction zones to successfully inject more atmospheric noble gases into the interior, making the dominant influx only mildly fractionated compared to seawater. However, with additional mantle source elemental abundance ratio data, this constraint can be loosened: mantle source elemental abundance patterns seem to reflect mixing between accreted components and influxed components with more strongly fractionated elemental abundance ratios than air-saturated seawater (Figures 7, 8; Parai, 2022; Williams and Mukhopadhyay, 2019).

Metasomatized subcontinental lithospheric mantle is potentially an important reservoir for surface volatiles that were expelled from slabs in the past, but did not return to the surface through arc volcanism (Barry and Broadley, 2021; Broadley et al., 2016; Matsumoto et al., 2001). Delamination of the subcontinental lithospheric mantle could carry these atmospheric volatiles into convecting mantle reservoirs (Parai et al., 2012; Sarda et al., 2000).

5.3 The timing of atmospheric influx

The magnitude of influx of surface volatiles into the mantle has changed over time. Secular cooling of the mantle has changed the pressure-temperature paths slabs experience during subduction, and accordingly the phases that could carry surface volatiles beyond depths of magma generation have likely changed. Prior to the onset of plate tectonics, atmospheric influx could have occurred through delamination or foundering of the lithosphere. There is a great amount of uncertainty about how things might have been different in the past.

The Xe isotopic system provides a powerful tool with which to investigate the atmospheric influx over time. Earth's atmosphere is depleted in Xe relative to other noble gases when compared

to potential atmospheric precursor materials, and atmospheric Xe isotopes exhibit a mass-dependent depletion in light isotopes compared to those precursors (Avice and Marty, 2020). Archives of ancient atmospheric Xe have illustrated that the process that drove Xe loss (Broadley et al., 2022) and generated the atmospheric Xe isotopic fractionation operated for the first ~2 Gyr of Earth history until the modern atmospheric composition was reached ~2.4 Ga (Ardoin et al., 2022; Avice et al., 2017; Avice et al., 2018; Broadley et al., 2022; Pujol et al., 2011; Pujol et al., 2009). Accordingly, the isotopic "fingerprint" of atmospheric Xe was changing for the first 2 Gyr of Earth history.

If atmospheric Xe was injected into the mantle throughout Earth history, then the mantle has received a mixture of modern and ancient atmospheric Xe isotopic compositions over time. Parai and Mukhopadhyay (2015) tested whether compiled mantle source Xe isotopic compositions could be explained well using the composition of atmospheric Xe from 3.5 Gyr old quartz samples (Pujol et al., 2011). The authors performed the linear least squares computation described in Section 4.2.1.2 to solve for the fraction of Xe from accretion, Pu-fission, U-fission, and ancient atmospheric Xe that best matches the modern mantle compositions. Parai and Mukhopadhyay (2015) noted that this exercise produced very poor fits, with residuals that were orders of magnitude higher than the best fits using the modern atmospheric composition for influxed Xe, and suggested that average composition of influxed atmospheric Xe retained in the mantle today was close to the modern composition. Péron and Moreira (2018) used their determination of MORB source $^{128}Xe/^{130}Xe$ and $^{136}Xe/^{130}Xe$ to place constraints on the weighted average age of influxed atmospheric Xe. The authors found that the maximum average age of influxed Xe was 2.8 ± 0.3 Ga. Neither of these approaches rules out some influx earlier in time, but if significant atmospheric gas were injected prior to ~2.8 Ga, then it must have been lost from the mantle by

subsequent outgassing. However, that outgassing would have consequences for Pu-fission and U-fission Xe isotopes.

To test potential histories of atmospheric influx and outgassing, Parai and Mukhopadhyay (2018) developed a forward model of mantle Xe isotopic evolution. Starting with an initial chondritic Xe composition, the Xe isotopic composition of the mantle was tracked over time for different model histories of outgassing, continental crust growth (which extracts Pu and U from the mantle), and atmospheric influx. Model inputs that generated present-day mantle compositions matching the estimated MORB source composition were identified. The model only succeeded in reproducing the modern MORB mantle Xe composition if the concentration of atmospheric Xe in slabs was low (<< the mantle Xe concentration) early in Earth history. The authors concluded that injection of atmospheric Xe was limited prior to ~2.5 Ga.

These distinct approaches all point towards the same result: for the first ~2 Gyr of Earth history, atmospheric Xe was not efficiently carried into the mantle. There are multiple lines of evidence for the initiation of plate tectonics and subduction prior to 2.5 Ga, including eclogitic inclusions in diamonds up to 3.0 Ga (Shirey and Richardson, 2011) and evidence from Hadean zircons (Hopkins et al., 2008). It is possible that subducted materials were less altered and hydrated early in Earth history, but high-temperature alteration of Archean crust in a Xe-rich early atmosphere seems like it would lead to high Xe concentrations in subducting materials. Rather, a hotter mantle may have led to quantitative expulsion of Xe from Archean slabs, such that the atmospheric Xe was efficiently returned to the surface through arc volcanism (Parai and Mukhopadhyay, 2018). The modern, colder style of subduction carrying an influx of atmospheric noble gases would then have started at some time after ~2.5 Ga.

6. SUMMARY AND FUTURE OUTLOOK

Mantle source noble gas compositions have recorded a story of volatile accretion, early differentiation, long-term volatile transport and convective mixing. While gases have been transferred between the mantle and atmosphere, the interior and surface reservoirs have been distinct since the Earth accreted and have never been homogenized. Likewise, there are at least two distinct reservoirs within the mantle: one that is the present-day MORB source mantle, and another that contributes to mantle plumes. The main points of the chapter can be summarized as follows (see Sections 3-5 for detailed references).

(1) The mantle noble gas record is most consistent with accretion of a mixture of solar nebular and carbonaceous chondritic gases.

(2) Given the extreme contrast in solar and chondritic elemental abundance patterns, solar contributions to Kr and Xe are miminal. Initial mantle Kr and Xe isotopes resembled the average carbonaceous chondrite composition, but with a deficit in ^{86}Kr that may be nucleosynthetic in origin, indicating primordial isotope heterogeneity among carbonaceous solids in the proto-planetary disk.

(3) Initial mantle He and Ne were dominantly from dissolution of solar nebular gas into a terrestrial magma ocean, indicating that at least one giant impact occurred before the nebular gas dissipated from the proto-planetary disk.

(4) The reservoir that contributes to mantle plumes was characterized by low I/Pu and low Xe concentrations early in Earth history compared to the reservoir that became the MORB source, likely due to a smaller proportion of gas accreted from volatile-rich carbonaceous solids.

(5) Numerous early-formed isotopic heterogeneities persist in modern mantle reservoirs. These include ^{129}Xe heterogeneity and I/Pu heterogeneity between plume and MORB sources. $^{3}He/^{22}Ne$ heterogeneity may also be a magma ocean signature.

(6) Long-term mantle processing by partial melting and convective mixing of slabs returned from the surface has affected the radiogenic noble gas isotopic compositions of both plume and MORB sources. MORB sources have signatures of stronger long-term outgassing (high $^{4}He/^{3}He$, $^{21}Ne/^{22}Ne_{E}$, and $^{40}Ar/^{36}Ar$; low $^{136}Xe_{Pu}/^{136}Xe_{TF}$) compared to plume sources.

(7) Influx of atmospheric Ne, Ar, Kr and Xe has affected both plume and MORB mantle source compositions. Influx of atmospheric noble gases became efficient some time after ~2.5 Ga.

(8) The noble gas elemental and isotopic compositions of MORB and plume sources do not require isolation within a hidden reservoir. Signatures of extensive outgassing and atmospheric influx in both sources require the integration of subducted slabs into both mantle reservoirs.

Given the role that luck plays in stumbling upon samples suitable to give mantle source compositions (low atmospheric contamination and little fractionation by degassing), massive analytical campaigns (including volcanic gas samples and solid rocks) are needed to build greater global coverage. Particular attention should be given to measurements in samples with anomalous tungsten isotopic compositions, in light of the complex but intriguing relationships between He and W isotopes (Day et al., 2022; Jackson et al., 2020; Mundl et al., 2017) and seismological features at the base of the mantle (Cottaar et al., 2022). It is notable that heterogeneities formed during accretion or produced by plate tectonics have persisted for billions of years in the plume mantle reservoir. This perhaps indicates that these heterogeneities were introduced into a reservoir that mixes sluggishly by nature, possibly due to a high viscosity or high density. The new

information gleaned from precise measurements (especially of Kr and Xe) must be paired with geophysical modeling studies to better understand what constraints the geochemistry can place on geodynamics.

Acknowledgments

The author thanks David Graham for a thorough and constructive review that greatly improved the manuscript, and is grateful for Catherine Chauvel's patience and smooth editorial handling. RP was supported by National Science Foundation Grant EAR 2145663 and Department of Energy Grant DE-NA0004094.

Figure captions

Figure 1. Decay curves for radioactive isotopes that produce noble gas isotopes. The abundance (N) of the radioactive isotope is shown over time, relative to the initial abundance (N_0). (a) There are two short-lived radioactive isotopes that decay to produce isotopes of Xe (Table 1). ^{129}I decays with a half-life of 16.1 Myr to produce ^{129}Xe, while ^{244}Pu undergoes spontaneous fission with a half-life of 80.0 Myr to produce isotopes of Xe. (b) Isotopes of He, Ne, Ar and Xe are produced by decay of long-lived radioactive isotopes ^{235}U, ^{238}U, ^{232}Th and ^{40}K.

Figure 2. Types of samples for noble gas analysis. Mantle noble gases are measured in a wide variety of samples. Gas samples from wells and springs are collected in (a) a Giggenbach-type sampling vessel and (b) a lead-glass container (panels a and b from Sano and Fischer, 2013). (c) Fresh glass chips from a pillow basalt dredged from the Southwest Indian Ridge (Parai et al., 2012). (d) 3D image obtained by X-ray computed microtomography of a vesicular basalt glass from Galápagos, along with a virtual slice showing interior vesicles. Sample was analyzed by laser ablation to pierce individual vesicles (Péron et al., 2016). I Olivine-bearing basalt glass from subglacial pillows in Iceland (Parai, 2023). (f) Olivines from the Cook-Austral Islands undergoing hand-picking to select clear, pale green crystals (Zhang et al., 2024). (g) Large feldspar crystals from a Greenland anorthosite. Samples in panels (c, e-g) were analyzed by step-crushing of large quantities of material using a steel pestle and hand-pumped hydraulic ram under vacuum.

Figure 3. Concentrations of primordial noble gas isotopes normalized to solar abundances in moles/g. Solar nebular concentrations were calculated based on Lodders (2021) proto-Solar isotopic compositions of the elements, by converting ^{22}Ne, ^{36}Ar, ^{84}Kr and ^{130}Xe atoms per 10^6 atoms of Si to moles per gram of solar nebular material following the approach of Dauphas and Morbidelli (2014; see Figure 62 in Brown, 1949 for a historical perspective). Note that all other concentrations are in moles per gram of rock, but are normalized to moles per gram of solar nebula (see Table 2 for concentrations used to generate the figure). CI chondrite concentrations were computed based on Dauphas and Morbidelli (2014), assuming a chondritic ^{20}Ne/^{22}Ne of 9.0 (Williams and Mukhopadhyay, 2019) and a chondritic ^{3}He/^{22}Ne of 0.89 (Tucker and Mukhopadhyay, 2014). The bulk mantle estimate is from Marty (2012). The MORB and plume mantle estimates are based on model ^{3}He concentrations from Parai (2022) required to explain N. Atlantic MORB 2ΠD43 and Icelandic basalt glass DICE, using elemental ratios from Mukhopadhyay (2012), Tucker and Mukhopadhyay (2014), Williams and Mukhopadhyay (2019) and Péron and Mukhopadhyay (2022). The chondritic pattern is depleted in all gases compared to solar, but most strongly depleted in He and Ne and least depleted in Xe. The enstatite chondrite

South Oman (bearing the subsolar composition; Crabb and Anders, 1981; Ott, 2014) is depleted in Ne and strongly enriched in Ar compared to carbonaceous chondrites. The mantle abundance pattern estimates are broadly in agreement, with the bulk mantle estimate from Marty (2012) most similar to the plume mantle estimate using Parai (2022). There are low overall gas concentrations in the MORB mantle. The mantle patterns are similar to chondrites for the heavy noble gases, with a notable deficit in Xe reflecting the large component of influxed atmosphere in the mantle that carries the "missing Xe" signature.

Figure 4. Highest measured mantle $^{20}Ne/^{22}Ne$ ratios compared to accreted components. Solar wind and solar nebula (Heber et al., 2012), Ne-B (Black, 1972b; Krietsch et al., 2021), Ne-A (Krietsch et al., 2021; Marty, 2022), and the atmospheric composition (Györe et al., 2024) are shown for reference. Error bars are 1σ. Highest measured $^{20}Ne/^{22}Ne$ ratios for dunite from the Kola peninsula in Russia (Yokochi and Marty, 2004), subglacial basalt glass from Iceland (Mukhopadhyay, 2012), and submarine basalt glass from section of the southern Mid-Atlantic Ridge influenced by the Discovery hotspot (Williams and Mukhopadhyay, 2019) are higher than and well-resolved from the Ne-B composition, and the Discovery measurement exceeds the estimate of ~12.9 for dust irradiated by solar wind in a turbulent disk (Moreira and Charnoz, 2016). Dissolution of solar nebular gas into a terrestrial magma ocean could account for such high measurements. The highest $^{20}Ne/^{22}Ne$ ratio measured with high precision in a MORB is ~12.6 (Parai and Mukhopadhyay, 2021).

Figure 5. Kr isotopes in well gases, volcanic gas and rocks. Error bars are 1σ. Well gas data are from Bravo Dome (Holland et al., 2009), Yellowstone volcanic gas is from Broadley et al. (2020), and Iceland and Galápagos basalts are from Péron et al. (2021). The atmospheric composition (Basford et al., 1973), average carbonaceous chondrite (AVCC; Péron et al., 2021), solar wind (Meshik et al., 2013; Ott, 2014), subsolar gas (a component found in some enstatite chondrites; data from South Oman; Crabb and Anders, 1981; Ott, 2014) and Phase Q (Busemann et al., 2000) are shown for comparison. Panel (a) shows $^{82}Kr/^{84}Kr$ plotted against $^{86}Kr/^{84}Kr$ to illustrate the good agreement between well gas the volcanic samples, and the deficit in ^{86}Kr in mantle samples compared to AVCC and Phase Q (Peron et al., 2021). Panel (b) shows $^{82}Kr/^{84}Kr$ plotted against $^{83}Kr/^{84}Kr$, as there is good separation between the AVCC and Phase Q compositions in this space. The Iceland Kr data is within uncertainty of the atmospheric composition in this isotope space. Yellowstone and Galápagos data indicate that mantle Kr is most similar to the average carbonaceous chondrite composition (AVCC).

Figure 6. Primordial Xe isotopes in well gases, volcanic gas and N. Atlantic MORB. High precision data well-resolved from the atmospheric composition are shown, and error bars are 1σ. Well gases are from Caffee et al. (1999) – Caroline, Harding County, Sheep Mountain; Holland et al. (2009) – Bravo Dome. Volcanic gas from Yellowstone (Broadley et al., 2020) and the N.

Atlantic MORB mantle source composition corrected for shallow atmospheric contamination (Péron and Moreira, 2018) are shown along with the atmospheric composition (Basford et al., 1973). Solar wind (Meshik et al., 2020), subsolar (from enstatite chondrite South Oman; Crabb and Anders, 1981; Ott, 2014), Phase Q (Busemann et al., 2000), and the average carbonaceous chondrite (AVCC) (Pepin, 2000) are shown for comparison. An orthogonal least squares best fit forced through atmosphere is shown along with a 1σ envelope. The mantle primordial Xe isotopic composition is most consistent with AVCC or Q. The mantle source composition corrected for shallow atmospheric contamination (Péron and Moreira, 2018) indicates that ~75% of ^{130}Xe in the MORB mantle is influxed atmospheric Xe, and ~25% is ^{130}Xe retained from accretion.

Figure 7. Primordial Ne isotopes versus ^{36}Ar/^{22}Ne (adapted from Williams and Mukhopadhyay, 2019). Mantle source estimates for Galápagos (Péron et al., 2021; Péron and Mukhopadhyay, 2022), Iceland (Mukhopadhyay, 2012), Rochambeau Rift (thought to sample the Samoan plume; Pető et al., 2013) and N. Atlantic MORB 2ΠD43 (separate estimates from Moreira et al., 1998; Parai and Mukhopadhyay, 2021) are consistent with mixing between solar nebula (Heber et al., 2012; Ott, 2014; Lodders, 2021), chondritic (Williams and Mukhopadhyay, 2019; Dauphas and Morbidelli, 2014) and influxed atmospheric Ar and Ne. If the Ne-B component provided Ne to the MORB source mantle, the high ^{36}Ar/^{22}Ne ratio of the MORB source would require addition of Ar from an extremely high ^{36}Ar/^{22}Ne component. The atmospheric composition is shown along with deep ocean water (Williams and Mukhopadhyay, 2019), which has the atmospheric isotopic composition but a fractionated elemental ratio due to differences in noble gas solubility in water. Ranges for altered oceanic crust (Chavrit et al., 2016) and serpentinites (or their metamorphosed equivalents; Kendrick et al., 2018) that could carry the atmospheric influx into the mantle are shown. MORB and plume sources may incorporate influxed atmospheric gas with distinct ^{36}Ar/^{22}Ne ratios, potentially with a higher ^{36}Ar/^{22}Ne in slab materials incorporated into plume sources.

Figure 8. Primordial Ne isotopes versus ^{130}Xe/^{22}Ne (adapted from Williams and Mukhopadhyay, 2019). Mantle source estimates for Galápagos (Péron et al., 2021; Péron and Mukhopadhyay, 2022), Iceland (Mukhopadhyay, 2012), Hawaii (Valbracht et al., 1997); Rochambeau Rift (thought to sample the Samoan plume; Pető et al., 2013) and N. Atlantic MORB 2ΠD43 (separate estimates with different mantle source ^{20}Ne/^{22}Ne: 12.5 from Moreira et al., 1998; 12.6 from Parai and Mukhopadhyay, 2021) are consistent with mixing between solar nebula (Heber et al., 2012; Ott, 2014; Lodders, 2021), chondritic (Williams and Mukhopadhyay, 2019; Dauphas and Morbidelli, 2014) and influxed atmospheric Xe and Ne. The MORB composition requires a greater contribution from non-solar components. Mixing model best fit ^{130}Xe/^{22}Ne for the atmospheric influx component in the N. Atlantic MORB mantle and Iceland mantle sources from Parai (2022) are shown. Other plume-influenced mantle sources are consistent with the Iceland mantle mixing model, and suggest that slabs subducted into plume sources are broadly

characterized by high $^{130}Xe/^{22}Ne$ compared to the N. Atlantic MORB mantle. The 2ΠD43 mantle composition estimated based on Moreira et al. (1998) is consistent with the MORB mixing model constructed using data from Parai and Mukhopadhyay (2021). Panel (b) shows zoomed-in detail of mantle sources and the Parai (2022) mixing models: the MORB mixing model has a greater contribution from chondrites in the mix of accreted volatiles (pink dashed line between solar nebula and CI chondrites; see Figure 26); influxed atmospheric gases are added to the accreted composition over time. Despite the similarity between MORB source $^{20}Ne/^{22}Ne$ and Ne-B (Ballentine et al., 2005), solar wind irradiated material (Ne-B) cannot provide all of the Ne in the MORB source mantle; a contribution from a component with an extremely high $^{130}Xe/^{22}Ne$ would be required to explain the high MORB source Xe/Ne ratio, and this component would then dominate the Xe isotopic composition of the MORB source mantle. Neither influxed atmospheric gas carried in slabs nor the subsolar component in enstatite chondrites (panel a; Crabb and Anders, 1981; Ott, 2014) can provide high Xe/Ne gas to the MORB source, as Xe primordial isotopes in MORB mantle samples are not consistent with either of those components (Figure 6).

Figure 9. $^{3}He/^{22}Ne$ in data from samples with unfractionated elemental ratios. Data are from Iceland (Mukhopadhyay, 2012), Galápagos (Péron et al., 2016), and the N. Atlantic MORB 2ΠD43 (Moreira et al., 1998; Parai and Mukhopadhyay, 2021). Error bars are 1σ. The solar nebula composition is shown for reference (Heber et al., 2012; Tucker and Mukhopadhyay, 2014). Only samples with $^{21}Ne^{*}/^{4}He$ ratios similar to the mantle production ratio (Graham, 2002; Yatsevich and Honda, 1997) are shown to avoid elemental fractionation due to magmatic degassing. The atmospheric composition is at the lower left. Variation in the step crush data reflects variable atmospheric contamination. Plume mantle source compositions have high $^{20}Ne/^{22}Ne$ and relatively low $^{3}He/^{22}Ne$, while the MORB sample with unfractionated He/Ne has a mantle source $^{20}Ne/^{22}Ne$ of ~12.6 and a higher $^{3}He/^{22}Ne$. Data from depleted MORB samples from the Equatorial Atlantic were corrected for fractionation during degassing, yielding higher MORB source values $^{3}He/^{22}Ne$ that extend beyond the values shown here (up to ~10; Tucker and Mukhopadhyay, 2014), potentially indicating MORB mantle $^{3}He/^{22}Ne$ heterogeneity.

Figure 10. $^{20}Ne/^{22}Ne$-$^{129}Xe/^{130}Xe$ mixing systematics in basalts analyzed by step-crushing. Samples that yielded a wide range of $^{20}Ne/^{22}Ne$ ratios were selected. MORB data are from the N. Mid-Atlantic Ridge (Moreira et al., 1998; Parai and Mukhopadhyay, 2021) and SWIR (Parai et al., 2012). Selected plume data are from Hawaii (Trieloff et al., 2000), Iceland (Mukhopadhyay, 2012), and Rochambeau Rift (thought to sample the Samoan plume; Pető et al., 2013). Error bars are 1σ. Syn– to post-eruptive atmospheric contamination generates hyperbolic mixing arrays between the atmospheric composition and mantle sources. Mantle source $^{129}Xe/^{130}Xe$ compositions at high $^{20}Ne/^{22}Ne$ ratios are high in MORB sources compared to plume sources.

Figure 11. He-Xe mixing systematics in basalts analyzed by step-crushing. Data for N. Atlantic MORB (Moreira et al., 1998; Parai and Mukhopadhyay, 2021), Iceland (Mukhopadhyay, 2012), and Rochambeau Rift (thought to sample the Samoan plume; Pető et al., 2013) are shown with 1σ error bars. To avoid samples with fractionated elemental ratios, only samples with $^{4}He/^{40}Ar^{*}$ and $^{4}He/^{21}Ne^{*}$ ratios similar to mantle production ratios are show. Syn- to post-eruptive atmospheric contamination generates linear mixing arrays between the atmospheric composition and mantle sources. The N. Atlantic MORB source has a high $^{129}Xe/^{130}Xe$ compared to the plume sources. The distinct slopes in this space indicate that the low $^{129}Xe/^{130}Xe$ in plume sources cannot be explained by different degrees of injection of atmospheric gas into these mantle sources, and that they instead reflect an early-formed mantle heterogeneity from decay of ^{129}I that has not been mixed away by ~4.45 Gyr of convection.

Figure 12. $^{128}Xe/^{130}Xe$ vs. $^{129}Xe/^{130}Xe$ evidence for early-formed $^{129}Xe/^{130}Xe$ heterogeneity. Average or most mantle-like compositions from plume-influenced and upper mantle samples are shown along with total least squares fits forced through the atmospheric composition. Error bars are 1σ. Iceland crush data point is from Parai (2023); Iceland and Galápagos screened accumulated gas data are from Péron et al. (2021). The individual measurements (small symbols) and average (large symbol) are shown for the Iceland screened gas, but only the average was used to compute the best plume slope and its uncertainty. Yellowstone volcanic gases are from Broadley et al. (2020) and Bekaert et al. (2023). The slope of the plume fit is strongly affected by the precisely-determined Yellowstone 4B average, which may reflect some mass-dependent fractionation in the hydrothermal system (Bekaert et al., 2023). The upper mantle fit is based on screened gas from the N. Atlantic popping rock (Péron and Moreira, 2018), Bravo Dome 20B well gas (Holland and Ballentine, 2006), and well gas data from Caffee et al. (1999). Despite a larger uncertainty in the plume fit, the plume and upper mantle fits have distinct slopes. Distinct trends radiating from atmosphere in $^{128}Xe/^{130}Xe$ vs. $^{129}Xe/^{130}Xe$ support an early-formed $^{129}Xe/^{130}Xe$ heterogeneity from I/Xe heterogeneity within the mantle during the lifetime of ^{129}I, not from differential influx of atmospheric Xe into mantle reservoirs.

Figure 13. Fissiogenic Xe isotopic compositions. AVCC, Pu fission Xe and U-fission Xe compositions are shown along with the modern and past atmospheric compositions (Alexander et al., 1971; Basford et al., 1973; Eikenberg et al., 1993; Hebeda et al., 1987; Hudson et al., 1989; Lewis, 1975; Pepin, 2000; Ragettli et al., 1994; Wetherill, 1953). The initial mantle composition (for both plume and MORB sources) is likely similar to average carbonaceous chondrites. Throughout Earth history, ingrowth of fissiogenic Xe has changed mantle isotopic compositions. Spontaneous fission of ^{244}Pu and ^{238}U produce $^{131,132,134,136}Xe$ in distinct, characteristic ratios, seen in this figure with the relatively high $^{136}Xe/^{132}Xe$ in the U-fission component compared to Pu-fission Xe. Pu-fission dominated for the first several hundred Myr, after which point U-fission

became the major source of fissiogenic Xe. Influx of atmospheric Xe would shift the mantle composition towards the atmospheric composition at the time.

Figure 14. $^{129}Xe^*/^{136}Xe_{Pu}$ vs. the fraction of fissiogenic Xe from Pu-fission in mantle sources. Plume Xe isotope ratios are shown for Iceland (Mukhopadhyay, 2012) and Rochambeau Rift (thought to sample the Samoan plume; Pető et al., 2013). Xe ratios are shown for MORB sources from the Equatorial Atlantic (Tucker et al., 2012), Southwest Indian Ridge Eastern and Western Orthogonal Supersegment (EOSS and WOSS; Parai et al., 2012), N. Mid-Atlantic Ridge (Parai and Mukhopadhyay, 2021). Mantle sources of CO_2 well gases (Caffee et al., 1999; Holland and Ballentine, 2006) are also shown and are consistent with the MORB source compositions. Medians and 68% confidence intervals are shown. Variation in $^{129}Xe^*/^{136}Xe_{Pu}$ (x-axis) could reflect the time that open system outgassing during accretion ceased (closure age), I/Pu heterogeneity, or a combination of these. Variation in the $^{136}Xe_{Pu}/^{136}Xe_{TF}$ (y-axis) reflects the extent of long-term outgassing. Plume and MORB source mantle compositions carry distinct signatures, with a difference in long-term processing superimposed on early heterogeneity.

Figure 15. Schematic diagram of mass transfer and gas transport during mantle processing. This illustration underpins some recent box models of mantle noble gas isotopic evolution (Gonnermann and Mukhopadhyay, 2009; Parai, 2022; Parai and Mukhopadhyay, 2018; Zhang et al., 2023). Boxes for the atmosphere, lithosphere, and a mantle reservoir are shown (only one mantle reservoir is shown for simplicity). A sequence of events is illustrated in this diagram; note that lower portion of the mantle reservoir box depicts steps later in the sequence and should not be interpreted as a depiction of a deeper portion of the mantle reservoir. The lithosphere includes sediments, the crust and lithospheric mantle (LM). For helium, atmospheric influx is thought to be insignificant (Section 5.1), whereas for heavier noble gases, influx of atmospheric gases beyond depths of magma generation adds gas with a distinct isotopic composition into the mantle. In the box labeled (1), partial melting of the mantle generates a melt and depleted residue. Mantle noble gases are concentrated in the melt. The mass of material in box (1) is transferred from the mantle to the lithosphere (and an equal mass of lithosphere is subducted into the mantle; box 3). During eruption at the surface (2), mantle gas is transported from the melt to the atmosphere, leaving the crust and depleted residue with low gas concentrations. The box labeled (3) represents subducted lithosphere. Atmospheric Ne, Ar, Kr and Xe may be carried by sediments, altered oceanic crust (AOC) or serpentinized lithospheric mantle in the subducting slab. If these gases are retained in the slab beyond depths of magma generation, the atmospheric gases are influxed to the mantle. Otherwise, they return to the surface through arc volcanism. Over time, subducted slabs (4) are stretched and incorporated into ambient mantle by convective mixing (5). In the case of no atmospheric influx (He), the concentration of mantle gas in the reservoir becomes progressively depleted by mixing in gas-poor crust and lithospheric mantle. In the case where atmospheric gas is influxed (heavy noble gases), the concentration of mantle gas in the reservoir becomes

progressively depleted but atmospheric gas is also added as slabs are mixed into the mantle reservoir.

Figure 16. $^{4}He/^{3}He$ in data compilations of oceanic basalts from (Moreira, 2013). OIBs exhibit a wider range of He isotope ratios, and MORBs fall in the central ~50% of that range. The median OIB has a lower $^{4}He/^{3}He$, signifying a less-outgassed mantle source. The highest $^{4}He/^{3}He$ ratios are generally found in HIMU OIBs (though inclusion of MORB data from the Chile Ridge would extend the MORB range up to ~200,000; Sturm et al., 1999). Using $^{3}He/^{4}He$ ratios normalized to atmosphere (R/Ra) makes the MORB range (~7-9 Ra) appear narrower and closer to the more-outgassed end of the OIB range (~4 to 62 Ra).

Figure 17. Correction for syn- to post-eruptive atmospheric contamination of Ne isotopes. Data generated by step-crushing of Galápagos basalt glass sample D22B are shown with 1σ error bars (Kurz et al., 2009; Péron et al., 2016; Péron et al., 2021). The ratio of two primordial isotopes ($^{20}Ne/^{22}Ne$) is plotted against the ratio of nucleogenic ^{21}Ne to primordial ^{22}Ne, and mixing is linear in this space. The step-crush data define a linear array reflecting variable syn- to post-eruptive atmospheric contamination of the mantle composition. The mantle source $^{21}Ne/^{22}Ne_E$ composition is determined by extrapolating the orthogonal least-squares line of best fit to a model mantle $^{20}Ne/^{22}Ne$ ratio, which assumed for Galápagos to be that in solar nebular gas (13.36). The mantle source composition corrected for syn- to post-eruptive atmospheric contamination can then be compared to other mantle source compositions.

Figure 18. Ne isotope arrays in selected mantle samples. Data generated by step-crushing of oceanic basalts are shown with 1σ error bars for the N. Mid-Atlantic Ridge (AL4818-003 from Péron et al., 2019; 2ΠD43 from Parai and Mukhopadhyay, 2021), SWIR (AG22 1-1&1-4 from Parai et al., 2012), Rochambeau Rift (thought to sample the Samoan plume; NLD-27 from Pető et al., 2013), Galápagos (D22B from Kurz et al., 2009; Péron et al., 2016; Péron et al., 2021), and Discovery Ridge segment of the southern Mid-Atlantic Ridge influenced by the Discovery plume (EW9309-5D from Williams and Mukhopadhyay, 2019). The solar nebula composition is from Heber et al. (2012). Syn- to post-eruptive atmospheric contamination generates linear arrays radiating out from the atmospheric composition. Mantle $^{21}Ne/^{22}Ne_E$ ratios in MORB sources are generally higher than those in plume sources, indicating a greater extent of outgassing. The mantle source $^{20}Ne/^{22}Ne$ ratios of MORB sources may be lower than those of plume sources. Mantle sources with plume and depleted mantle mixtures may have intermediate source $^{20}Ne/^{22}Ne$ along with intermediate $^{21}Ne/^{22}Ne_E$ (Pető et al., 2013; Williams and Mukhopadhyay, 2019). The lower source $^{20}Ne/^{22}Ne$ could reflect a greater contribution from chondrites during accretion and greater atmospheric influx of Ne (Figures 15, 25; Parai, 2022).

Figure 19. $^{4}He/^{3}He$ vs. $^{21}Ne/^{22}Ne_E$ in MORBs and OIBs (from Moreira, 2013 with annotations added in pink). He and Ne from Baffin Island picrites (Horton et al., 2021; Horton et al., 2023) and Rochambeau Rift (Pető et al., 2013) are added to the compilation, with $^{21}Ne/^{22}Ne_E$ computed at a mantle source $^{20}Ne/^{22}Ne$ of 12.5 for consistency with the rest of the data compilation. Mixing between two components, A and B, in this space generates a hyperbola with curvature factor r = $(^{3}He/^{22}Ne)_B/(^{3}He/^{22}Ne)_A$. A strong contrast in $^{3}He/^{22}Ne$ ratios between mixing components translates to a strongly curved hyperbola. The dominant curvature evident in this compilation indicates that the more-outgassed component with high $^{4}He/^{3}He$ and high $^{21}Ne/^{22}Ne_E$ (MORB sources) has a high $^{3}He/^{22}Ne$ ratio compared to the less-outgassed component (plume sources). However, there is scatter in the compiled data and other curvatures may be evident in the array (*e.g.,* Baffin, Loihi, Rochambeau Rift).

Figure 20. Correction for syn- to post-eruptive atmospheric contamination of Ar isotopes. Data generated by step-crushing of a basalt glass from the SWIR (AII107-6 57-5; Parai et al., 2012) are shown with 1σ error bars. The ratio of two primordial isotopes ($^{20}Ne/^{22}Ne$) is plotted against the ratio of radiogenic ^{40}Ar to primordial ^{36}Ar. The step-crush data define a hyperbolic array reflecting variable syn- to post-eruptive atmospheric contamination of the mantle composition. The mantle source $^{40}Ar/^{36}Ar_E$ composition is determined by extrapolating the orthogonal least-squares hyperbola of best fit to a model mantle $^{20}Ne/^{22}Ne$ ratio, which was assumed for this MORB to be 12.5. The mantle source composition corrected for syn- to post-eruptive atmospheric contamination can then be compared to mantle source compositions for other localities.

Figure 21. $^{20}Ne/^{22}Ne$-$^{40}Ar/^{36}Ar$ mixing systematics in basalts analyzed by step-crushing. Samples that yielded a wide range of $^{20}Ne/^{22}Ne$ ratios were selected for plotting with 1σ error bars. MORB data are from the N. Mid-Atlantic Ridge (Moreira et al., 1998; Parai and Mukhopadhyay, 2021; Péron et al., 2019) and SWIR (Parai et al., 2012). Selected plume data are from Hawaii (Trieloff et al., 2000), Réunion (Trieloff et al., 2002), Iceland (Mukhopadhyay, 2012), and Galápagos (Péron et al., 2016). Syn- to post-eruptive atmospheric contamination generates hyperbolic mixing arrays between the atmospheric composition and mantle sources. Mantle source $^{40}Ar/^{36}Ar$ compositions at high $^{20}Ne/^{22}Ne$ ratios are high in MORB sources compared to plume sources.

Figure 22. Iceland fissiogenic Xe isotopes and models of mantle Xe isotopic evolution, adapted from Parai (2022). The Iceland composition (2σ error bars) requires a contribution from Pu-fission. In the reference case, the initial model mantle $^{130}Xe_i$ concentration is 1.5×10^{8} atoms/g and 3 reservoir masses are processed over Earth history (N_{res} = 3). Model mantle compositions start at AVCC and incorporate fissiogenic and regassed atmospheric Xe over time. Arrays of present-day outcomes radiate from atmosphere, reflecting variable mixtures of atmospheric Xe

influx, fissiogenic and initial gas retained in the mantle today. (a) The effect of changing the extent of mantle processing given a constant $^{130}Xe_i$. Limiting the amount of outgassing generates present-day compositions where Pu-fission dominates over U-fission Xe, but the overall impact of fission can be muted because the initial gas budget is largely retained; reducing N_{res} in panel (a) rotates outcome arrays towards AVCC, and cannot explain Iceland Xe. Stronger outgassing cannot explain the Iceland composition either: higher N_{res} depletes initial Xe and Pu-fission Xe, and arrays rotate towards, but never past, a mixing line between atmospheric and U-fission Xe (see overlap between outcomes for N_{res} of 8 and 15). (b) The effect of changing the initial $^{130}Xe_i$ concentration given a constant N_{res}. Decreasing $^{130}Xe_i$ rotates arrays away from AVCC. Low $^{130}Xe_i$ can explain Iceland Xe.

Figure 23. Best fit model input parameters to explain plume and MORB He-Ne-Xe isotopes, adapted from Parai (2022). The Iceland and N. Mid-Atlantic Ridge compositions are well-explained by a forward model of He-Ne-Xe isotopic evolution. The score for a given pairing is the sum of squared sigma-normalized residuals for He, Ne and Xe isotope ratios, with Xe isotope ratio residuals weighted double. Only scores below 50 are shown in the figure, and the lowest scores (darkest colors) represent the best fits. The isotopic evolution model succeeds in simultaneously reproducing present-day mantle He, Ne and Xe isotopic and elemental ratios for model realizations that pair low extents of outgassing with low initial ^{130}Xe concentrations in the plume source relative to the MORB source. However, the initial ^{3}He and ^{22}Ne concentrations in the model plume mantle are higher than those in the MORB mantle due to higher, more solar-like $^{3}He/^{130}Xe$ and $^{22}Ne/^{130}Xe$ (Figures 8, 11). A difference in the extent of outgassing is necessary but not sufficient to explain plume and MORB noble gas signatures; a difference in initial gas concentrations and abundance patterns is also required.

Figure 24. Results of the linear least squares analysis of mantle source Xe isotope compositions, adapted from Parai (2022). (a) Precisely-determined mantle source compositions for Iceland (Mukhopadhyay, 2012) and N. Mid-Atlantic Ridge MORB (Parai and Mukhopadhyay, 2021) are shown in $^{136}Xe/^{132}Xe$ – $^{130}Xe/^{132}Xe$ space (2σ error bars). The atmospheric composition is shown as a cyan square and mixing towards the average carbonaceous chondrite (AVCC) Xe composition is illustrated with stars marking the proportions of ^{130}Xe from an influx of atmospheric gas into the mantle. Lines showing addition of Pu-fission Xe or U-fission Xe are shown radiating out from the stars, mapping out variable mixtures of the four components in this isotope space. Best-fit contributions of ^{132}Xe from regassed atmosphere, initial Xe from accretion, Pu-fission and U-fission can be determined by linear least squares using multiple Xe isotope ratios. Median solutions for component contributions of ^{132}Xe for the (b) Iceland sample DICE and (c) N. Atlantic popping rock 2ΠD43 both illustrate that mantle sources are dominated by influxed atmospheric Xe contributions. The fissiogenic Xe signature of the Iceland mantle source is

dominated by Pu-fission Xe, while the 2ΠD43 MORB mantle source Xe composition is consistent with a stronger U-fission Xe signature.

Figure 25. Mantle source He, Ne, Ar and Xe isotopic compositions in selected localities, modified from Parai et al. (2019). Mantle source compositions for plume-influenced locations show signatures of lower extents of outgassing (low $^{4}He/^{3}He$ and low $^{40}Ar/^{36}Ar_{E}$). However, among MORBs from the SWIR, there are large variations in $^{40}Ar/^{36}Ar_{E}$ and $^{129}Xe/^{130}Xe_{E}$ for a narrow range of $^{4}He/^{3}He$ ratios. These variations are not likely to reflect variable outgassing of the mantle source, and instead may reflect atmospheric influx related to the Dupal anomaly.

Figure 26. Proportions of ^{22}Ne from solar, chondritic or influxed atmosphere origins, adapted from Parai (2022). Solutions are shown for Iceland mantle source (Mukhopadhyay, 2012) and N. Atlantic MORB mantle source (Parai and Mukhopadhyay, 2021). Solar contributions dominate mantle Ne. The MORB source requires a greater contribution of chondritic Ne during accretion, consistent with the higher initial Xe concentration (Figure 23). The MORB source also shows a greater contribution from influxed atmospheric Ne, consistent with the greater extent of processing (Figure 23) which would bring more subducted slabs bearing atmospheric gas into the MORB source (Figure 15).

Fig 1.

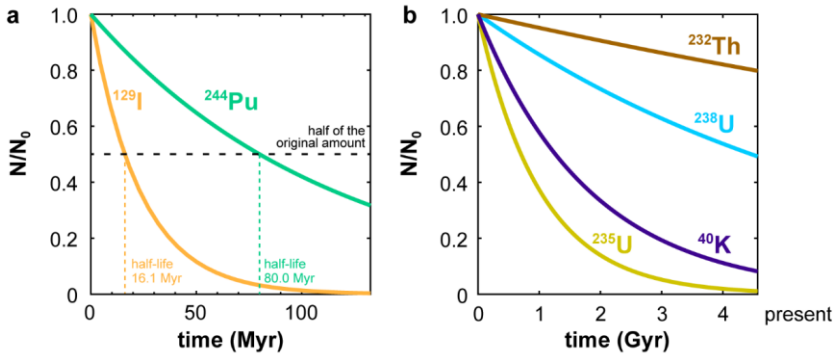
a
b
N/N0
1.0
0.8
0.6
0.4
0.2
0
129I
244Pu
half of the original amount
half-life 16.1 Myr
half-life 80.0 Myr
0
50
100
time (Myr)
232Th
238U
235U
40K
1
2
3
4
present
time (Gyr)

Fig. 2

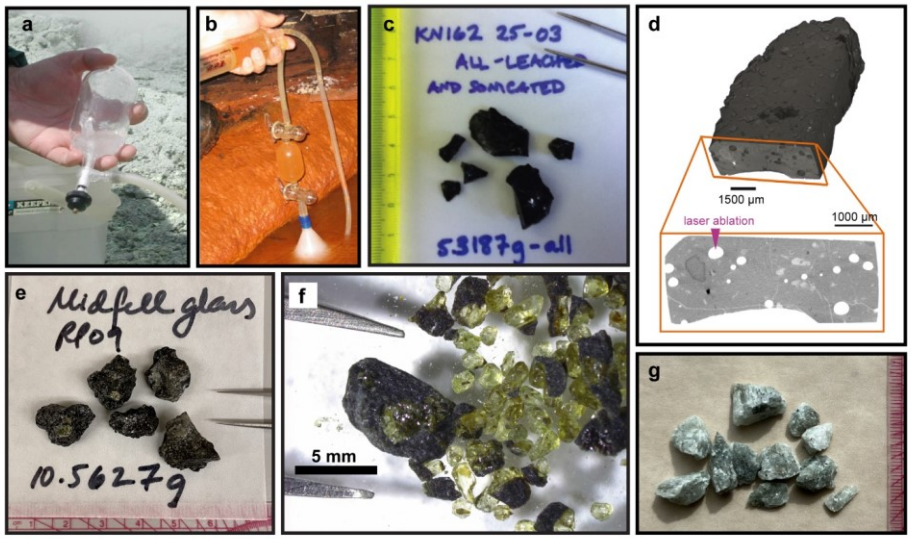
a
b
c
KN162 25-03
ALL-LEACHED
AND SONICATED
53187g-all
d
1500 µm
laser ablation
1000 µm
e
Midfell glass
Rlog
10.5627g
f
5 mm
g

Fig. 3

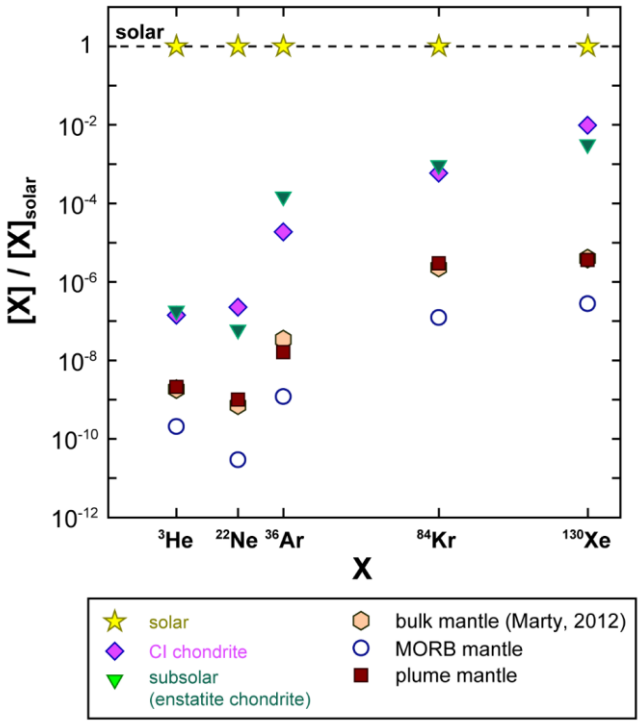
solar
1
10^{-2}
10^{-4}
10^{-6}
10^{-8}
10^{-10}
10^{-12}
[X] / [X]solar
^{3}He
^{22}Ne
^{36}Ar
^{84}Kr
^{130}Xe
X
solar
CI chondrite
subsolar
(enstatite chondrite)
bulk mantle (Marty, 2012)
MORB mantle
plume mantle

Fig. 4

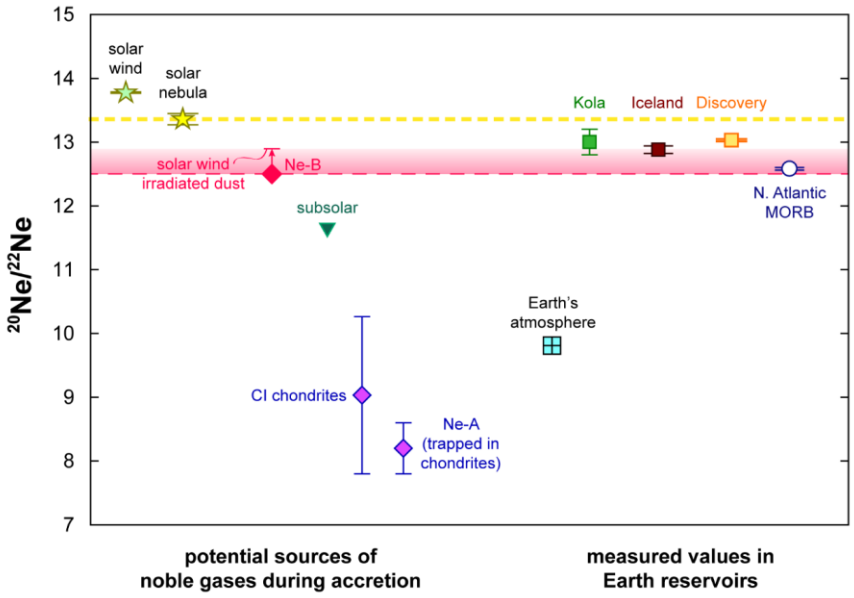
15
14
13
12
11
10
9
8
7
$^{20}Ne/^{22}Ne$
solar wind
solar nebula
solar wind irradiated dust
Ne-B
subsolar
CI chondrites
Ne-A (trapped in chondrites)
Earth's atmosphere
Kola
Iceland
Discovery
N. Atlantic MORB
potential sources of noble gases during accretion
measured values in Earth reservoirs

Fig. 5

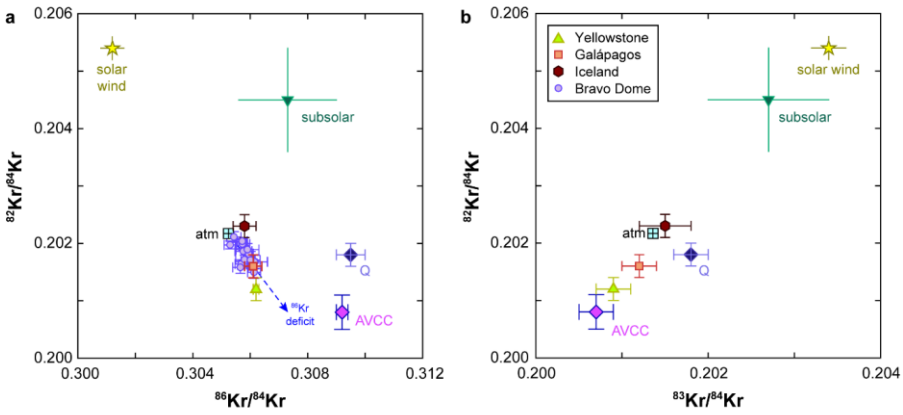
a
b
solar wind
subsolar
atm
Q
AVCC
^{86}Kr deficit
Yellowstone
Galápagos
Iceland
Bravo Dome
^{82}Kr/^{84}Kr
^{86}Kr/^{84}Kr
^{83}Kr/^{84}Kr
0.200
0.202
0.204
0.206
0.300
0.304
0.308
0.312

Fig. 6

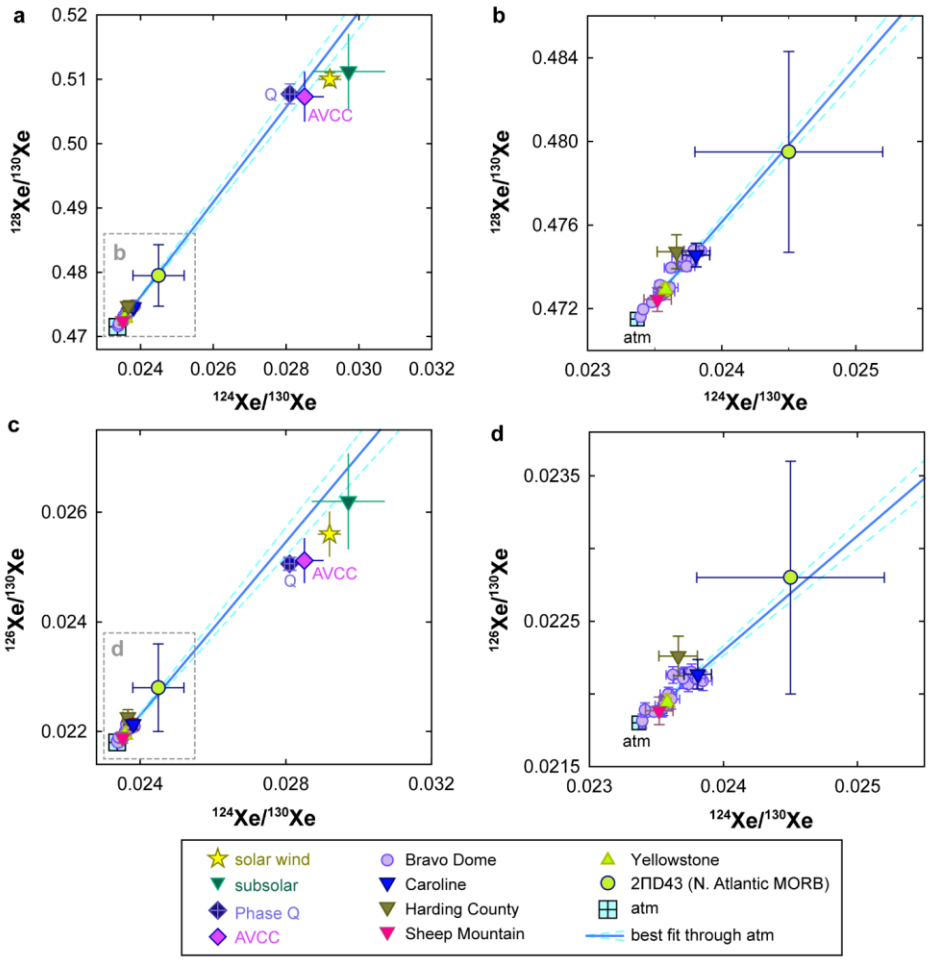
a
b
c
d
$^{128}Xe/^{130}Xe$
$^{124}Xe/^{130}Xe$
$^{126}Xe/^{130}Xe$
Q
AVCC
atm
solar wind
subsolar
Phase Q
AVCC
Bravo Dome
Caroline
Harding County
Sheep Mountain
Yellowstone
2ПД43 (N. Atlantic MORB)
atm
best fit through atm

Fig. 7

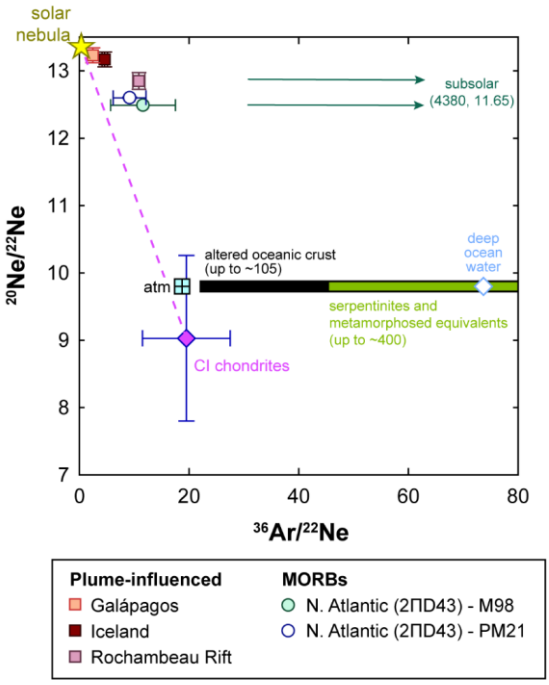
solar nebula
subsolar (4380, 11.65)
altered oceanic crust (up to ~105)
deep ocean water
atm
serpentinites and metamorphosed equivalents (up to ~400)
CI chondrites
$^{20}Ne/^{22}Ne$
$^{36}Ar/^{22}Ne$
13
12
11
10
9
8
7
0
20
40
60
80
Plume-influenced
Galápagos
Iceland
Rochambeau Rift
MORBs
N. Atlantic (2ПД43) - M98
N. Atlantic (2ПД43) - PM21

Fig. 8

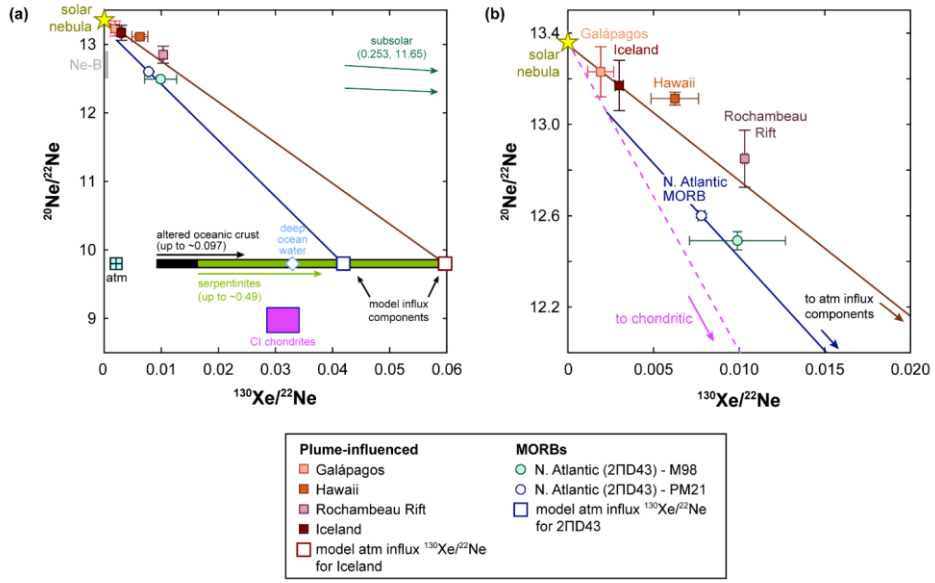
(a)
solar nebula
Ne-B
subsolar (0.253, 11.65)
altered oceanic crust (up to ~0.097)
deep ocean water
atm
serpentinites (up to ~0.49)
model influx components
CI chondrites
$^{20}Ne/^{22}Ne$
$^{130}Xe/^{22}Ne$
(b)
Galápagos
Iceland
solar nebula
Hawaii
Rochambeau Rift
N. Atlantic MORB
to chondritic
to atm influx components
$^{20}Ne/^{22}Ne$
$^{130}Xe/^{22}Ne$
Plume-influenced
Galápagos
Hawaii
Rochambeau Rift
Iceland
model atm influx $^{130}Xe/^{22}Ne$ for Iceland
MORBs
N. Atlantic (2ΠD43) - M98
N. Atlantic (2ΠD43) - PM21
model atm influx $^{130}Xe/^{22}Ne$ for 2ΠD43

Fig. 9

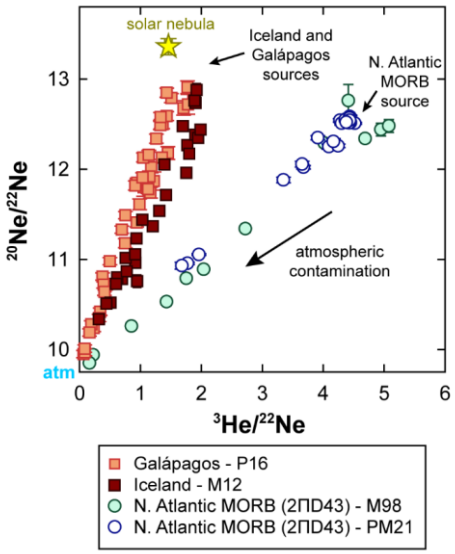
solar nebula
Iceland and Galápagos sources
N. Atlantic MORB source
atmospheric contamination
atm
$^{20}Ne/^{22}Ne$
$^{3}He/^{22}Ne$
0
1
2
3
4
5
6
10
11
12
13
Galápagos - P16
Iceland - M12
N. Atlantic MORB (2ПД43) - M98
N. Atlantic MORB (2ПД43) - PM21

Fig. 10

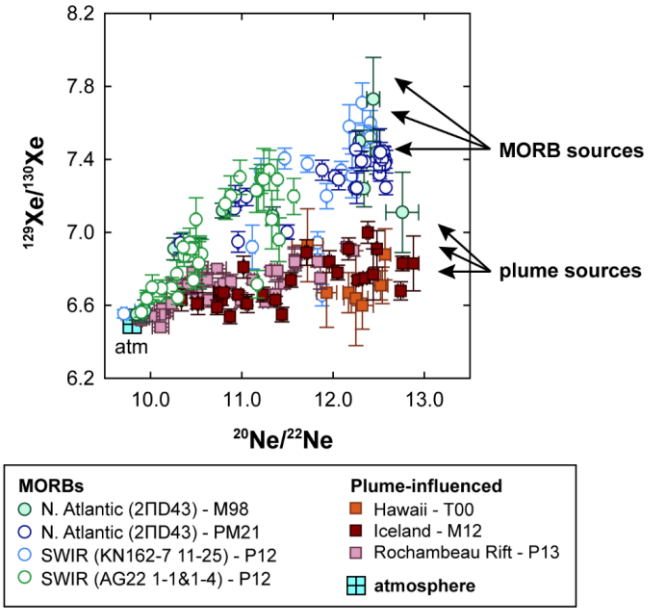
8.2
7.8
7.4
7.0
6.6
6.2
10.0
11.0
12.0
13.0
$^{129}Xe/^{130}Xe$
$^{20}Ne/^{22}Ne$
atm
MORB sources
plume sources
MORBs
N. Atlantic (2ПД43) - M98
N. Atlantic (2ПД43) - PM21
SWIR (KN162-7 11-25) - P12
SWIR (AG22 1-1&1-4) - P12
Plume-influenced
Hawaii - T00
Iceland - M12
Rochambeau Rift - P13
atmosphere

Fig. 11

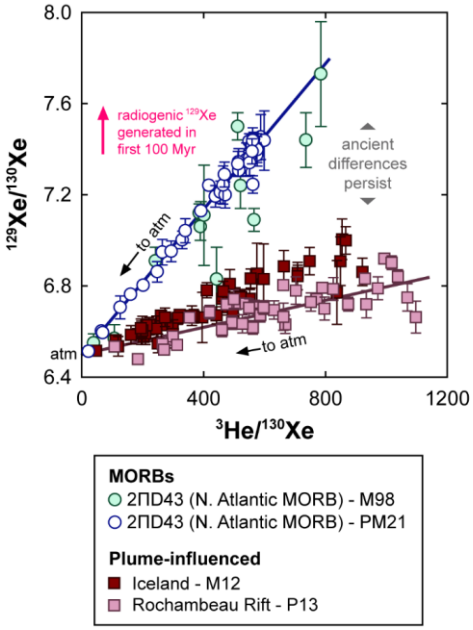
8.0
7.6
7.2
6.8
6.4
atm
0
400
800
1200
$^{129}Xe/^{130}Xe$
$^{3}He/^{130}Xe$
radiogenic ^{129}Xe generated in first 100 Myr
ancient differences persist
to atm
to atm
MORBs
2ПD43 (N. Atlantic MORB) - M98
2ПD43 (N. Atlantic MORB) - PM21
Plume-influenced
Iceland - M12
Rochambeau Rift - P13

Fig. 12

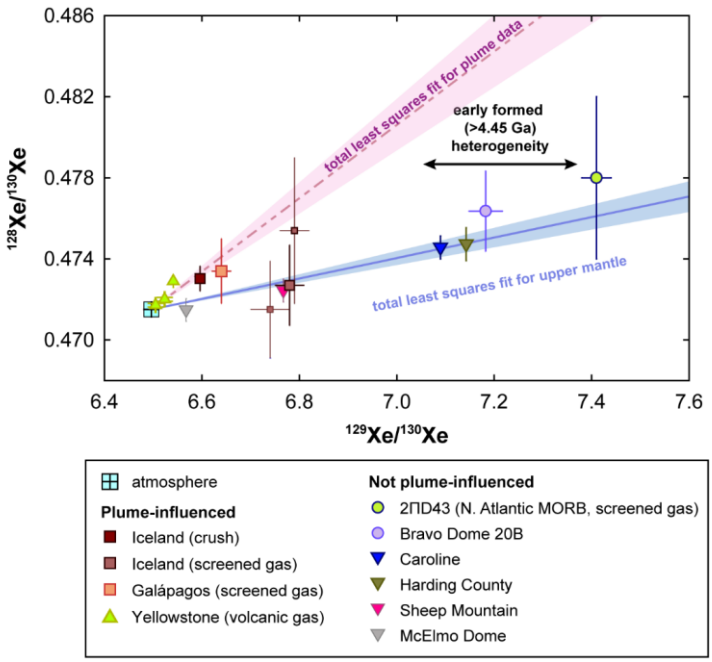
0.486
0.482
0.478
0.474
0.470
$^{128}Xe/^{130}Xe$
6.4
6.6
6.8
7.0
7.2
7.4
7.6
$^{129}Xe/^{130}Xe$
total least squares fit for plume data
early formed
(>4.45 Ga)
heterogeneity
total least squares fit for upper mantle
atmosphere
Plume-influenced
Iceland (crush)
Iceland (screened gas)
Galápagos (screened gas)
Yellowstone (volcanic gas)
Not plume-influenced
2ΠD43 (N. Atlantic MORB, screened gas)
Bravo Dome 20B
Caroline
Harding County
Sheep Mountain
McElmo Dome

Fig. 13

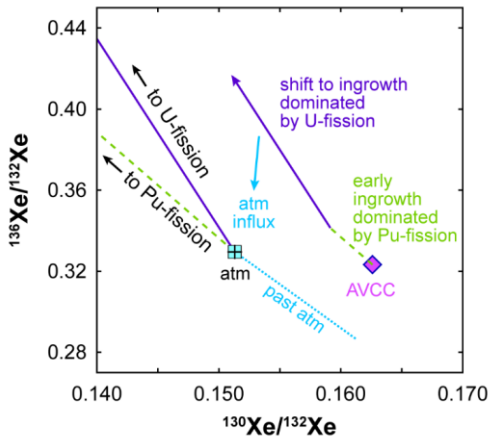
0.44
0.40
0.36
0.32
0.28
0.140
0.150
0.160
0.170
$^{136}Xe/^{132}Xe$
$^{130}Xe/^{132}Xe$
to U-fission
to Pu-fission
shift to ingrowth
dominated
by U-fission
atm
influx
early
ingrowth
dominated
by Pu-fission
atm
AVCC
past atm

Fig. 14

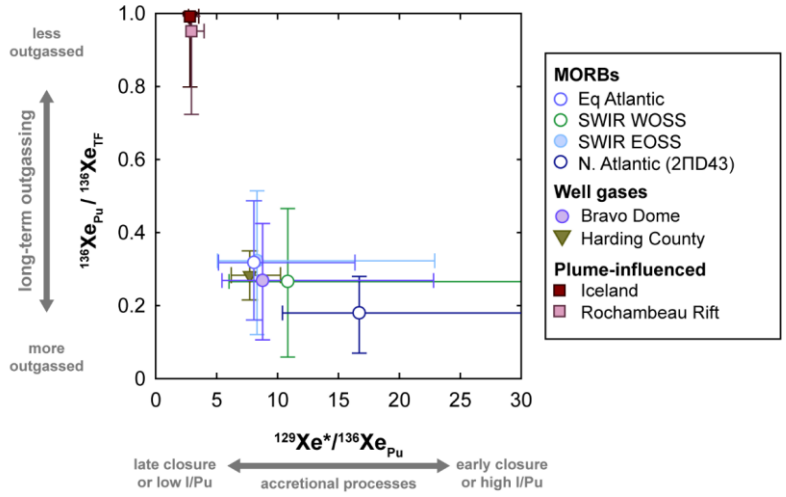
less outgassed
long-term outgassing
more outgassed
$^{136}Xe_{Pu}$ / $^{136}Xe_{TF}$
1.0
0.8
0.6
0.4
0.2
0
0
5
10
15
20
25
30
$^{129}Xe^{*}/^{136}Xe_{Pu}$
late closure or low I/Pu
accretional processes
early closure or high I/Pu
MORBs
Eq Atlantic
SWIR WOSS
SWIR EOSS
N. Atlantic (2ПD43)
Well gases
Bravo Dome
Harding County
Plume-influenced
Iceland
Rochambeau Rift

Fig. 15

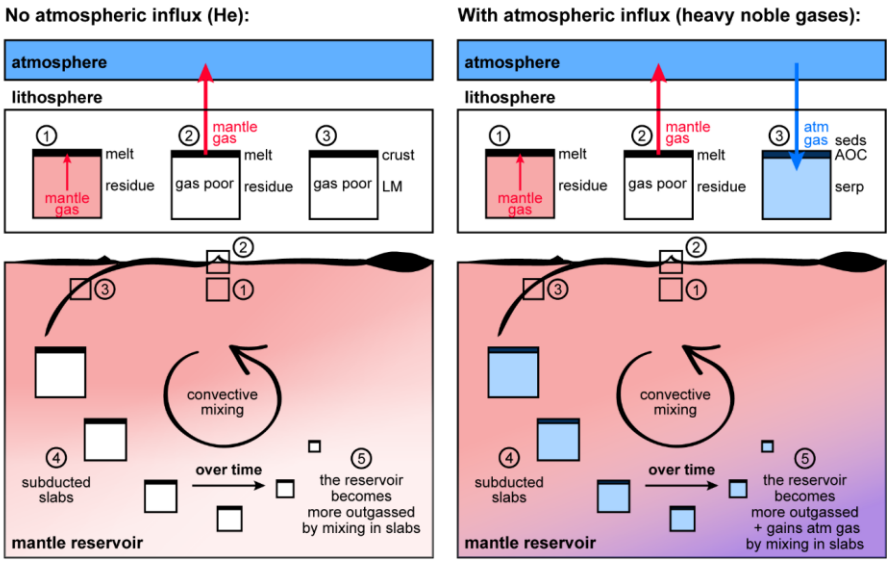
No atmospheric influx (He):
With atmospheric influx (heavy noble gases):
atmosphere
lithosphere
mantle gas
melt
residue
gas poor
crust
LM
atm gas
seds
AOC
serp
convective mixing
subducted slabs
over time
the reservoir becomes more outgassed by mixing in slabs
the reservoir becomes more outgassed + gains atm gas by mixing in slabs
mantle reservoir

Fig. 16

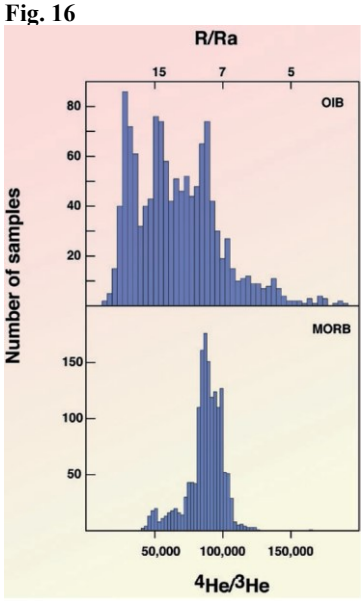
R/Ra
15
7
5
OIB
80
60
40
20
MORB
150
100
50
Number of samples
50,000
100,000
150,000
4He/3He

Fig. 17

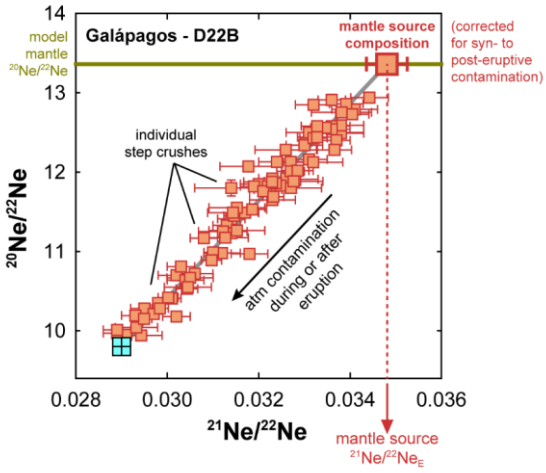
Galápagos - D22B
model mantle $^{20}Ne/^{22}Ne$
mantle source composition
(corrected for syn- to post-eruptive contamination)
individual step crushes
atm contamination during or after eruption
$^{20}Ne/^{22}Ne$
$^{21}Ne/^{22}Ne$
mantle source $^{21}Ne/^{22}Ne_E$
14
13
12
11
10
0.028
0.030
0.032
0.034
0.036

Fig. 18

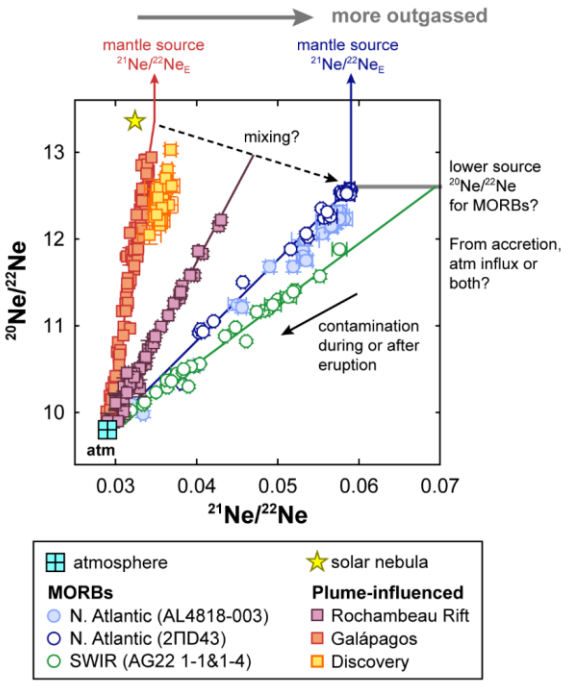
more outgassed
mantle source
$^{21}Ne/^{22}Ne_E$
mantle source
$^{21}Ne/^{22}Ne_E$
mixing?
lower source
$^{20}Ne/^{22}Ne$
for MORBs?
From accretion,
atm influx or
both?
contamination
during or after
eruption
atm
13
12
11
10
0.03
0.04
0.05
0.06
0.07
$^{20}Ne/^{22}Ne$
$^{21}Ne/^{22}Ne$
atmosphere
solar nebula
MORBs
N. Atlantic (AL4818-003)
N. Atlantic (2ΠD43)
SWIR (AG22 1-1&1-4)
Plume-influenced
Rochambeau Rift
Galápagos
Discovery

Fig. 19

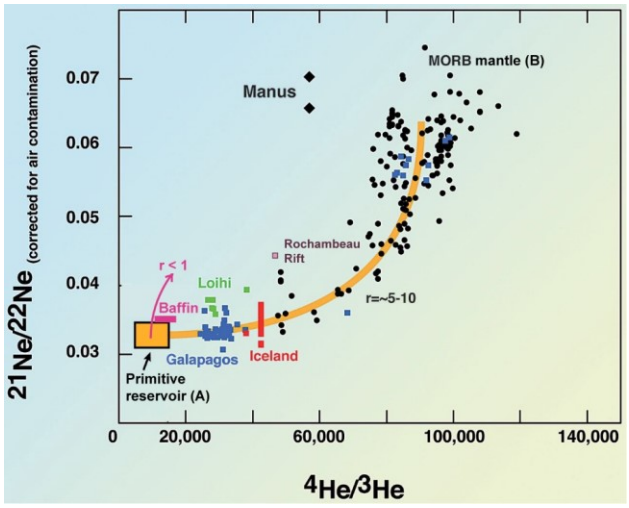
MORB mantle (B)
Manus
Rochambeau
Rift
r < 1
Loihi
Baffin
r=~5-10
Galapagos
Iceland
Primitive
reservoir (A)
0.07
0.06
0.05
0.04
0.03
0
20,000
60,000
100,000
140,000
21Ne/22Ne (corrected for air contamination)
4He/3He

Fig. 20

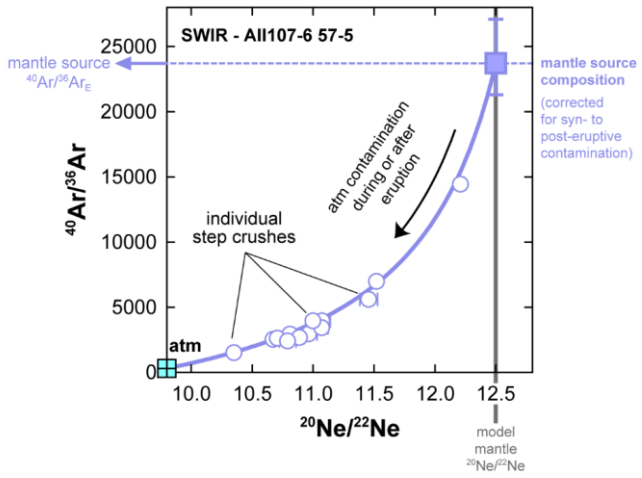
SWIR - All107-6 57-5
mantle source
$^{40}Ar/^{36}Ar_E$
mantle source composition
(corrected for syn- to post-eruptive contamination)
atm contamination during or after eruption
individual step crushes
atm
$^{40}Ar/^{36}Ar$
$^{20}Ne/^{22}Ne$
model mantle $^{20}Ne/^{22}Ne$
25000
20000
15000
10000
5000
0
10.0
10.5
11.0
11.5
12.0
12.5

Fig. 21

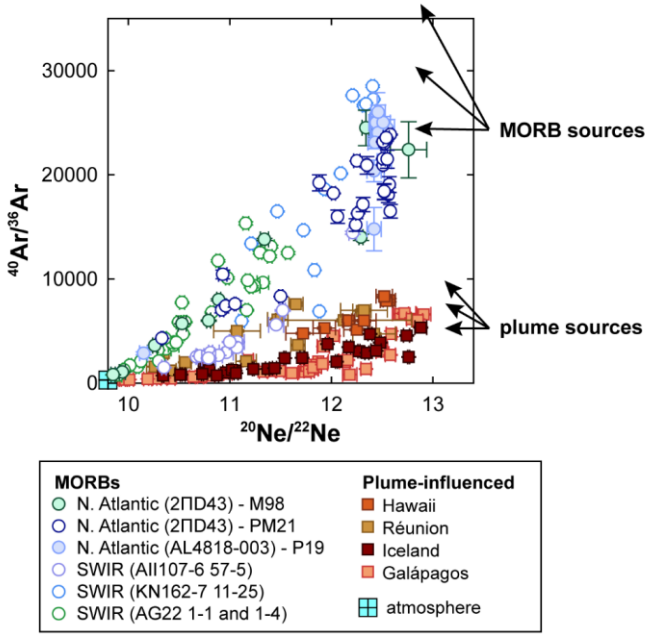
30000
20000
10000
0
10
11
12
13
$^{40}Ar/^{36}Ar$
$^{20}Ne/^{22}Ne$
MORB sources
plume sources
MORBs
N. Atlantic (2ПD43) - M98
N. Atlantic (2ПD43) - PM21
N. Atlantic (AL4818-003) - P19
SWIR (AII107-6 57-5)
SWIR (KN162-7 11-25)
SWIR (AG22 1-1 and 1-4)
Plume-influenced
Hawaii
Réunion
Iceland
Galápagos
atmosphere

Fig. 22

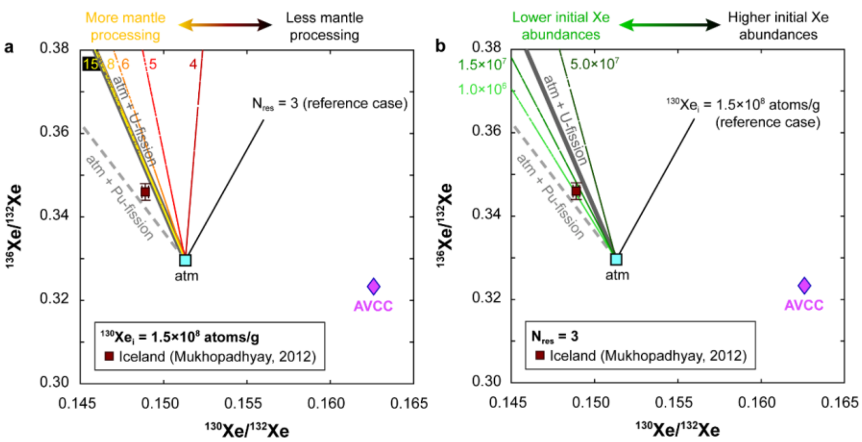
a
More mantle processing
Less mantle processing
15
8
6
5
4
N_{res} = 3 (reference case)
atm + U-fission
atm + Pu-fission
atm
AVCC
$^{130}Xe_i$ = 1.5×10^8 atoms/g
Iceland (Mukhopadhyay, 2012)
$^{136}Xe/^{132}Xe$
$^{130}Xe/^{132}Xe$
0.38
0.36
0.34
0.32
0.30
0.145
0.150
0.155
0.160
0.165
b
Lower initial Xe abundances
Higher initial Xe abundances
1.5×10^7
1.0×10^6
5.0×10^7
$^{130}Xe_i$ = 1.5×10^8 atoms/g (reference case)
atm + U-fission
atm + Pu-fission
atm
AVCC
N_{res} = 3
Iceland (Mukhopadhyay, 2012)
$^{136}Xe/^{132}Xe$
$^{130}Xe/^{132}Xe$
0.38
0.36
0.34
0.32
0.30
0.145
0.150
0.155
0.160
0.165

Fig. 23

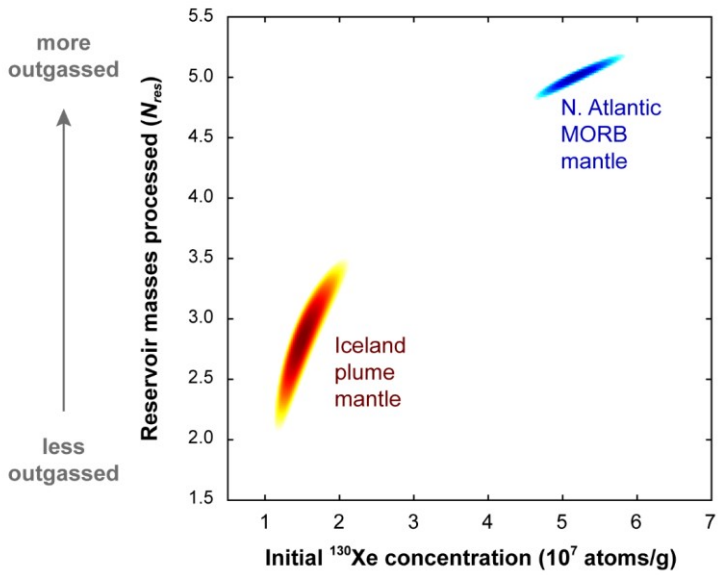
more outgassed
less outgassed
Reservoir masses processed (N_{res})
5.5
5.0
4.5
4.0
3.5
3.0
2.5
2.0
1.5
1
2
3
4
5
6
7
Initial ^{130}Xe concentration (10^7 atoms/g)
N. Atlantic MORB mantle
Iceland plume mantle

Fig. 24

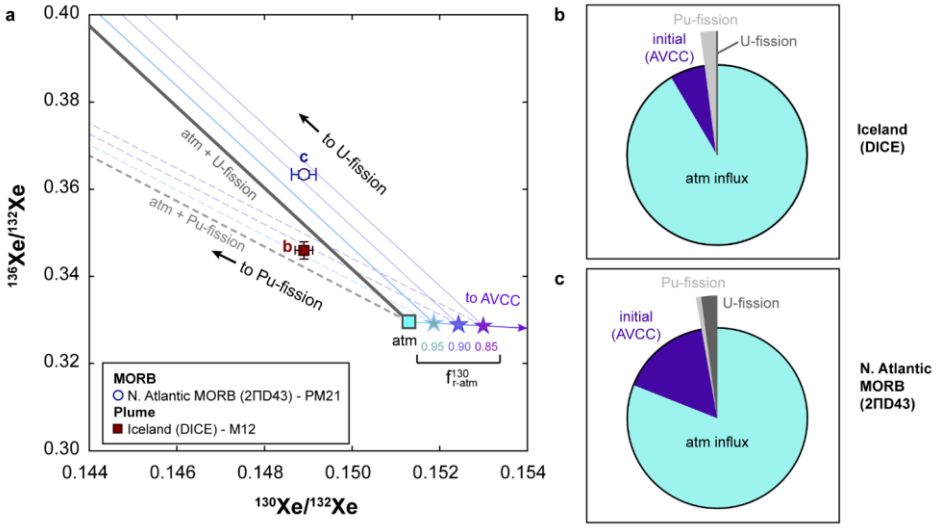
a
b
c
0.40
0.38
0.36
0.34
0.32
0.30
0.144
0.146
0.148
0.150
0.152
0.154
$^{136}Xe/^{132}Xe$
$^{130}Xe/^{132}Xe$
atm + U-fission
atm + Pu-fission
to U-fission
to Pu-fission
to AVCC
atm
0.95 0.90 0.85
$f^{130}_{r\text{-}atm}$
MORB
N. Atlantic MORB (2ΠD43) - PM21
Plume
Iceland (DICE) - M12
Pu-fission
initial (AVCC)
U-fission
atm influx
Iceland (DICE)
N. Atlantic MORB (2ΠD43)

Fig. 25

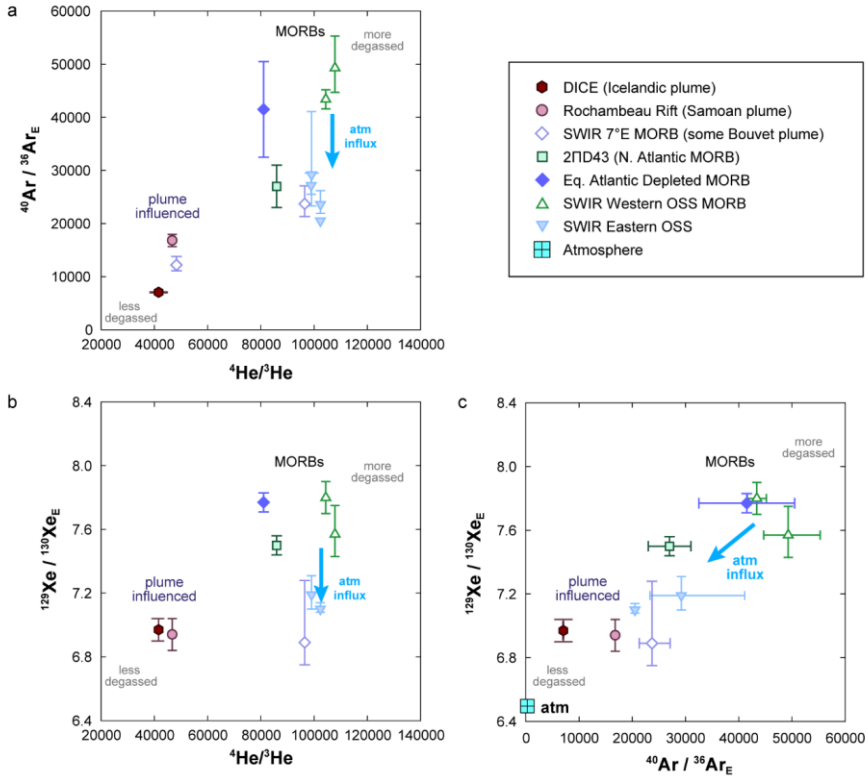
a
b
c
MORBs
more degassed
plume influenced
less degassed
atm influx
atm
DICE (Icelandic plume)
Rochambeau Rift (Samoan plume)
SWIR 7°E MORB (some Bouvet plume)
2ΠD43 (N. Atlantic MORB)
Eq. Atlantic Depleted MORB
SWIR Western OSS MORB
SWIR Eastern OSS
Atmosphere
40Ar / 36ArE
4He/3He
129Xe / 130XeE
40Ar / 36ArE

Fig. 26

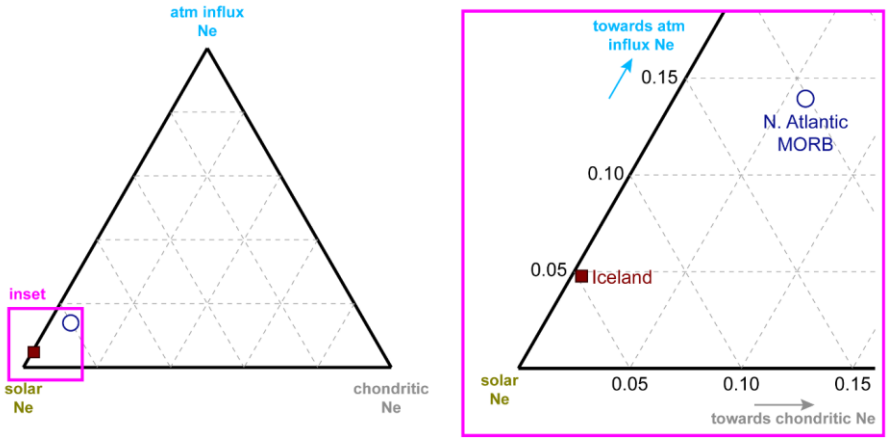
atm influx
Ne
inset
solar
Ne
chondritic
Ne
towards atm
influx Ne
0.15
0.10
0.05
N. Atlantic
MORB
Iceland
solar
Ne
0.05
0.10
0.15
towards chondritic Ne

References (353 total)

Akram, W., Schönbächler, M., Bisterzo, S., Gallino, R., 2015. Zirconium isotope evidence for the heterogeneous distribution of s-process materials in the solar system. Geochimica et Cosmochimica Acta 165, 484-500.

Alexander, E.C., Lewis, R.S., Reynolds, J.H., Michel, M.C., 1971. Plutonium-244 – Confirmation as an extinct radioactivity. Science 172, 837-840.

Allègre, C.J., Sarda, P., Staudacher, T., 1993. Speculations about the cosmic origin of He and Ne in the interior of the Earth. Earth and Planetary Science Letters 117, 229-233.

Allègre, C.J., Staudacher, T., Sarda, P., Kurz, M., 1983. Constraints on evolution of Earth's mantle from rare gas systematics. Nature 303, 762.

Amari, S., Anders, E., Virag, A., Zinner, E., 1990. Interstellar graphite in meteorites. Nature 345, 238-240.

Anderson, D.L., 1993. Helium-3 from the mantle: primordial signal or cosmic dust? Science 261, 170-176.

Ardoin, L., Broadley, M., Almayrac, M., Avice, G., Byrne, D., Tarantola, A., Lepland, A., Saito, T., Komiya, T., Shibuya, T., 2022. The end of the isotopic evolution of atmospheric xenon. Geochemical Perspectives Letters 20, 43-47.

Armytage, R.M., Jephcoat, A.P., Bouhifd, M., Porcelli, D., 2013. Metal–silicate partitioning of iodine at high pressures and temperatures: Implications for the Earth's core and 129∗ Xe budgets. Earth and Planetary Science Letters 373, 140-149.

Audi, G., Bersillon, O., Blachot, J., Wapstra, A.H., 2003. The NUBASE evaluation of nuclear and decay properties. Nuclear physics A 729, 3-128.

Avice, G., Marty, B., 2020. Perspectives on atmospheric evolution from noble gas and nitrogen isotopes on Earth, Mars & Venus. Space Science Reviews 216, 1-18.

Avice, G., Marty, B., Burgess, R., 2017. The origin and degassing history of the Earth's atmosphere revealed by Archean xenon. Nature communications 8, 1-9.

Avice, G., Marty, B., Burgess, R., Hofmann, A., Philippot, P., Zahnle, K., Zakharov, D., 2018. Evolution of atmospheric xenon and other noble gases inferred from Archean to Paleoproterozoic rocks. Geochimica et Cosmochimica Acta 232, 82-100.

Baldwin, S.L., Das, J., 2015. Atmospheric Ar and Ne returned from mantle depths to the Earth's surface by forearc recycling. Proceedings of the National Academy of Sciences 112, 14174-14179.

Ballentine, C.J., Barfod, D.N., 2000. The origin of air-like noble gases in MORB and OIB. Earth and Planetary Science Letters 180, 39-48.

Ballentine, C.J., Marty, B., Lollar, B.S., Cassidy, M., 2005. Neon isotopes constrain convection and volatile origin in the Earth's mantle. Nature 433, 33-38.

Ballentine, C.J., Van Keken, P.E., Porcelli, D., Hauri, E.H., 2002. Numerical models, geochemistry and the zero–paradox noble–gas mantle. Philosophical Transactions of the Royal Society of London. Series A: Mathematical, Physical and Engineering Sciences 360, 2611-2631.

Bar-Nun, A., Notesco, G., Owen, T., 2007. Trapping of N2, CO and Ar in amorphous ice—Application to comets. Icarus 190, 655-659.

Barfod, D.N., Ballentine, C.J., Halliday, A.N., Fitton, J.G., 1999. Noble gases in the Cameroon line and the He, Ne, and Ar isotopic compositions of high μ (HIMU) mantle. Journal of Geophysical Research: Solid Earth 104, 29509-29527.

Barry, P.H., Broadley, M.W., 2021. Nitrogen and noble gases reveal a complex history of metasomatism in the Siberian lithospheric mantle. Earth and Planetary Science Letters 556, 116707.

Basford, J.R., Dragon, J.C., Pepin, R.O., Coscio, M.R., Jr., Murthy, V.R., 1973. Krypton and xenon in lunar fines. Proceedings of the Lunar Science Conference, Geochimica Et Cosmochimica Acta Supplement 4 1915-1955.

Behrens, H., 2010. Noble gas diffusion in silicate glasses and melts. Reviews in Mineralogy and Geochemistry 72, 227-267.

Bekaert, D., Turner, S., Broadley, M., Barnes, J., Halldórsson, S., Labidi, J., Wade, J., Walowski, K., Barry, P., 2021. Subduction-driven volatile recycling: A global mass balance. Annual Review of Earth and Planetary Sciences 49, 37-70.

Bekaert, D.V., Barry, P.H., Broadley, M.W., Byrne, D.J., Marty, B., Ramírez, C.J., de Moor, J.M., Rodriguez, A., Hudak, M.R., Subhas, A.V., 2023. Ultrahigh-precision noble gas isotope analyses reveal pervasive subsurface fractionation in hydrothermal systems. Science Advances 9, eadg2566.

Bekaert, D.V., Broadley, M.W., Caracausi, A., Marty, B., 2019. Novel insights into the degassing history of Earth's mantle from high precision noble gas analysis of magmatic gas. Earth and Planetary Science Letters 525, 115766.

Bellotti, E., Broggini, C., Di Carlo, G., Laubenstein, M., Menegazzo, R., 2015. Precise measurement of the 222Rn half-life: A probe to monitor the stability of radioactivity. Physics Letters B 743, 526-530.

Bermingham, K.R., Füri, E., Lodders, K., Marty, B., 2020. The NC-CC Isotope Dichotomy: Implications for the Chemical and Isotopic Evolution of the Early Solar System. Space Science Reviews 216, 133.

Bianchi, D., Sarmiento, J.L., Gnanadesikan, A., Key, R.M., Schlosser, P., Newton, R., 2010. Low helium flux from the mantle inferred from simulations of oceanic helium isotope data. Earth and Planetary Science Letters 297, 379-386.

Black, D., Pepin, R., 1969. Trapped neon in meteorites—II. Earth and Planetary Science Letters 6, 395-405.

Black, D.C., 1972a. On the origins of trapped helium, neon and argon isotopic variations in meteorites—I. Gas-rich meteorites, lunar soil and breccia. Geochimica et Cosmochimica Acta 36, 347-375.

Black, D.C., 1972b. On the origins of trapped helium, neon and argon isotopic variations in meteorites—II. Carbonaceous meteorites. Geochimica et Cosmochimica Acta 36, 377-394.

Bohlin, R.C., Savage, B.D., Drake, J.F., 1978. A survey of interstellar H I from Lalpha absorption measurements. II. The Astrophysical Journal 224, 132-142.

Bottinga, Y., Javoy, M., 1989. MORB degassing: evolution of CO2. Earth and Planetary Science Letters 95, 215-225.

Bouhifd, M.A., Jephcoat, A., Porcelli, D., Kelley, S., Marty, B., 2020. Potential of Earth's core as a reservoir for noble gases: Case for helium and neon. Geochemical Perspectives Letters, 15-18.

Boulos, M.S., Manuel, O.K., 1971. Xenon Record Of Extinct Radioactivities In Earth. Science 174, 1334-&.
Broadhurst, C., Drake, M., Hagee, B., Bernatowicz, T., 1992. Solubility and partitioning of Ne, Ar, Kr and Xe in minerals and synthetic basaltic melts. Geochimica et Cosmochimica Acta 56, 709-723.
Broadley, M.W., Bekaert, D.V., Piani, L., Füri, E., Marty, B., 2022. Origin of life-forming volatile elements in the inner Solar System. Nature 611, 245-255.
Broadley, M., Byrne, D., Ardoin, L., Almayrac, M., Bekaert, D., Marty, B., 2022. High precision noble gas measurements of hydrothermal quartz reveal variable loss rate of Xe from the Archean atmosphere. Earth and Planetary Science Letters 588, 117577.
Broadley, M.W., Ballentine, C.J., Chavrit, D., Dallai, L., Burgess, R., 2016. Sedimentary halogens and noble gases within Western Antarctic xenoliths: Implications of extensive volatile recycling to the sub continental lithospheric mantle. Geochimica et Cosmochimica Acta 176, 139-156.
Broadley, M.W., Barry, P.H., Bekaert, D.V., Byrne, D.J., Caracausi, A., Ballentine, C.J., Marty, B., 2020. Identification of chondritic krypton and xenon in Yellowstone gases and the timing of terrestrial volatile accretion. Proceedings of the National Academy of Sciences 117, 13997-14004.
Brown, H. (1949) Rare gases and the formation of the Earth's atmosphere. In G. P. Kuiper, The atmospheres of the Earth and planets, Chapter 9, pp. 258-266.
Buikin, A., Trieloff, M., Hopp, J., Althaus, T., Korochantseva, E., Schwarz, W.H., Altherr, R., 2005. Noble gas isotopes suggest deep mantle plume source of late Cenozoic mafic alkaline volcanism in Europe. Earth and Planetary Science Letters 230, 143-162.
Burkhardt, C., Spitzer, F., Morbidelli, A., Budde, G., Render, J.H., Kruijer, T.S., Kleine, T., 2021. Terrestrial planet formation from lost inner solar system material. Science advances 7, eabj7601.
Burnard, P., 2004. Diffusive fractionation of noble gases and helium isotopes during mantle melting. Earth and Planetary Science Letters 220, 287-295.
Burnard, P., Graham, D., Turner, G., 1997. Vesicle-specific noble gas analyses of "popping rock": implications for primordial noble gases in Earth. Science 276, 568-571.
Burnard, P., Harrison, D., Turner, G., Nesbitt, R., 2003. Degassing and contamination of noble gases in Mid-Atlantic Ridge basalts. Geochemistry, Geophysics, Geosystems 4, 1-20.
Burnard, P., Zimmermann, L., Sano, Y., 2013. The noble gases as geochemical tracers: history and background. Springer.
Burnett, D., Team, G.S., 2011. Solar composition from the Genesis Discovery mission. Proceedings of the National Academy of Sciences 108, 19147-19151.
Busemann, H., Baur, H., Wieler, R., 2000. Primordial noble gases in "phase Q" in carbonaceous and ordinary chondrites studied by closed-system stepped etching. Meteoritics & Planetary Science 35, 949-973.
Busemann, H., Eugster, O., 2002. The trapped noble gas component in achondrites. Meteoritics & Planetary Science 37, 1865-1891.
Busemann, H., Lorenzetti, S., Eugster, O., 2006. Noble gases in D'Orbigny, Sahara 99555 and D'Orbigny glass—Evidence for early planetary processing on the angrite parent body. Geochimica et cosmochimica acta 70, 5403-5425.

Butler, W.A., Jeffery, P.M., Reynolds, J.H., Wasserburg, G.J., 1963. Isotopic Variations In Terrestrial Xenon. Journal of Geophysical Research 68, 3283-&.
Caffee, M.W., Hudson, G.U., Velsko, C., Huss, G.R., Alexander, E.C., Chivas, A.R., 1999. Primordial noble gases from Earth's mantle: Identification of a primitive volatile component. Science 285, 2115-2118.
Cameron, A.G.W., Ward, W.R., 1976. The Origin of the Moon. Abstracts of the Lunar and Planetary Science Conference 7, 120-122.
Caracausi, A., Avice, G., Burnard, P.G., Füri, E., Marty, B., 2016. Chondritic xenon in the Earth's mantle. Nature 533, 82-85.
Carroll, M.R., Stolper, E.M., 1993. Noble gas solubilities in silicate melts and glasses: New experimental results for argon and the relationship between solubility and ionic porosity. Geochimica et Cosmochimica Acta 57, 5039-5051.
Carroll, M.R., Webster, J.D., 1994. Solubilities of sulfur, noble gases, nitrogen, chlorine, and fluorine in magmas. Reviews in Mineralogy and Geochemistry 30, 231-279.
Charnoz, S., Avice, G., Hyodo, R., Pignatale, F.C., Chaussidon, M., 2021. Forming pressure traps at the snow line to isolate isotopic reservoirs in the absence of a planet. A&A 652, A35.
Chauvel, C., Hofmann, A.W., Vidal, P., 1992. HIMU-EM: the French Polynesian connection. Earth and Planetary Science Letters 110, 99-119.
Chavrit, D., Burgess, R., Sumino, H., Teagle, D.A., Droop, G., Shimizu, A., Ballentine, C.J., 2016. The contribution of hydrothermally altered ocean crust to the mantle halogen and noble gas cycles. Geochimica et Cosmochimica Acta 183, 106-124.
Chou, C.-L., 1978. Fractionation of Siderophile Element Ratios in the Earth's Upper Mantle and Lunar Samples, pp. 163-165.
Christensen, U.R., Hofmann, A.W., 1994. Segregation of subducted oceanic crust in the convecting mantle. Journal of Geophysical Research: Solid Earth 99, 19867-19884.
Clarke, W.B., Beg, M., Craig, H., 1969. Excess 3He in the sea: Evidence for terrestrial primodal helium. Earth and Planetary Science Letters 6, 213-220.
Class, C., Goldstein, S.L., 2005. Evolution of helium isotopes in the Earth's mantle. Nature 436, 1107-1112.
Class, C., Goldstein, S.L., Stute, M., Kurz, M.D., Schlosser, P., 2005. Grand Comore Island: a well-constrained "low 3He/4He" mantle plume. Earth and Planetary Science Letters 233, 391-409.
Colin, A., Moreira, M., Gautheron, C., Burnard, P., 2015. Constraints on the noble gas composition of the deep mantle by bubble-by-bubble analysis of a volcanic glass sample from Iceland. Chemical Geology 417, 173-183.
Coltice, N., Marty, B., Yokochi, R., 2009. Xenon isotope constraints on the thermal evolution of the early Earth. Chemical Geology 266, 4-9.
Condomines, M., Grönvold, K., Hooker, P.J., Muehlenbachs, K., O'Nions, R.K., Óskarsson, N., Oxburgh, E.R., 1983. Helium, oxygen, strontium and neodymium isotopic relationships in Icelandic volcanics. Earth and Planetary Science Letters 66, 125-136.
Connolly, J.A., 2010. The mechanics of metamorphic fluid expulsion. Elements 6, 165-172.
Cottaar, S., Martin, C., Li, Z., Parai, R., 2022. The root to the Galápagos mantle plume on the core-mantle boundary. Seismica 1.
Crabb, J., Anders, E., 1981. Noble gases in E-chondrites. Geochimica et Cosmochimica Acta 45, 2443-2464.

Craig, H., Lupton, J., 1976. Primordial neon, helium, and hydrogen in oceanic basalts. Earth and Planetary Science Letters 31, 369-385.
Crisp, J.A., 1984. Rates of magma emplacement and volcanic output. Journal of Volcanology and Geothermal Research 20, 177-211.
Crowther, S., Gilmour, J., 2013. The Genesis solar xenon composition and its relationship to planetary xenon signatures. Geochimica et Cosmochimica Acta 123, 17-34.
Dauphas, N., Hopp, T., Nesvorný, D., 2024. Bayesian inference on the isotopic building blocks of Mars and Earth. Icarus 408, 115805.
Dauphas, N., Morbidelli, A., 2014. 6.1 – Geochemical and Planetary Dynamical Views on the Origin of Earth's Atmosphere and Oceans, in: Holland, H.D., Turekian, K.K. (Eds.), Treatise on Geochemistry (Second Edition). Elsevier, Oxford, pp. 1-35.
Day, J.M., 2022. Noble gas isotope systematics in the Canary Islands and implications for refractory mantle components. Geochimica et Cosmochimica Acta 331, 35-47.
Day, J.M., Hilton, D.R., 2011. Origin of 3He/4He ratios in HIMU-type basalts constrained from Canary Island lavas. Earth and Planetary Science Letters 305, 226-234.
Day, J.M., Jones, T.D., Nicklas, R.W., 2022. Mantle sources of ocean islands basalts revealed from noble gas isotope systematics. Chemical Geology 587, 120626.
Donnelly, K.E., Goldstein, S.L., Langmuir, C.H., Spiegelman, M., 2004. Origin of enriched ocean ridge basalts and implications for mantle dynamics. Earth and Planetary Science Letters 226, 347-366.
Dunai, T.J., Porcelli, D., 2002. Storage and transport of noble gases in the subcontinental lithosphere. Reviews in mineralogy and geochemistry 47, 371-409.
Dupré, B., Allègre, C.J., 1983. Pb–Sr isotope variation in Indian Ocean basalts and mixing phenomena. Nature 303, 142-146.
Dygert, N., Jackson, C.R., Hesse, M.A., Tremblay, M.M., Shuster, D.L., Gu, J.T., 2018. Plate tectonic cycling modulates Earth's 3He/22Ne ratio. Earth and Planetary Science Letters 498, 309-321.
Eberhardt, P., Eugster, O., Marti, K., 1965b. A redetermination of the isotopic composition of atmospheric neon. Zeitschrift für Naturforschung A 20, 623-624.
Eberhardt, P., Geiss, J., Grögler, N., 1965a. Über die Verteilung der Uredelgase im Meteoriten Khor Temiki. Tschermaks mineralogische und petrographische Mitteilungen 10, 535-551.
Eikenberg, J., Signer, P., Wieler, R., 1993. U-Xe, U-Kr, and U-Pb systematics for dating uranium minerals and investigations of the production of nucleogenic neon and argon. Geochimica Et Cosmochimica Acta 57, 1053-1069.
Farley, K., Maier-Reimer, E., Schlosser, P., Broecker, W., 1995. Constraints on mantle 3He fluxes and deep-sea circulation from an oceanic general circulation model. Journal of Geophysical Research: Solid Earth 100, 3829-3839.
Farley, K., Neroda, E., 1998. Noble gases in the earth's mantle. Annual Review of Earth and Planetary Sciences 26, 189-218.
Farley, K., Poreda, R., 1993. Mantle neon and atmospheric contamination. Earth and Planetary Science Letters 114, 325-339.
Fischer-Gödde, M., Elfers, B.-M., Münker, C., Szilas, K., Maier, W.D., Messling, N., Morishita, T., Van Kranendonk, M., Smithies, H., 2020. Ruthenium isotope vestige of Earth's pre-late-veneer mantle preserved in Archaean rocks. Nature 579, 240-244.

Fisher, D.E., 1975. Trapped helium and argon and the formation of the atmosphere by degassing. Nature 256, 113-114.
Fisher, D.E., 1983. Rare gases from the undepleted mantle? Nature 305, 298-300.
Fisher, D.E., 1985. Noble gases from oceanic island basalts do not require an undepleted mantle source. Nature 316, 716-718.
Fisher, D.E., 1997. Helium, argon, and xenon in crushed and melted MORB. Geochimica et cosmochimica acta 61, 3003-3012.
Fisher, D.E., Perfit, M.R., 1990. Evidence from rare gases for magma-chamber degassing of highly evolved mid-ocean-ridge basalt. Nature 343, 450-452.
Fukushima, N., Sumino, H., Kobayashi, M., Kagi, H., 2024. Two metasomatic events recorded by noble gas characteristics in the Finero mantle wedge: Extreme fractionation (He, Ar) and seawater penetration into the mantle deformation zone. Chemical Geology 644, 121829.
García-Toraño, E., Altzitzoglou, T., Auerbach, P., Bé, M.-M., Bobin, C., Cassette, P., Chartier, F., Dersch, R., Fernández, M., Isnard, H., 2018. The half-life of 129I. Applied Radiation and Isotopes 140, 157-162.
Gautheron, C., Moreira, M., 2002. Helium signature of the subcontinental lithospheric mantle. Earth and Planetary Science Letters 199, 39-47.
Gautheron, C., Moreira, M., Allègre, C., 2005. He, Ne and Ar composition of the European lithospheric mantle. Chemical Geology 217, 97-112.
Geiss, J., Bühler, F., Cerutti, H., Eberhardt, P., Filleux, C., Meister, J., Signer, P., 2004. The Apollo SWC Experiment: Results, Conclusions, Consequences. Space Science Reviews 110, 307-335.
Gonnermann, H.M., Mukhopadhyay, S., 2007. Non-equilibrium degassing and a primordial source for helium in ocean-island volcanism. Nature 449, 1037-1040.
Gonnermann, H.M., Mukhopadhyay, S., 2009. Preserving noble gases in a convecting mantle. Nature 459, 560-563.
Graham, D., Christie, D., Harpp, K., Lupton, J., 1993. Mantle plume helium in submarine basalts from the Galápagos platform. Science 262, 2023-2026.
Graham, D.W., 2002. Noble Gas Isotope Geochemistry of Mid-Ocean Ridge and Ocean Island Basalts: Characterization of Mantle Source Reservoirs. Reviews in Mineralogy and Geochemistry 47, 247-317.
Graham, D.W., Humphris, S.E., Jenkins, W.J., Kurz, M.D., 1992a. Helium isotope geochemistry of some volcanic rocks from Saint Helena. Earth and Planetary Science Letters 110, 121-131.
Graham, D.W., Jenkins, W.J., Schilling, J.G., Thompson, G., Kurz, M.D., Humphris, S.E., 1992b. Helium Isotope Geochemistry of Midocean Ridge Basalts from the South-Atlantic. Earth and Planetary Science Letters 110, 133-147.
Graham, D.W., Michael, P.J., Shea, T., 2016. Extreme incompatibility of helium during mantle melting: Evidence from undegassed mid-ocean ridge basalts. Earth and Planetary Science Letters 454, 192-202.
Gray, C.M., Papanastassiou, D.A., Wasserburg, G.J., 1973. The identification of early condensates from the solar nebula. Icarus 20, 213-239.
Grimberg, A., Baur, H., Bochsler, P., Bühler, F., Burnett, D.S., Hays, C.C., Heber, V.S., Jurewicz, A.J., Wieler, R., 2006. Solar wind neon from Genesis: Implications for the lunar noble gas record. Science 314, 1133-1135.

Grimberg, A., Baur, H., Bühler, F., Bochsler, P., Wieler, R., 2008. Solar wind helium, neon, and argon isotopic and elemental composition: Data from the metallic glass flown on NASA's Genesis mission. Geochimica et Cosmochimica Acta 72, 626-645.
Grimberg, A., Burnett, D., Bochsler, P., Baur, H., Wieler, R., 2007. Composition of light solar wind noble gases in the bulk metallic glass flown on the Genesis mission. The Composition of Matter, 293-300.
Gülcher, A.J., Gebhardt, D.J., Ballmer, M.D., Tackley, P.J., 2020. Variable dynamic styles of primordial heterogeneity preservation in the Earth's lower mantle. Earth and Planetary Science Letters 536, 116160.
Györe, D., Sumino, H., Yang, I., Palcsu, L., László, E., Bishop, M.C., Mukhopadhyay, S., Stuart, F.M., 2024. Inter-laboratory re-determination of the atmospheric 22Ne/20Ne. Chemical Geology 645, 121900.
Hallis, L.J., Huss, G.R., Nagashima, K., Taylor, G.J., Halldórsson, S.A., Hilton, D.R., Mottl, M.J., Meech, K.J., 2015. Evidence for primordial water in Earth's deep mantle. Science 350, 795-797.
Hanan, B., Graham, D., 1996. Lead and helium isotope evidence from oceanic basalts for a common deep source of mantle plumes. Science 272, 991-995.
Hanyu, T., Kaneoka, I., 1997. The uniform and low 3He/4He ratios of HIMU basalts as evidence for their origin as recycled materials. Nature 390, 273-276.
Hanyu, T., Kaneoka, I., 1998. Open system behavior of helium in case of the HIMU source area. Geophysical research letters 25, 687-690.
Hanyu, T., Kaneoka, I., Nagao, K., 1999. Noble gas study of HIMU and EM ocean island basalts in the Polynesian region. Geochimica et Cosmochimica Acta 63, 1181-1201.
Hanyu, T., Kawabata, H., Tatsumi, Y., Kimura, J.-I., Hyodo, H., Sato, K., Miyazaki, T., Chang, Q., Hirahara, Y., Takahashi, T., 2014. Isotope evolution in the HIMU reservoir beneath St. Helena: Implications for the mantle recycling of U and Th. Geochimica et Cosmochimica Acta 143, 232-252.
Hanyu, T., Tatsumi, Y., Kimura, J.-I., 2011. Constraints on the origin of the HIMU reservoir from He–Ne–Ar isotope systematics. Earth and Planetary Science Letters 307, 377-386.
Harper, C.L., Jacobsen, S.B., 1996. Noble gases and Earth's accretion. Science 273, 1814-1818.
Hart, S.R., Hauri, E.H., Oschmann, L.A., Whitehead, J.A., 1992. Mantle plumes and entrainment – isotopic evidence. Science 256, 517-520.
Hebeda, E.H., Schultz, L., Freundel, M., 1987. Radiogenic, fissiogenic and nucleogenic noble gases in zircons. Earth and Planetary Science Letters 85, 79-90.
Heber, V.S., Baur, H., Bochsler, P., McKeegan, K.D., Neugebauer, M., Reisenfeld, D.B., Wieler, R., Wiens, R.C., 2012. Isotopic mass fractionation of solar wind: Evidence from fast and slow solar wind collected by the Genesis mission. The Astrophysical Journal 759, 121.
Heber, V.S., Brooker, R.A., Kelley, S.P., Wood, B.J., 2007. Crystal–melt partitioning of noble gases (helium, neon, argon, krypton, and xenon) for olivine and clinopyroxene. Geochimica et Cosmochimica Acta 71, 1041-1061.
Heber, V.S., Wieler, R., Baur, H., Olinger, C., Friedmann, T.A., Burnett, D.S., 2009. Noble gas composition of the solar wind as collected by the Genesis mission. Geochimica et Cosmochimica Acta 73, 7414-7432.
Hillenbrand, L.A., 2008. Disk-dispersal and planet-formation timescales. Physica Scripta 2008, 014024.

Hilton, D., McMurtry, G., Goff, F., 1998. Large variations in vent fluid CO2/3He ratios signal rapid changes in magma chemistry at Loihi seamount, Hawaii. Nature 396, 359-362.
Hilton, D.R., Fischer, T.P., Marty, B., 2002. Noble gases and volatile recycling at subduction zones. Reviews in mineralogy and geochemistry 47, 319-370.
Hilton, D.R., Macpherson, C.G., Elliott, T.R., 2000. Helium isotope ratios in mafic phenocrysts and geothermal fluids from La Palma, the Canary Islands (Spain): Implications for HIMU mantle sources. Geochimica Et Cosmochimica Acta 64, 2119-2132.
Hilton, D.R., Porcelli, D., 2014a. 3.7 – Noble Gases as Mantle Tracers, in: Holland, H.D., Turekian, K.K. (Eds.), Treatise on Geochemistry (Second Edition). Elsevier, Oxford, pp. 293-325.
Hilton, D.R., Porcelli, D., 2014b. 3.8 – Noble Gases as Tracers of Mantle Processes, in: Holland, H.D., Turekian, K.K. (Eds.), Treatise on Geochemistry (Second Edition). Elsevier, Oxford, pp. 327-353.
Hiyagon, H., Ozima, M., Marty, B., Zashu, S., Sakai, H., 1992. Noble gases in submarine glasses from mid-oceanic ridges and Loihi seamount: constraints on the early history of the Earth. Geochimica et Cosmochimica Acta 56, 1301-1316.
Hofmann, A.W., White, W.M., 1982. Mantle plumes from ancient oceanic crust. Earth and Planetary Science Letters 57, 421-436.
Holland, G., Ballentine, C.J., 2006. Seawater subduction controls the heavy noble gas composition of the mantle. Nature 441, 186-191.
Holland, G., Cassidy, M., Ballentine, C.J., 2009. Meteorite Kr in Earth's mantle suggests a late accretionary source for the atmosphere. Science 326, 1522-1525.
Holzer, M., DeVries, T., Bianchi, D., Newton, R., Schlosser, P., Winckler, G., 2017. Objective estimates of mantle 3He in the ocean and implications for constraining the deep ocean circulation. Earth and Planetary Science Letters 458, 305-314.
Honda, M., McDougall, I., 1998. Primordial helium and neon in the Earth—a speculation on early degassing. Geophysical research letters 25, 1951-1954.
Honda, M., McDougall, I., Patterson, D.B., Doulgeris, A., Clague, D.A., 1991. Possible solar noble-gas component in Hawaiian basalts. Nature 349, 149-151.
Honda, M., McDougall, I., Patterson, D.B., Doulgeris, A., Clague, D.A., 1993. Noble gases in submarine pillow basalt glasses from Loihi and Kilauea, Hawaii: a solar component in the Earth. Geochimica et Cosmochimica Acta 57, 859-874.
Honda, M., Reynolds, J., Roedder, E., Epstein, S., 1987. Noble gases in diamonds: Occurrences of solarlike helium and neon. Journal of Geophysical Research: Solid Earth 92, 12507-12521.
Hopkins, M., Harrison, T.M., Manning, C.E., 2008. Low heat flow inferred from >4[thinsp]Gyr zircons suggests Hadean plate boundary interactions. Nature 456, 493-496.
Hopp, T., Dauphas, N., Spitzer, F., Burkhardt, C., Kleine, T., 2022. Earth's accretion inferred from iron isotopic anomalies of supernova nuclear statistical equilibrium origin. Earth and Planetary Science Letters 577, 117245.
Hoppe, P., Leitner, J., Kodolányi, J., Borrmann, S., Jones, A.P., 2022. Dust from supernovae and their progenitors in the solar nebula. Nature Astronomy 6, 1027-1034.
Horton, F., Asimow, P., Farley, K., Curtice, J., Kurz, M., Blusztajn, J., Biasi, J., Boyes, X., 2023. Highest terrestial 3He/4He credibly from the core. Nature, 1-5.

Horton, F., Curtice, J., Farley, K., Kurz, M., Asimow, P., Treffkorn, J., Boyes, X., 2021. Primordial neon in high-3He/4He Baffin Island olivines. Earth and Planetary Science Letters 558, 116762.
Horton, F., Farley, K., Jackson, M., 2019. Helium distributions in ocean island basalt olivines revealed by X-ray computed tomography and single-grain crushing experiments. Geochimica et Cosmochimica Acta 244, 467-477.
Huang, J., Andrews, S.M., Dullemond, C.P., Isella, A., Pérez, L.M., Guzmán, V.V., Öberg, K.I., Zhu, Z., Zhang, S., Bai, X.-N., 2018. The disk substructures at high angular resolution project (DSHARP). II. Characteristics of annular substructures. The Astrophysical Journal Letters 869, L42.
Hudson, G.B., Kennedy, B.M., Podosek, F.A., Hohenberg, C.M., 1989. The early Solar System abundance of Pu-244 as inferred from the St. Severin chondrite, Proceedings of the 19th Lunar and Planetary Science Conference, pp. 547-557. Lunar and Planetary Institute, Houston, TX, pp. 547-557.
Izidoro, A., Dasgupta, R., Raymond, S.N., Deienno, R., Bitsch, B., Isella, A., 2022. Planetesimal rings as the cause of the Solar System's planetary architecture. Nature Astronomy 6, 357-366.
Jackson, C.R., Parman, S.W., Kelley, S.P., Cooper, R.F., 2013a. Constraints on light noble gas partitioning at the conditions of spinel-peridotite melting. Earth and Planetary Science Letters 384, 178-187.
Jackson, C.R., Parman, S.W., Kelley, S.P., Cooper, R.F., 2013b. Noble gas transport into the mantle facilitated by high solubility in amphibole. Nature Geoscience 6, 562-565.
Jackson, C.R., Parman, S.W., Kelley, S.P., Cooper, R.F., 2015. Light noble gas dissolution into ring structure-bearing materials and lattice influences on noble gas recycling. Geochimica et Cosmochimica Acta 159, 1-15.
Jackson, C.R.M., Bennett, N.R., Du, Z., Cottrell, E., Fei, Y., 2018. Early episodes of high-pressure core formation preserved in plume mantle. Nature 553, 491-495.
Jackson, M.G., Blichert-Toft, J., Halldórsson, S.A., Mundl-Petermeier, A., Bizimis, M., Kurz, M.D., Price, A.A., Harðardóttir, S., Willhite, L.N., Breddam, K., Becker, T.W., Fischer, R.A., 2020. Ancient helium and tungsten isotopic signatures preserved in mantle domains least modified by crustal recycling. Proceedings of the National Academy of Sciences 117, 30993-31001.
Jackson, M.G., Kurz, M.D., Hart, S.R., Workman, R.K., 2007. New Samoan lavas from Ofu Island reveal a hemispherically heterogeneous high 3He/4He mantle. Earth and Planetary Science Letters 264, 360-374.
Jaffey, A., Flynn, K., Glendenin, L., Bentley, W.t., Essling, A., 1971. Precision measurement of half-lives and specific activities of U 235 and U 238. Physical review C 4, 1889.
Jambon, A., Weber, H., Braun, O., 1986. Solubility of He, Ne, Ar, Kr and Xe in a basalt melt in the range 1250–1600 C. Geochemical implications. Geochimica et Cosmochimica Acta 50, 401-408.
Jeffery, P., 1971. Isotopic composition of xenon from a Greenland anorthosite. Nature 233, 260-261.
Jenkins, W.J., 2020. Using excess 3He to estimate Southern Ocean upwelling time scales. Geophysical Research Letters 47, e2020GL087266.

Johnson, L., Burgess, R., Turner, G., Milledge, H., Harris, J., 2000. Noble gas and halogen geochemistry of mantle fluids: comparison of African and Canadian diamonds. Geochimica et Cosmochimica Acta 64, 717-732.
Kallenbach, R., Ipavich, F., Bochsler, P., Hefti, S., Hovestadt, D., Grünwaldt, H., Hilchenbach, M., Axford, W., Balsiger, H., Bürgi, A., 1997. Isotopic composition of solar wind neon measured by CELIAS/MTOF on board SOHO. Journal of Geophysical Research: Space Physics 102, 26895-26904.
Kaneoka, I., Takaoka, N., 1978. Excess 129Xe and high 3He/4He ratios in olivine phenocrysts of Kapuho lava and xenolithic dunites from Hawaii. Earth and Planetary Science Letters 39, 382-386.
Kaneoka, I., Takaoka, N., 1980. Rare gas isotopes in Hawaiian ultramafic nodules and volcanic rocks: constraint on genetic relationships. Science 208, 1366-1368.
Kaneoka, I., Takaoka, N., Aoki, K., 1978. Rare gases in mantle-derived rocks and minerals, in: Alexander, E.C. (Ed.), Terrestrial Rare Gases. Japan Scientific Society Press, Tokyo, pp. 71-83.
Kaneoka, I., Takaoka, N., Clague, D.A., 1983. Noble gas systematics for coexisting glass and olivine crystals in basalts and dunite xenoliths from Loihi Seamount. Earth and Planetary Science Letters 66, 427-437.
Kellogg, L., Wasserburg, G., 1990. The role of plumes in mantle helium fluxes. Earth and Planetary Science Letters 99, 276-289.
Kendrick, M.A., Honda, M., Pettke, T., Scambelluri, M., Phillips, D., Giuliani, A., 2013. Subduction zone fluxes of halogens and noble gases in seafloor and forearc serpentinites. Earth and Planetary Science Letters 365, 86-96.
Kendrick, M.A., Scambelluri, M., Hermann, J., Padrón-Navarta, J.A., 2018. Halogens and noble gases in serpentinites and secondary peridotites: Implications for seawater subduction and the origin of mantle neon. Geochimica et Cosmochimica Acta 235, 285-304.
Kendrick, M.A., Scambelluri, M., Honda, M., Phillips, D., 2011. High abundances of noble gas and chlorine delivered to the mantle by serpentinite subduction. Nature Geoscience 4, 807-812.
Kennedy, B., 1988. Noble gases in vent water from the Juan de Fuca Ridge. Geochimica et Cosmochimica Acta 52, 1929-1935.
Kleine, T., Budde, G., Burkhardt, C., Kruijer, T., Worsham, E., Morbidelli, A., Nimmo, F., 2020. The non-carbonaceous–carbonaceous meteorite dichotomy. Space Science Reviews 216, 1-27.
Krantz, J.A., Parman, S.W., Kelley, S.P., 2019. Recycling of heavy noble gases by subduction of serpentinite. Earth and Planetary Science Letters 521, 120-127.
Krietsch, D., Busemann, H., Riebe, M.E., King, A.J., Alexander, C.M.D., Maden, C., 2021. Noble gases in CM carbonaceous chondrites: Effect of parent body aqueous and thermal alteration and cosmic ray exposure ages. Geochimica et Cosmochimica Acta 310, 240-280.
Kruijer, T.S., Kleine, T., Borg, L.E., 2020. The great isotopic dichotomy of the early Solar System. Nature Astronomy 4, 32-40.
Kumagai, H., Dick, H.J., Kaneoka, I., 2003. Noble gas signatures of abyssal gabbros and peridotites at an Indian Ocean core complex. Geochemistry, Geophysics, Geosystems 4.
Kunz, J., 1999. Is there solar argon in the Earth's mantle? Nature 399, 649-650.

Kunz, J., Staudacher, T., Allegre, C.J., 1998. Plutonium-fission xenon found in Earth's mantle. Science 280, 877-880.
Kurz, M., Jenkins, W., 1981. The distribution of helium in oceanic basalt glasses. Earth and Planetary Science Letters 53, 41-54.
Kurz, M.D., Curtice, J., Fornari, D., Geist, D., Moreira, M., 2009. Primitive neon from the center of the Galápagos hotspot. Earth and Planetary Science Letters 286, 23-34.
Kurz, M.D., Jenkins, W.J., Hart, S.R., 1982a. Helium Isotopic Systematics of Oceanic Islands and Mantle Heterogeneity. Nature 297, 43-47.
Kurz, M.D., Jenkins, W.J., Hart, S.R., Clague, D., 1983. Helium isotopic variations in volcanic rocks from Loihi Seamount and the Island of Hawaii. Earth and Planetary Science Letters 66, 388-406.
Kurz, M.D., Jenkins, W.J., Schilling, J.G., Hart, S.R., 1982b. Helium Isotopic Variations in the Mantle beneath the Central-North Atlantic-Ocean. Earth and Planetary Science Letters 58, 1-14.
Kurz, M.D., Gurney, J.J., Jenkins, W.J., Lott III, D.E., 1987. Helium isotopic variability within single diamonds from the Orapa kimberlite pipe. Earth and planetary science letters 86, 57-68.
Kyser, T.K., Rison, W., 1982. Systematics of rare gas isotopes in basic lavas and ultramafic xenoliths. Journal of Geophysical Research: Solid Earth 87, 5611-5630.
Lewis, R.S., 1975. Rare-gases in separated whitlockite from St. Severin chondrite - Xenon and krypton from fission extinct Pu-244. Geochimica Et Cosmochimica Acta 39, 417-432.
Lewis, R.S., Ming, T., Wacker, J.F., Anders, E., Steel, E., 1987. Interstellar diamonds in meteorites. Nature 326, 160-162.
Lichtenberg, T., Drążkowska, J., Schönbächler, M., Golabek, G.J., Hands, T.O., 2021. Bifurcation of planetary building blocks during Solar System formation. Science 371, 365-370.
Lock, S.J., Bermingham, K.R., Parai, R., Boyet, M., 2020. Geochemical constraints on the origin of the Moon and preservation of ancient terrestrial heterogeneities. Space science reviews 216, 109.
Lock, S.J., Stewart, S.T., Petaev, M.I., Leinhardt, Z., Mace, M.T., Jacobsen, S.B., Cuk, M., 2018. The origin of the Moon within a terrestrial synestia. Journal of Geophysical Research: Planets 123, 910-951.
Lodders, K., 2003. Solar system abundances and condensation temperatures of the elements. The Astrophysical Journal 591, 1220.
Lodders, K., 2021. Relative Atomic Solar System Abundances, Mass Fractions, and Atomic Masses of the Elements and Their Isotopes, Composition of the Solar Photosphere, and Compositions of the Major Chondritic Meteorite Groups. Space Science Reviews 217, 44.
Lott III, D.E., 2001. Improvements in noble gas separation methodology: A nude cryogenic trap. Geochemistry, Geophysics, Geosystems 2.
Lupton, J., Craig, H., 1975. Excess 3He in oceanic basalts: evidence for terrestrial primordial helium. Earth and Planetary Science Letters 26, 133-139.
Lux, G., 1987. The behavior of noble gases in silicate liquids: Solution, diffusion, bubbles and surface effects, with applications to natural samples. Geochimica et Cosmochimica Acta 51, 1549-1560.

Mahaffy, P., Donahue, T.M., Atreya, S., Owen, T., Niemann, H., 1998. Galileo probe measurements of D/H and 3He/4He in Jupiter's atmosphere. Space Science Reviews 84, 251-263.
Marrocchi, Y., Derenne, S., Marty, B., Robert, F., 2005. Interlayer trapping of noble gases in insoluble organic matter of primitive meteorites. Earth and Planetary Science Letters 236, 569-578.
Marty, B., 1989. Neon and xenon isotopes in MORB: implications for the earth-atmosphere evolution. Earth and Planetary Science Letters 94, 45-56.
Marty, B., 2012. The origins and concentrations of water, carbon, nitrogen and noble gases on Earth. Earth and Planetary Science Letters 313, 56-66.
Marty, B., 2022. Meteoritic noble gas constraints on the origin of terrestrial volatiles. Icarus, 115020.
Marty, B., Altwegg, K., Balsiger, H., Bar-Nun, A., Bekaert, D., Berthelier, J.-J., Bieler, A., Briois, C., Calmonte, U., Combi, M., 2017. Xenon isotopes in 67P/Churyumov-Gerasimenko show that comets contributed to Earth's atmosphere. Science 356, 1069-1072.
Marty, B., Tolstikhin, I.N., 1998. CO2 fluxes from mid-ocean ridges, arcs and plumes. Chemical Geology 145, 233-248.
Marty, B., Zashu, S., Ozima, M., 1983. Two noble gas components in a Mid-Atlantic Ridge basalt. Nature 302, 238-240.
Marty, B., Zimmermann, L., 1999. Volatiles (He, C, N, Ar) in mid-ocean ridge basalts: Assesment of shallow-level fractionation and characterization of source composition. Geochimica et Cosmochimica Acta 63, 3619-3633.
Matsumoto, T., Chen, Y., Matsuda, J.-i., 2001. Concomitant occurrence of primordial and recycled noble gases in the Earth's mantle. Earth and Planetary Science Letters 185, 35-47.
Mazor, E., Heymann, D., Anders, E., 1970. Noble gases in carbonaceous chondrites. Geochimica et Cosmochimica Acta 34, 781-824.
Meshik, A., Hohenberg, C., Pravdivtseva, O., Burnett, D., 2013. Xenon Isotopes in Aluminum Solar Wind Collectors in from Genesis Mission, 44th Annual Lunar and Planetary Science Conference, p. 3103.
Meshik, A., Hohenberg, C., Pravdivtseva, O., Burnett, D., 2014. Heavy noble gases in solar wind delivered by Genesis mission. Geochimica et cosmochimica acta 127, 326-347.
Meshik, A., Pravdivtseva, O., Burnett, D., 2020. Refined composition of solar wind xenon delivered by Genesis NASA mission: comparison with xenon captured by extraterrestrial regolith soils. Geochimica et Cosmochimica Acta 276, 289-298.
Mizuno, H., Nakazawa, K., Hayashi, C., 1980. Dissolution of the primordial rare gases into the molten Earth's material. Earth and Planetary Science Letters 50, 202-210.
Morbidelli, A., 2020. Planet formation by pebble accretion in ringed disks. Astronomy & Astrophysics 638, A1.
Morbidelli, A., Lunine, J.I., O'Brien, D.P., Raymond, S.N., Walsh, K.J., 2012. Building terrestrial planets. Annual Review of Earth and Planetary Sciences 40, 251-275.
Moreira, M., 2007. Constraints on the origin of the 129Xe on Earth using the tellurium double beta decay. Earth and Planetary Science Letters 264, 114-122.
Moreira, M., 2013. Noble Gas Constraints on the Origin and Evolution of Earth's Volatiles. Geochemical Perspectives 2, 229-403.

Moreira, M., Charnoz, S., 2016. The origin of the neon isotopes in chondrites and on Earth. Earth and Planetary Science Letters 433, 249-256.
Moreira, M., Kunz, J., Allegre, C., 1998. Rare gas systematics in Popping Rock: Isotopic and elemental compositions in the upper mantle. Science 279, 1178-1181.
Moreira, M., Kurz, M., 2013. Noble gases as tracers of mantle processes and magmatic degassing. The noble gases as geochemical tracers, 371-391.
Moreira, M., Kurz, M.D., 2001. Subducted oceanic lithosphere and the origin of the 'high μ'basalt helium isotopic signature. Earth and Planetary Science Letters 189, 49-57.
Moreira, M., Raquin, A., 2007. The origin of rare gases on Earth: The noble gas 'subduction barrier'revisited. Comptes Rendus Geoscience 339, 937-945.
Moreira, M., Rouchon, V., Muller, E., Noirez, S., 2018. The xenon isotopic signature of the mantle beneath Massif Central. Geochem. Perspect. Lett 6, 28-32.
Morgan, W.J., 1971. Convection plumes in the lower mantle. Nature 230, 42-43.
Mukhopadhyay, S., 2012. Early differentiation and volatile accretion recorded in deep-mantle neon and xenon. Nature 486, 101-U124.
Mukhopadhyay, S., Ackert Jr, R.P., Pope, A.E., Pollard, D., DeConto, R.M., 2012. Miocene to recent ice elevation variations from the interior of the West Antarctic ice sheet: constraints from geologic observations, cosmogenic nuclides and ice sheet modeling. Earth and Planetary Science Letters 337, 243-251.
Mukhopadhyay, S., Parai, R., 2019. Noble gases: a record of Earth's evolution and mantle dynamics. Annual Review of Earth and Planetary Sciences 47, 389-419.
Mundl, A., Touboul, M., Jackson, M.G., Day, J.M., Kurz, M.D., Lekic, V., Helz, R.T., Walker, R.J., 2017. Tungsten-182 heterogeneity in modern ocean island basalts. Science 356, 66-69.
Mungall, J.E., Bagdassarov, N.S., Romano, C., Dingwell, D.B., 1996. Numerical modelling of stress generation and microfracturing of vesicle walls in glassy rocks. Journal of Volcanology and Geothermal Research 73, 33-46.
Nakamura, T., Nagao, K., Takaoka, N., 1999. Microdistribution of primordial noble gases in CM chondrites determined by in situ laser microprobe analysis: decipherment of nebular processes. Geochimica et Cosmochimica Acta 63, 241-255.
Naumenko-Dèzes, M.O., Nägler, T.F., Mezger, K., Villa, I.M., 2018. Constraining the 40K decay constant with 87Rb-87Sr – 40K-40Ca chronometer intercomparison. Geochimica et Cosmochimica Acta 220, 235-247.
Niedermann, S., Bach, W., Erzinger, J., 1997. Noble gas evidence for a lower mantle component in MORBs from the southern East Pacific Rise: Decoupling of helium and neon isotope systematics. Geochimica et Cosmochimica Acta 61, 2697-2715.
Notesco, G., Bar-Nun, A., Owen, T., 2003. Gas trapping in water ice at very low deposition rates and implications for comets. Icarus 162, 183-189.
O'Nions, R., Oxburgh, E., 1983. Heat and helium in the Earth. Nature 306, 429-431.
Okazaki, R., Takaoka, N., Nagao, K., Nakamura, T., 2010. Noble gases in enstatite chondrites released by stepped crushing and heating. Meteoritics & Planetary Science 45, 339-360.
Okazaki, R., Takaoka, N., Nagao, K., Sekiya, M., Nakamura, T., 2001. Noble-gas-rich chondrules in an enstatite meteorite. Nature 412, 795-798.
Olson, P., Sharp, Z.D., 2018. Hydrogen and helium ingassing during terrestrial planet accretion. Earth and Planetary Science Letters 498, 418-426.

Olson, P.L., Sharp, Z.D., 2022. Primordial Helium-3 Exchange Between Earth's Core and Mantle. Geochemistry, Geophysics, Geosystems 23, e2021GC009985.
Ott, U., 2014. Planetary and pre-solar noble gases in meteorites. Geochemistry 74, 519-544.
Ott, U., Mack, R., Sherwood, C., 1981. Noble-gas-rich separates from the Allende meteorite. Geochimica et Cosmochimica Acta 45, 1751-1788.
Owen, T.C., Bar-Nun, A., 2000. Volatile contributions from icy planetesimals. Origin of the Earth and Moon 10, 459.
Ozima, M., 1989. Gases in diamonds. Annual Review of Earth and Planetary Sciences 17, 361-384.
Ozima, M., Podosek, F., Igarashi, G., 1985. Terrestrial xenon isotope constraints on the early history of the Earth. Nature 315, 471-474.
Ozima, M., Zashu, S., 1983. Noble gases in submarine pillow volcanic glasses. Earth and Planetary Science Letters 62, 24-40.
Parai, R., 2022. A dry ancient plume mantle from noble gas isotopes. Proceedings of the National Academy of Sciences 119, e2201815119.
Parai, R., 2023. Primordial noble gas isotopes from immoderate crushing of an Icelandic basalt glass. Geochemical Perspectives Letters 27, 32-37.
Parai, R., Mukhopadhyay, S., 2012. How large is the subducted water flux? New constraints on mantle regassing rates. Earth and Planetary Science Letters 317, 396-406.
Parai, R., Mukhopadhyay, S., 2015. The evolution of MORB and plume mantle volatile budgets: Constraints from fission Xe isotopes in Southwest Indian Ridge basalts. Geochemistry, Geophysics, Geosystems 16, 719-735.
Parai, R., Mukhopadhyay, S., 2018. Xenon isotopic constraints on the history of volatile recycling into the mantle. Nature 560, 223.
Parai, R., Mukhopadhyay, S., 2021. Heavy noble gas signatures of the North Atlantic Popping Rock 2ΠD43: Implications for mantle noble gas heterogeneity. Geochimica et Cosmochimica Acta 294, 89-105.
Parai, R., Mukhopadhyay, S., Lassiter, J.C., 2009. New constraints on the HIMU mantle from neon and helium isotopic compositions of basalts from the Cook-Austral Islands. Earth and Planetary Science Letters 277, 253-261.
Parai, R., Mukhopadhyay, S., Standish, J.J., 2012. Heterogeneous upper mantle Ne, Ar and Xe isotopic compositions and a possible Dupal noble gas signature recorded in basalts from the Southwest Indian Ridge. Earth and Planetary Science Letters 359, 227-239.
Parai, R., Mukhopadhyay, S., Tucker, J.M., Pető, M.K., 2019. The emerging portrait of an ancient, heterogeneous and continuously evolving mantle plume source. Lithos 346-347, 105153.
Parman, S.W., Kurz, M.D., Hart, S.R., Grove, T.L., 2005. Helium solubility in olivine and implications for high (3)He/(4)He in ocean island basalts. Nature 437, 1140-1143.
Patterson, D., Honda, M., McDougall, I., 1990. Atmospheric contamination: A possible source for heavy noble gases in basalts from Loihi seamount, Hawaii. Geophysical Research Letters 17, 705-708.
Patterson, D., Honda, M., McDougall, I., 1991. Contamination of Loihi magmas with atmosphere derived noble gases: A Reply to Comments by T. Staudacher, P. Sarda and C. Allegre. Geophysical Research Letters 18, 749-752.
Patzer, A., Schultz, L., 2002. Noble gases in enstatite chondrites II: The trapped component. Meteoritics & Planetary Science 37, 601-612.

Patzer, A., Schultz, L., Franke, L., 2003. New noble gas data of primitive and differentiated achondrites including Northwest Africa 011 and Tafassasset. Meteoritics & Planetary Science 38, 1485-1497.
Paulatto, M., Laigle, M., Galve, A., Charvis, P., Sapin, M., Bayrakci, G., Evain, M., Kopp, H., 2017. Dehydration of subducting slow-spread oceanic lithosphere in the Lesser Antilles. Nature communications 8, 15980.
Pepin, R., 1998. Isotopic evidence for a solar argon component in the Earth's mantle. Nature 394, 664-667.
Pepin, R., Becker, R., 1990. Isotopic compositions of solar wind neon, argon and krypton. Meteoritics, Vol. 25, p. 398 25, 398.
Pepin, R., Nyquist, L., Phinney, D., Black, D.C., 1970. Isotopic composition of rare gases in lunar samples. Science 167, 550-553.
Pepin, R.O., 1967. Trapped neon in meteorites. Earth and Planetary Science Letters 2, 13-18.
Pepin, R.O., 2000. On the isotopic composition of primordial xenon in terrestrial planet atmospheres. Space Science Reviews 92, 371-395.
Pepin, R.O., Porcelli, D., 2002. Origin of Noble Gases in the Terrestrial Planets. Reviews in Mineralogy and Geochemistry 47, 191-246.
Pepin, R.O., Schlutter, D.J., Becker, R.H., Reisenfeld, D.B., 2012. Helium, neon, and argon composition of the solar wind as recorded in gold and other Genesis collector materials. Geochimica et Cosmochimica Acta 89, 62-80.
Péron, S., Moreira, M., 2018. Onset of volatile recycling into the mantle determined by xenon anomalies. Geochemical Perspectives Letters 9, 21-25.
Péron, S., Moreira, M., Agranier, A., 2018. Origin of light noble gases (He, Ne, and Ar) on Earth: A review. Geochemistry, Geophysics, Geosystems 19, 979-996.
Péron, S., Moreira, M., Colin, A., Arbaret, L., Putlitz, B., Kurz, M.D., 2016. Neon isotopic composition of the mantle constrained by single vesicle analyses. Earth and Planetary Science Letters 449, 145-154.
Péron, S., Moreira, M.A., Kurz, M.D., Curtice, J., Blusztajn, J.S., Putlitz, B., Wanless, V.D., Jones, M.P., Soule, S.A., Mittelstaedt, E., 2019. Noble gas systematics in new popping rocks from the Mid-Atlantic Ridge (14° N): evidence for small-scale upper mantle heterogeneities. Earth and Planetary Science Letters 519, 70-82.
Péron, S., Mukhopadhyay, S., 2022. Pre-subduction mantle noble gas elemental pattern reveals larger missing xenon in the deep interior compared to the atmosphere. Earth and Planetary Science Letters 593, 117655.
Péron, S., Mukhopadhyay, S., Huh, M., 2020. A new dual stainless steel cryogenic trap for efficient separation of krypton from argon and xenon. Journal of Analytical Atomic Spectrometry 35, 2663-2671.
Péron, S., Mukhopadhyay, S., Kurz, M.D., Graham, D.W., 2021. Deep-mantle krypton reveals Earth's early accretion of carbonaceous matter. Nature 600, 462-467.
Petaev, M.I., Wood, J.A., 1998. The condensation with partial isolation (CWPI) model of condensation in the solar nebula. Meteoritics & Planetary Science 33, 1123-1137.
Pető, M.K., Mukhopadhyay, S., Kelley, K.A., 2013. Heterogeneities from the first 100 million years recorded in deep mantle noble gases from the Northern Lau Back-arc Basin. Earth and Planetary Science Letters 369, 13-23.

Phinney, D., Tennyson, J., Frick, U., 1978. Xenon In CO2 Well Gas Revisited. Journal of Geophysical Research 83, 2313-2319.
Plank, T., Manning, C.E., 2019. Subducting carbon. Nature 574, 343-352.
Podosek, F.A., 1978. Isotopic structures in solar system materials. Annual Review of Astronomy and Astrophysics 16, 293-334.
Porcelli, D., Ballentine, C.J., Wieler, R., 2002. An overview of noble gas geochemistry and cosmochemistry. Reviews in mineralogy and geochemistry 47, 1-19.
Porcelli, D., Elliott, T., 2008. The evolution of He isotopes in the convecting mantle and the preservation of high 3He/4He ratios. Earth and Planetary Science Letters 269, 175-185.
Porcelli, D., Halliday, A., 2001. The core as a possible source of mantle helium. Earth and Planetary Science Letters 192, 45-56.
Porcelli, D., O'nions, R., O'reilly, S., 1986. Helium and strontium isotopes in ultramafic xenoliths. Chemical geology 54, 237-249.
Porcelli, D., Pepin, R.O., 2014. 6.17 - The Origin of Noble Gases and Major Volatiles in the Terrestrial Planets, in: Holland, H.D., Turekian, K.K. (Eds.), Treatise on Geochemistry (Second Edition). Elsevier, Oxford, pp. 383-406.
Porcelli, D., Stone, J., O'nions, R., 1987. Enhanced 3He4He ratios and cosmogenic helium in ultramafic xenoliths. Chemical Geology 64, 25-33.
Porcelli, D., Wasserburg, G., 1995a. Mass transfer of helium, neon, argon, and xenon through a steady-state upper mantle. Geochimica et Cosmochimica Acta 59, 4921-4937.
Porcelli, D., Wasserburg, G.J., 1995b. Mass transfer of xenon through a steady-state upper mantle. Geochimica et Cosmochimica Acta 59, 1991-2007.
Porcelli, D., Woolum, D., Cassen, P., 2001. Deep Earth rare gases: initial inventories, capture from the solar nebula, and losses during Moon formation. Earth and Planetary Science Letters 193, 237-251.
Poreda, R., Farley, K., 1992. Rare gases in Samoan xenoliths. Earth and Planetary Science Letters 113, 129-144.
Poreda, R., Radicati di Brozolo, F., 1984. Neon isotope variations in Mid-Atlantic Ridge basalts. Earth and planetary science letters 69, 277-289.
Poreda, R., Schilling, J., Craig, H., 1986. Helium and hydrogen isotopes in ocean-ridge basalts north and south of Iceland. Earth and Planetary Science Letters 78, 1-17.
Pujol, M., Marty, B., Burgess, R., 2011. Chondritic-like xenon trapped in Archean rocks: A possible signature of the ancient atmosphere. Earth and Planetary Science Letters 308, 298-306.
Pujol, M., Marty, B., Burnard, P., Philippot, P., 2009. Xenon in Archean barite: Weak decay of 130Ba, mass-dependent isotopic fractionation and implication for barite formation. Geochimica et Cosmochimica Acta 73, 6834-6846.
Ragettli, R.A., Hebeda, E.H., Signer, P., Wieler, R., 1994. Uranium Xenon Chronology - Precise Determination of Lambda(SF)* Y136(SF) for Spontaneous Fission of U-238. Earth and Planetary Science Letters 128, 653-670.
Raquin, A., Moreira, M., 2009. Atmospheric (38)Ar/(36)Ar in the mantle: Implications for the nature of the terrestrial parent bodies. Earth and Planetary Science Letters 287, 551-558.
Raquin, A., Moreira, M.A., Guillon, F., 2008. He, Ne and Ar systematics in single vesicles: Mantle isotopic ratios and origin of the air component in basaltic glasses. Earth and Planetary Science Letters 274, 142-150.

Raymond, S.N., Morbidelli, A., 2022. Planet formation: key mechanisms and global models. Demographics of Exoplanetary Systems: Lecture Notes of the 3rd Advanced School on Exoplanetary Science, 3-82.
Render, J., Fischer-Gödde, M., Burkhardt, C., Kleine, T., 2017. The cosmic molybdenum-neodymium isotope correlation and the building material of the Earth. Geochem. Perspect. Lett 3, 170-178.
Renne, P.R., Mundil, R., Balco, G., Min, K., Ludwig, K.R., 2010. Joint determination of 40K decay constants and 40Ar∗/40K for the Fish Canyon sanidine standard, and improved accuracy for 40Ar/39Ar geochronology. Geochimica et Cosmochimica Acta 74, 5349-5367.
Reynolds, J., Hohenberg, C., Lewis, R., Davis, P., Kaiser, W., 1970. Isotopic analysis of rare gases from stepwise heating of lunar fines and rocks. Science 167, 545-548.
Reynolds, J., Jeffery, P., McCrory, G., Varga, P., 1978. Improved charcoal trap for rare gas mass spectrometry. American Institute of Physics.
Reynolds, J., Turner, G., 1964. Rare gases in the chondrite Renazzo. Journal of Geophysical Research 69, 3263-3281.
Rison, W., Craig, H., 1983. Helium isotopes and mantle volatiles in Loihi Seamount and Hawaiian Island basalts and xenoliths. Earth and Planetary Science Letters 66, 407-426.
Rizo, H., Walker, R.J., Carlson, R.W., Horan, M.F., Mukhopadhyay, S., Manthos, V., Francis, D., Jackson, M.G., 2016. Preservation of Earth-forming events in the tungsten isotopic composition of modern flood basalts. Science 352, 809-812.
Roubinet, C., Moreira, M.A., 2018. Atmospheric noble gases in Mid-Ocean Ridge Basalts: Identification of atmospheric contamination processes. Geochimica et Cosmochimica Acta 222, 253-268.
Rubin, M., Altwegg, K., Balsiger, H., Bar-Nun, A., Berthelier, J.-J., Briois, C., Calmonte, U., Combi, M., De Keyser, J., Fiethe, B., 2018. Krypton isotopes and noble gas abundances in the coma of comet 67P/Churyumov-Gerasimenko. Science advances 4, eaar6297.
Saffer, D.M., Tobin, H.J., 2011. Hydrogeology and mechanics of subduction zone forearcs: Fluid flow and pore pressure. Annual Review of Earth and Planetary Sciences 39, 157-186.
Sandoval-Velasquez, A., Rizzo, A., Casetta, F., Ntaflos, T., Aiuppa, A., Alonso, M., Padrón, E., Pankhurst, M., Mundl-Petermeier, A., Zanon, V., 2023. The noble gas signature of the 2021 Tajogaite eruption (La Palma, Canary Islands). Journal of Volcanology and Geothermal Research 443, 107928.
Sano, Y., Fischer, T.P., 2013. The analysis and interpretation of noble gases in modern hydrothermal systems. The noble gases as geochemical tracers, 249-317.
Sarda, P., 2004. Surface noble gas recycling to the terrestrial mantle. Earth and Planetary Science Letters 228, 49-63.
Sarda, P., Moreira, M., Staudacher, T., Schilling, J.G., Allègre, C.J., 2000. Rare gas systematics on the southernmost Mid-Atlantic Ridge: Constraints on the lower mantle and the Dupal source. Journal of Geophysical Research: Solid Earth 105, 5973-5996.
Sarda, P., Staudacher, T., Allegre, C.J., 1985. 40Ar36Ar in MORB glasses: constraints on atmosphere and mantle evolution. Earth and Planetary Science Letters 72, 357-375.
Sarda, P., Staudacher, T., Allègre, C.J., 1988. Neon isotopes in submarine basalts. Earth and Planetary Science Letters 91, 73-88.

Sasaki, S., Nakazawa, K., 1988. Origin of isotopic fractionation of terrestrial Xe: hydrodynamic fractionation during escape of the primordial H2He atmosphere. Earth and planetary science letters 89, 323-334.
Schlitzer, R., 2016. Quantifying He fluxes from the mantle using multi-tracer data assimilation. Philosophical Transactions of the Royal Society A: Mathematical, Physical and Engineering Sciences 374, 20150288.
Schönbächler, M., Carlson, R., Horan, M., Mock, T., Hauri, E., 2010. Heterogeneous accretion and the moderately volatile element budget of Earth. Science 328, 884-887.
Schultz, L., Weber, H., Begemann, F., 1990. Planetary noble gases in H3-and H4-chondrite falls. Meteoritics 25, 405.
Schultz, L., Weber, H., Begemann, F., 1991. Noble gases in H-chondrites and potential differences between Antarctic and non-Antarctic meteorites. Geochimica et Cosmochimica Acta 55, 59-66.
Seltzer, A.M., Bekaert, D.V., 2022. A unified method for measuring noble gas isotope ratios in air, water, and volcanic gases via dynamic mass spectrometry. International Journal of Mass Spectrometry 478, 116873.
Shibata, T., Takahashi, E., Matsuda, J.-i., 1998. Solubility of neon, argon, krypton, and xenon in binary and ternary silicate systems: a new view on noble gas solubility. Geochimica et Cosmochimica Acta 62, 1241-1253.
Shirey, S.B., Richardson, S.H., 2011. Start of the Wilson cycle at 3 Ga shown by diamonds from subcontinental mantle. Science 333, 434-436.
Signer, P., Suess, H., 1963. Rare gases in the sun, in the atmosphere, and in meteorites. Earth science and meteorites, 125-146.
Smye, A.J., Jackson, C.R., Konrad-Schmolke, M., Hesse, M.A., Parman, S.W., Shuster, D.L., Ballentine, C.J., 2017. Noble gases recycled into the mantle through cold subduction zones. Earth and Planetary Science Letters 471, 65-73.
Starkey, N.A., Stuart, F.M., Ellam, R.M., Fitton, J.G., Basu, S., Larsen, L.M., 2009. Helium isotopes in early Iceland plume picrites: Constraints on the composition of high 3He/4He mantle. Earth and Planetary Science Letters 277, 91-100.
Staudacher, T., Allegre, C.J., 1982. Terrestrial Xenology. Earth and Planetary Science Letters 60, 389-406.
Staudacher, T., Allègre, C.J., 1988. Recycling of oceanic crust and sediments: the noble gas subduction barrier. Earth and Planetary Science Letters 89, 173-183.
Staudacher, T., Sarda, P., Richardson, S., Allègre, C., Sagna, I., Dmitriev, L., 1989. Noble gases in basalt glasses from a Mid-Atlantic Ridge topographic high at 14 N: geodynamic consequences. Earth and Planetary Science Letters 96, 119-133.
Stroncik, N., Niedermann, S., 2016. Atmospheric contamination of the primary Ne and Ar signal in mid-ocean ridge basalts and its implications for ocean crust formation. Geochimica et Cosmochimica Acta 172, 306-321.
Stuart, F.M., Lass-Evans, S., Fitton, J.G., Ellam, R.M., 2003. High 3He/4He ratios in picritic basalts from Baffin Island and the role of a mixed reservoir in mantle plumes. Nature 424, 57-59.
Suess, H., Wänke, H., Wlotzka, F., 1964. On the origin of gas-rich meteorites. Geochimica et Cosmochimica Acta 28, 595-607.

Suess, H.E., Wänke, H., 1965. On the possibility of a helium flux through the ocean floor. Progress in oceanography 3, 347-353.
Tolstikhin, I., Mamyrin, B., Khabarin, L., Erlikh, E., 1974. Isotope composition of helium in ultrabasic xenoliths from volcanic rocks of Kamchatka. Earth and Planetary Science Letters 22, 75-84.
Tolstikhin, I., Marty, B., Porcelli, D., Hofmann, A., 2014. Evolution of volatile species in the earth's mantle: A view from xenology. Geochimica et Cosmochimica Acta 136, 229-246.
Trieloff, M., Kunz, J., Allègre, C.J., 2002. Noble gas systematics of the Réunion mantle plume source and the origin of primordial noble gases in Earth's mantle. Earth and Planetary Science Letters 200, 297-313.
Trieloff, M., Kunz, J., Clague, D.A., Harrison, D., Allegre, C.J., 2000. The nature of pristine noble gases in mantle plumes. Science 288, 1036-1038.
Trinquier, A., Elliott, T., Ulfbeck, D., Coath, C., Krot, A.N., Bizzarro, M., 2009. Origin of nucleosynthetic isotope heterogeneity in the solar protoplanetary disk. Science 324, 374-376.
Tucker, J.M., Mukhopadhyay, S., 2014. Evidence for multiple magma ocean outgassing and atmospheric loss episodes from mantle noble gases. Earth and Planetary Science Letters 393, 254-265.
Tucker, J.M., Mukhopadhyay, S., Gonnermann, H.M., 2018. Reconstructing mantle carbon and noble gas contents from degassed mid-ocean ridge basalts. Earth and Planetary Science Letters 496, 108-119.
Tucker, J.M., Mukhopadhyay, S., Schilling, J.G., 2012. The heavy noble gas composition of the depleted MORB mantle (DMM) and its implications for the preservation of heterogeneities in the mantle. Earth and Planetary Science Letters 355, 244-254.
Tucker, J.M., van Keken, P.E., Ballentine, C.J., 2022. Earth's missing argon paradox resolved by recycling of oceanic crust. Nature Geoscience 15, 85-90.
Valbracht, P.J., Staudacher, T., Malahoff, A., Allègre, C.J., 1997. Noble gas systematics of deep rift zone glasses from Loihi Seamount, Hawaii. Earth and Planetary Science Letters 150, 399-411.
van Keken, P.E., Ballentine, C.J., Porcelli, D., 2001. A dynamical investigation of the heat and helium imbalance. Earth and Planetary Science Letters 188, 421-434.
Villa, I.M., Holden, N.E., Possolo, A., Ickert, R.B., Hibbert, D.B., Renne, P.R., Bonardi, M.L., De Bievre, P., 2022. IUGS–IUPAC recommendations and status reports on the half-lives of 87Rb, 146Sm, 147Sm, 234U, 235U, and 238U (IUPAC Technical Report). Pure and applied chemistry 94, 1085-1092.
Vogel, N., Heber, V.S., Baur, H., Burnett, D.S., Wieler, R., 2011. Argon, krypton, and xenon in the bulk solar wind as collected by the Genesis mission. Geochimica et Cosmochimica Acta 75, 3057-3071.
Vogel, N., Heber, V.S., Bochsler, P., Burnett, D.S., Maden, C., Wieler, R., 2019. Noble gas elemental abundances in three solar wind regimes as recorded by the Genesis mission. Geochimica et Cosmochimica Acta 263, 182-194.
Vollmer, R., 1983. Earth degassing, mantle metasomatism, and isotopic evolution of the mantle. Geology 11, 452-454.
Wänke, H., 1965. Der Sonnenwind als Quelle der Uredelgase in steinmeteoriten. Zeitschrift für Naturforschung A 20, 946-949.

Warren, P.H., 2011. Stable-isotopic anomalies and the accretionary assemblage of the Earth and Mars: A subordinate role for carbonaceous chondrites. Earth and Planetary Science Letters 311, 93-100.
Wasserburg, G., Mazor, E., 1965. Spontaneous fission xenon in natural gases. In: Fluids in Subsurface Environments, A Symposium, American Association of Petroleum Geologists Memoir 4, 386-398.
Weingartner, J.C., Draine, B., 2001. Dust grain-size distributions and extinction in the milky way, large magellanic cloud, and small magellanic cloud. The Astrophysical Journal 548, 296.
Weis, D., Harpp, K.S., Harrison, L.N., Boyet, M., Chauvel, C., Farnetani, C.G., Finlayson, V.A., Lee, K.K., Parai, R., Shahar, A., 2023. Earth's mantle composition revealed by mantle plumes. Nature Reviews Earth & Environment, 1-22.
Weston, B., Burgess, R., Ballentine, C.J., 2015. Disequilibrium degassing model determination of the 3He concentration and $^{3}He/^{22}Ne$ of the MORB and OIB mantle sources. Earth and Planetary Science Letters 410, 128-139.
Wetherill, G.W., 1953. Spontaneous fission yields from uranium and thorium. Physical Review 92, 907-912.
Wetherill, G.W., 1954. Variations in the isotopic abundances of neon and argon extracted from radioactive minerals. Physical Review 96, 679.
Wetherill, G.W., 1975. Radiometric chronology of early Solar-System. Annual Review of Nuclear and Particle Science 25, 283-328.
White, W. M. 1985. Sources of oceanic basalts: Radiogenic isotopic evidence. Geology, 13, 115-118.
Wieler, R., 2002. Noble gases in the solar system. Reviews in Mineralogy and geochemistry 47, 21-70.
Wieler, R., 2023. A Journey in Noble Gas Cosmochemistry and Geochemistry. Geochemical Perspectives 12, 1-2.
Wieler, R., Baur, H., Signer, P., 1986. Noble gases from solar energetic particles revealed by closed system stepwise etching of lunar soil minerals. Geochimica et Cosmochimica Acta 50, 1997-2017.
Wiens, R.C., Bochsler, P., Burnett, D.S., Wimmer-Schweingruber, R.F., 2004. Solar and solar wind isotopic compositions. Earth and Planetary Science Letters 226, 549-565.
Williams, C.D., Mukhopadhyay, S., 2019. Capture of nebular gases during Earth's accretion is preserved in deep-mantle neon. Nature 565, 78-81.
Yatsevich, I., Honda, M., 1997. Production of nucleogenic neon in the Earth from natural radioactive decay. Journal of Geophysical Research: Solid Earth 102, 10291-10298.
Yokochi, R., Marty, B., 2004. A determination of the neon isotopic composition of the deep mantle. Earth and Planetary Science Letters 225, 77-88.
Yokochi, R., Marty, B., 2005. Geochemical constraints on mantle dynamics in the Hadean. Earth and Planetary Science Letters 238, 17-30.
York, D., 1969. Least squares fitting of a straight line with correlated errors. Earth and Planetary Science Letters 5, 320-&.
York, D., Evensen, N.M., Martinez, M.L., Delgado, J.D., 2004. Unified equations for the slope, intercept, and standard errors of the best straight line. American Journal of Physics 72, 367-375.

Zartman, R.E., Wasserburg, G., Reynolds, J., 1961. Helium, argon, and carbon in some natural gases. Journal of geophysical research 66, 277-306.
Zeitler, P.K., Tremblay, M.M., 2020. Measuring noble gases for thermochronology. Elements 16, 343-344.
Zhang, X.J., Avice, G., Parai, R., 2023. Noble gas insights into early impact delivery and volcanic outgassing to Earth's atmosphere: A limited role for the continental crust. Earth and Planetary Science Letters 609, 118083.
Zhang, X.J., Parai, R., Lassiter, J.C., 2024. Primordial and recycled noble gases in the Cook-Austral HIMU mantle: insights into the onset of volatile subduction. Earth and Planetary Science Letters accepted, in press.
Zhang, Y., 2014. 6.2 - Degassing History of Earth, in: Holland, H.D., Turekian, K.K. (Eds.), Treatise on Geochemistry (Second Edition). Elsevier, Oxford, pp. 37-69.
Zindler, A., Hart, S., 1986. Chemical geodynamics. Annual Review of Earth and Planetary Sciences 14, 493-571.
Zindler, A., Jagoutz, E., Goldstein, S., 1982. Nd, Sr and Pb isotopic systematics in a 3-component mantle - a new perspective. Nature 298, 519-523.
Zinner, E., 2014. 1.4 - Presolar Grains, in: Holland, H.D., Turekian, K.K. (Eds.), Treatise on Geochemistry (Second Edition). Elsevier, Oxford, pp. 181-213.
Zinner, E., Ming, T., Anders, E., 1987. Large isotopic anomalies of Si, C, N and noble gases in interstellar silicon carbide from the Murray meteorite. Nature 330, 730-732.